Multielectron Dynamics of Singlet Fission in the Condensed Phase

by

Paul Emery Teichen

B.S., Western Washington University, 2009

A thesis submitted to the

Faculty of the Graduate School of the

University of Colorado in partial fulfillment

of the requirements for the degree of

Doctor of Philosophy, Chemical Physics

Department of Chemistry and Biochemistry

2015

This thesis entitled:
Multielectron Dynamics of Singlet Fission in the Condensed Phase
written by Paul Emery Teichen
has been approved for the Department of Chemistry and Biochemistry

Joel David Eaves

Prof. David Jonas

Prof. Rex Skodje

Date

The final copy of this thesis has been examined by the signatories, and we find that both the content and the form meet acceptable presentation standards of scholarly work in the above mentioned discipline.

Teichen, Paul Emery (Ph.D., Chemical Physics)

Multielectron Dynamics of Singlet Fission in the Condensed Phase

Thesis directed by Prof. Joel David Eaves

Elementary energy and electron transfer processes are ubiquitous in the renewable energy science of the last half of the 20^{th} century. As global energy demands increase, researchers are inclined to explore chemical physics that is outside the scope of the single electron paradigm using new theoretical concepts and methods. This thesis advances theories of two specific condensed phase phenomena: singlet fission, and energy transfer in photosynthetic light harvesting complexes. Some photoactive organic molecules relax through a multielectron process known as singlet fission, where a photon excites a chromophore that can down-convert the energy of a singlet excitation by relaxing to two triplet excitations. Singlet fission may lead to unprecedented solar power conversion efficiencies, but its many-body chemical physics can be challenging to model. We explore the fundamental role of thermal energy in singlet fission in liquids and solids over multiple timescales. Using quantum master equations and diabatic representations of the single and double electronic excitations, we study the scope of the Markovian approximation for the chemical environment's response to singlet fission. To better understand how singlet delocalization and triplet localization impact quantum yields in molecular crystals, we develop a theory for delocalized singlets interacting with a dense band of two triplet excitations that includes biexciton interactions. We use the Bethe Ansatz for the two triplets and calculate an entanglement for indistinguishable bipartite systems to analyze the triplet-triplet entanglement born out of singlet fission.

Dedication

For my mother and father.

Acknowledgements

My love of science has developed and matured over the course of many years. Kirby Zornes, Peter Saxby, and Mike Town were important secondary school teachers to me. Kirbey Zornes taught a joyful explorative science and lent me popular science videos outside of the core curriculum. At Western Washington University I was fortunate to receive many exceptional lectures in science and mathematics from Andrew Boudreaux, Takele Seda, Branko Curgus, and Jeff Young. Branko Curgus taught me about limits and infinite series and would become so passionate in lectures that he would break chalk. Takele Seda offered a course on Special Relativity in which we learned to supplement calculation with thought experiments and graphics. At the University of Colorado, Casey Hynes and Victor Gurarie taught me theories of electron transfer, the Ising model, and the Renormalization group. They demonstrated a mastery of chemical physics and statistical mechanics that I will forever aspire to achieve.

Science research requires a patience and rigour that my undergraduate advisor, Prof. Elizabeth Raymond, strongly emphasized. Prof. Raymond would hold weekly meetings with me and Brendan Abolins to discuss second harmonic generation and surface chemistry. Brendan and I were granted the freedom to explore many aspects of nonlinear optics that are often excluded from undergraduate coursework in chemistry. These early experiences were vital as I began to take ownership of my research.

Joel Eaves taught quantum mechanics my first semester of graduate school. As I looked for a research advisor, Joel assigned extracurricular calculations of quantum dissipative systems. I appreciated the firm connection between coursework and research, and quickly decided to work on

various charge and energy transfer problems in the Eaves Group. Joel's perspectives on chemical physics share a clear lineage with theorists such as Robert Silbey, David Chandler, and David Reichman. I hope to highlight their ground-breaking work in this thesis.

This dissertation would not be possible without the constant support of my friends and family. I would like to especially thank my sisters, Brenna and Jamie Teichen, as well as my closest friends: Jayden Wilson, Abigail Pleiss, Scott Delbecq, Laina Mercer, Dmitry Baranov, and Vivek Tiwari. Although I could not always be with my friends in person, they have indulged me with long conversations about science and society, work, and personal life. I will forever be indebted to them.

Contents

Chapter

Chapter 1 Introduction **1**

1.1 Energy and Electron Transfer in Condensed Phases 1

1.1.1 The History of Electron Transfer Theory 1

1.2 Singlet Fission 3

1.2.1 Background and Motivation 3

1.2.2 Singlet Fission is a Multielectron Process 4

1.3 Photosynthetic Light Harvesting 5

1.3.1 Background and Motivation 5

1.3.2 Recent Advances in Theories of Coherent Energy Transfer 5

1.4 Organization of the Thesis 6

Chapter 2 A Microscopic Model of Singlet Fission **7**

2.1 Abstract 7

2.2 Introduction 7

2.3 Methods 11

2.3.1 The Electronic Hamiltonian 11

2.3.2 Hamiltonian of the Dissipative System 16

2.3.3 Equation of Motion for the Populations of the Diabatic States 17

2.3.4 Rate Theories 19

2.4 Results and Discussion 20

2.5 Appendix 2A - Quantum Master Equations . . . 29
2.6 Appendix 2B - Biexciton Interactions and Spin Relaxation Measured using Magnetic Fields . . . 30
Chapter 3 Collective Aspects of Singlet Fission in Molecular Crystals **33**
3.1 Abstract . . . 33
3.2 Introduction. . . . 33
3.3 A Model Hamiltonian for Fission. . . . 40
3.3.1 The Jordan-Wigner Transformation and Matrix Representations . . . 44
3.4 The Singlet Self-Energy and the Rate of Singlet Fission. . . . 46
3.4.1 SF from a Localized Singlet State . . . 51
3.5 Biexciton Interactions . . . 54
3.6 Characterizing the Fission Product: Structure Functions. . . . 54
3.7 Bound States from the Bethe Ansatz. . . . 56
3.8 Triplet-Triplet Entanglement and the Slater Decomposition . . . 62
3.9 Conclusions. . . . 65
3.10 Acknowledgements . . . 67
3.11 Appendix 3A - Triplet Hamiltonian Matrix Elements. . . . 68
3.12 Appendix 3B - Pair Distribution Functions . . . 70
3.13 Appendix 3C - Bosonification on a Square Lattice . . . 72
Chapter 4 Dynamic Fluctuations Facilitate Vibronic Energy Transfer in Light-Harvesting Antennas **75**
4.1 Introduction . . . 75
4.2 A Model for Photosynthetic Antennas . . . 79
4.3 Vibronic Energy Transfer . . . 84
4.3.1 The HEOM and Redfield Theory . . . 84
4.4 Zeno and Anti-Zeno Effects . . . 94
4.5 Conclusion . . . 97

4.6 Appendix 4A - Calculating Low Temperature Transitions with the Numerical Renormalization Group 100

Bibliography **103**

Appendix

Chapter A Stochastic Modeling of the Vibrational FID in s-SNOM of PTFE **126**

A.1 Introduction 126

A.2 Nonergodic FID at Nanometer s-SNOM Resolution 127

A.3 Coherence Transfer between Local Vibrations 131

Figures

Figure

2.1 Fluctuations and SF . . . 10

2.2 Energy Level Diagram . . . 13

2.3 Slater Determinants . . . 15

2.4 FD Theory . . . 22

2.5 NonMarkovian Lineshapes . . . 24

2.6 Dipolar Coupling Schematic . . . 25

2.7 Marcus Rates . . . 26

2.8 Clebsch-Gordon Coefficients . . . 32

3.1 Dynamics of Singlet and Triplet Excitons . . . 43

3.2 Schematic of Ground State Absorption and Singlet Fission . . . 47

3.3 Singlet Fission as a Scattering Process . . . 48

3.4 Rate of Singlet Fission for Zero Biexciton Interactions . . . 52

3.5 Rate of Singlet Fission for Nonzero Biexciton Interactions . . . 55

3.6 The Static Structure Factor . . . 57

3.7 The Bethe Ansatz . . . 61

3.8 The Slater Decomposition . . . 64

4.1 Diagram of a Photoantenna . . . 76

4.2 One-Exciton Diabatic and Adiabatic Energies of a Dimer . . . 78

4.3 Polaron Energy Level Diagram 82
4.4 Population of the Donor State using Correlated Fluctuations 92
4.5 Population of the Acceptor State using Correlated Fluctuations 93
4.6 Population of the Donor State for Initially Vibrationally Hot Initial Conditions . . . 95
4.7 Population of the Acceptor State for Initially Vibrationally Hot Initial Conditions . 96
4.8 Energy Level Diagram of the FMO Complex with a Reaction Center 96
4.9 The Zeno Effect 98
4.10 The Trapping Time 99
4.11 NRG Ohmic Flow Diagrams 102

A.1 Linear Response of a Finite Set of Local Symmetric Vibrations 130
A.2 Linear Response of a Finite Set of Local Symmetric and Antisymmetric Vibrations . 131

Chapter 1

Introduction

1.1 Energy and Electron Transfer in Condensed Phases

The demand for efficient and cost-effective renewable energy has prompted fundamental physics and chemistry research of charge and energy transfer in solutions, crystals, and disordered solids, all to be used in novel photovoltaic cells and electrocatalysts. This thesis focuses on dynamical aspects of how the energy of electronic excitations is relaxed in these condensed systems.

1.1.1 The History of Electron Transfer Theory

In 1957, Kubo[1] published his seminal theory of electron transfer in liquids and solids, where many degrees of freedom relax and equilibrate about the electron's position.[2] If the electron experiences a *linear* restoring force for small displacements from local equilibrium, then the chemical environment behaves as a large "bath" of *harmonic* oscillators.[1, 3, 4, 5, 6] Kubo's work led to a generic class of microscopic models where the electronic system *linearly* couples to the bath and thermal motion modulates the electronic frequencies. These ideas will form the bedrock of our electronic and vibronic energy transfer theories.

When dephasing times are fast, the quantum dynamics become an incoherent rate process, and the Liouville equation reduces to a quantum master equation. For simple models, the isolated dynamics of the system and bath can be solved exactly. But when the system interacts with the bath we are forced to use reduced descriptions of the quantum dynamics by projecting out the system degrees of freedom from the harmonic reservoir. From the nonadiabatic perspective,

nuclear motion and the electromagnetic field of the surroundings help traverse free energy barriers between two localized charge distributions, and also dissipate energy once the barriers have been crossed. When temperature is much larger than any frequency of the heat bath, the environment can be treated as a classical reservoir. Marcus modeled electron transfer in the high temperature limit as the quantum analogue of the Kramers problem,[3] where the electron is quantal and the second order cumulant expansion of the Kubo response function is exact.[7, 8] In this case, the quantum tunneling between two localized diabats is slow, and transition rates are given by Fermi's Golden Rule. Energy transfer shares many similarities with electron transfer, and we will show that Marcus theory can serve as a benchmark for high temperature singlet fission rates.

In this thesis we are concerned with energy transfer processes that occur over picosecond and subpicosecond timescales, when the environment's response to electronic transitions may be slow. This *nonMarkovian* scenario has been analyzed by Kubo with the generalized Langevin equation,[9] by Grote and Hynes with transition state theory,[10, 9] and by Golosov and Reichman[11] who tackled the problem of delocalized charge transfer. Motivated by Jang, Jung, and Silbey's 2002 generalized Förster-Dexter theory,[12] we evaluate nonequilibrium singlet fission in Chapter 2.

In the opposite limit, where the electronic coupling is large relative to the reorganization energy, second order time-dependent perturbation theory in the system-bath coupling can well approximate the quantum relaxation dynamics if the bath cutoff frequency is much larger than the reorganization energy. In this regime, the Redfield rate equations for the reduced density matrix help us establish microscopic connections between phenomenological models and coherent energy transfer. In Chapter 4 we show that this limit is realized in the case of photosynthetic energy transfer.

1.2 Singlet Fission

1.2.1 Background and Motivation

The first attempts to design commercial solar cells that convert radiant energy from the sun into electrical and chemical work date back to Bell Laboratories in the late 1950's. Over half a century later, modern solar cells have yet to quench the global energy demand. Shockley and Queisser's analysis of one photon generating one electron-hole pair provides an upper bound for power conversion efficiency of about 30 %.[13] To break this efficiency ceiling, research has turned to new materials that might be able to down-convert excitation energy through many-body scattering.[14, 15]

Carrier multiplication from a single photon may fall outside the scope of effective one-body problems. In semiconductors, multiple electron-hole pairs can be generated and separated if the system is excited above or at twice the bandgap, and also if the electron-hole pairs can diffuse to overcome their Coulombic binding.[16, 17, 14, 15] In molecular systems, multiple excitations can be generated if the excited singlet can relax through an internal conversion whereby the electronic wavefunction acquires multiply-excited character, and if two triplet excitations can be separated.[18, 19] The former is referred to as multiple exciton generation (MEG) while the latter is its molecular analogue, singlet fission (SF). SF has the distinct advantages of not competing with intraband relaxation, and of producing long-lived triplet excitations. Despite these advantages, few of the candidate SF chromophores exhibit SF that can out-compete all other relaxation pathways. Research has focused on chemically tuning the electronic structure of chromophores in order to achieve an energy matching that favors charge injection from the triplet excitations rather than charge injection from the initially excited singlet.[18, 19, 20, 21, 22, 23, 24, 25, 26] In this thesis, we focus on the dynamical picture of singlet fission, using nonperturbative and perturbative methodologies to examine many-body aspects of the phenomenon.

1.2.2 Singlet Fission is a Multielectron Process

Singlet fission can not be understood as an effective one-body problem. Multielectron exchange interactions are essential for the energy matching condition of singlet fission, and SF on picosecond and subpicosecond timescales conserves the total spin angular momentum of multiple electrons by "impulsively" exciting quantum beats between triplet sublevels. Moreover, in molecular crystals the singlet excitations delocalize across many molecules via Coulomb interactions. Although electronic structure calculations can simulate static singlet delocalization and triplet localization, it remains unclear why these qualitative features correspond to efficient singlet fission.

In the first few years of my graduate studies, it was not known whether thermal energy would activate or dampen singlet fission. Chapter 2 is adapted from our 2012 publication that explores the role of thermal energy and nonMarkovian friction over ultrafast timescales. Although we calculated rates with a four orbital and four electron representation, the effects of solvation are analogous to the effects of low frequency lattice phonons in molecular crystals. In a perfect crystal, optical transitions access the completely delocalized singlet from the ground state. The excited singlet can then scatter and localize as two triplets at two molecules anywhere in the lattice. We draw an analogy between this idealized fission and the Anderson model in Chapter 3. In 1961, Anderson[27] showed that an "impurity" acquires a finite and nonzero self-energy through interactions with a continuum that irreversibly relaxes the impurity. Lattice defects and electron-phonon interactions may distort this model, leading to a somewhat disordered solid with disparate exciton localizations.

To enhance photocurrent in photovoltaic devices, the two triplets must be separated. However, triplet-triplet correlation has been largely overlooked in the literature. In the 1970s, Johnson and Merrifield[28, 29] explored spin-correlation arising from the spin-dipole interaction that breaks the spin symmetry on nanosecond timescales. In Chapter 4 we consider the entanglement of the spatial component of the triplet wavefunctions, and the effects of local biexciton interactions in ultrafast singlet fission. Local exchange interactions have been known to correlate plane waves in the Heisenberg model of spin-1/2 chains.[30, 31] We borrow concepts from quantum information theory,

such as the preparation of separable states through local operations and classical communications (LOCC).[31]

1.3 Photosynthetic Light Harvesting

1.3.1 Background and Motivation

Efficient energy transfer in the pigment-protein complexes of photosynthesis has stimulated theoretical chemical physics for nearly two decades.[32, 33, 34, 35, 36, 37] In green sulfur bacteria, energy transport hinges upon the Fenna-Matthews-Olson (FMO) complex, which acts like a bridge between the chlorosome and the reaction center in photoantenna. The intramolecular pigment vibrations in the FMO complex couple to the transfer of electronic excitation energy.[32] These pigments are also strongly bound to a protein network whose low frequency vibrations affect the electronic dynamics.[38] Although two-dimensional electronic spectroscopy (2DES) has measured the coherent quantum dynamics of pigment-protein complexes,[39, 32, 33, 40, 35, 36, 41] the role of pigment and protein vibrational motion is not fully understood.[36, 41, 32]

1.3.2 Recent Advances in Theories of Coherent Energy Transfer

Tiwari, Peters, and Jonas[32] have shown, using static vibronic transition frequencies, that the anticorrelated inter-pigment vibration mixes local pigment electronic diabats,[42, 32] corresponding to signatures of anticorrelated vibrations on the ground state in 2DES.[32] In Chapter 4 we explore whether or not fluctuations that lead to dynamic vibronic transition frequencies can "activate" the correlated inter-pigment vibration. We model the transfer of electronic energy out of the FMO complex and into the reaction center as a trapping event, analogous to measurement in quantum information theory. If an increase in the measurement frequency suppresses decay, the system can be said to exhibit a quantum Zeno effect.

1.4 Organization of the Thesis

The outline of this dissertation is as follows: In Chapter 2, we assess the role of thermal fluctuations in the singlet fission phenomenon. From the diabatic perspective, fluctuations facilitate fission via charge transfer intermediate electronic states up to some critical threshold, past which the system becomes self-trapped. In Chapter 3, we develop a model of singlet fission in molecular crystals, whose translational symmetry leads to a "momentum selection" rule that, taken together with the energy matching condition of singlet fission, governs the lifetime of the initial singlet excitation. By calculating the two-triplet density of states, the static structure factor, the Bethe Ansatz wavefunction, and the Slater decomposition when biexciton interactions are of the same order of magnitude as the triplet bandwidth, we demonstrate that biexciton interactions correlate the two triplets born out of singlet fission. We predict a threshold for bound triplet pairs and show that the two-triplet system can exhibit significant entanglement even if unbound. In Chapter 4, we model photosynthetic energy transfer as a vibronic energy transfer, using a polaronic system of pigments in the FMO complex, a thermal reservoir to model the protein scaffolding that introduces dynamic modulation of the exciton transition frequencies, and an anti-Hermitian operator describing the transport of electronic excitation energy from the pigment-protein complex to the reaction center. The polaron transformation rigorously shows that it is only the anticorrelated pigment vibrations that couple to the transfer of electronic excitation energy. Using the exact hierarchical equations of motion (HEOM), we validate simulations which solve the Redfield equation for a significant range of values for the Kubo parameter.

Chapter 2

A Microscopic Model of Singlet Fission

2.1 Abstract

Singlet fission, where an electronically excited singlet on one chromophore converts into a doubly excited state on two, has gone from a curiosity in organic photophysics to a potential pathway for increasing solar energy conversion efficiencies. Focusing on the role of solvent-induced energy level fluctuations that would be present in a dye-sensitized solar cell, we present a microscopic model for singlet fission. Starting from an electronic model Hamiltonian, we construct diabatic states in a manifold of single and double excitations with total singlet multiplicity and then develop a multilevel non-Markovian theory of dynamics for electronic populations in the presence of energy level fluctuations. Depending on the energy scales, energy gap fluctuations can either facilitate or hinder interconversion steps that lead to singlet fission. We critically assess the Markovian approximation that leads to golden rule rates and study the role of intramolecular solvation dynamics and electron transfer.

The contents of this chapter have been reprinted with permission from

P. E. Teichen and J. D. Eaves. A microscopic model of singlet fission. *J. of Phys. Chem. B*, 116:11473-11481, 2012.

2.2 Introduction

Developing solar technology that is cost-competitive with fossil fuels will require considerable advances in fundamental science. In 1961, Shockley and Queisser [13] argued that a single junction

solar cell could never have power conversion efficiency larger than about 30 %. Their argument considered only the most basic physics; one photon absorbed above the band gap yields one electron-hole pair, and that the cell is operating in steady-state. While these arguments are elementary, no single junction solar cell to date has broken the Shockley-Queisser limit. To do so, a new generation of materials has been proposed that yield more than one electron-hole pair per photon absorbed. In these materials, carriers that have energy in excess of the absorption threshold relax by emitting a second electron-hole pair rather than cooling by phonon emission or other nonradiative relaxation pathways. Multiple exciton generation (MEG), the name given to this process in semiconductors and semiconducting nanocrystals, has received the most attention in recent years [14, 15, 43, 44]. The great deal of debate surrounding the results and yields of MEG in nanocrystals highlights a fundamental weakness in our current understanding of the basic principles that might enable the one photon to multiple electron-hole pair paradigm.

Singlet fission is the molecular analog of MEG, where a singlet excited state S_1 on one chromophore decays into two excitations, T_1T_1, on different chromophores [18] (2.1). Unlike singlet to triplet conversion via intersystem crossing, the initial and final states are simultaneous eigenstates of the total spin operator, $\mathcal{S}^2$, and the operator for the z-component of the total spin, $\mathcal{S}_z$. Singlet fission is a form of internal conversion from S_1 to T_1T_1, is spin-allowed, and may take place on the sub-picosecond timescale [45, 46, 47, 48, 49].

Singlet fission was first invoked in the late 1960's to explain the photophysics of anthracene and tetracene crystals [28, 29]. In the past 40 years, it has been observed in molecular crystals and quantified with a variety of methods [18]. But the potential of singlet fission in solar applications was not realized until 2006, when Hanna and Nozik [14] proposed that singlet fission chromophores could enhance the efficiency of dye-sensitized solar cells [50, 51].

The singlet fission mechanism is highly system-specific. Singlet fission is a two-electron interconversion process that can proceed via direct coupling between the initial singlet excitation and the T_1T_1 states [52, 53]. It may also occur through concerted or stepwise electron transfer events that involve virtual or real intermediates, respectively [18, 54, 55]. Similar to the compounds

studied in Refs. [54, 56], we consider a class of chromophores whose relevant excited states can be described within frontier molecular orbital theory [18]. These states are weakly coupled, and the initial excited state is localized. Our treatment describes singlet fission within the stepwise, or "mediated" mechanism, in the language of Ref. [18]. Extensions of our model to higher-order perturbation theories that would describe concerted events through virtual state transitions, are straightforward. [57]

Clearly, computation has a role to play in locating molecules that might undergo singlet fission, but the calculations are demanding, and state-of-the-art calculations are done with molecules in isolation. But dye-sensitized solar cells are in polar solutions [14, 15, 43, 16] where interactions with solvent molecules induce electronic energy level fluctuations that can be on the order of 0.1-0.2 eV [58, 59, 60]; comparable to electronic energy level splittings of isolated singlet fission chromophores calculated with the highest available levels of theory [61, 52, 62, 63, 64, 65]. Solvent polarization fluctuations enable transitions between states by activating the system and bringing it to a crossing point. They also dissipate the energy of excited states [66] and stabilize products. From a design perspective, one may actually be able to exploit fluctuations to enable singlet fission when the energies of the S_1 and T_1T_1 states are not exactly degenerate. Clearly, a quantitative model of fluctuations needs to be part of a comprehensive theory for singlet fission.

In this chapter, we develop a microscopic model of singlet fission that is capable of describing dynamics on picosecond and subpicosecond timescales in the presence of solvent induced energy level fluctuations. First, we propose a physically reasonable electronic model Hamiltonian that is based on frontier molecular orbital theory. We then derive an exact quantum master equation for the populations of the electronic states and analyze it in the limit of weak-coupling between them. We analyze rate theories in the Markovian limit, when the timescale between relaxation is well-separated from the timescale for interconversion. Here, one imagines that solvation and relaxation timescales, as quantified through a time-dependent Stokes shift, are on the timescale of picoseconds, while interconversion timescales are at least an order of magnitude longer. The rate theories align with the Förster/Dexter theory of energy and electron transfer [67, 68]. Using plausible model

Figure 2.1: Conceptual diagram of singlet fission and the role of fluctuations. **(A)** Two chromophores, Left and Right, have energy levels where the doubly-excited state is nearly half the energy of the singlet S_1 state. The electron (solid blue circle) and hole (empty circle) undergo singlet fission, which is an internal conversion process that leaves the system with two excitations, one on each chromophore. **(B)** Electronic configurations that participate in singlet fission. A singlet (top) can go through a charge transfer state (middle) and then to a doubly-excited state (bottom). The states in both **A** and **B** are **schematic** because if taken literally, these states are not eigenstates of the total electron spin angular momentum. In addition to satisfying spin selection rules, interconversion must satisfy energy conservation. An initial state, $| i \rangle$, cannot transition to another state, $| f \rangle$, unless energy is conserved. For a system in relative isolation **(C)**, a large energy difference between states forbids transitions. In **(D)**, the solvent induces energy level fluctuations that broaden the relevant densities of states between $| i \rangle$ and $| f \rangle$. Provided that selection rules are satisfied, transitions can occur when two states have the same energies (purple overlap).

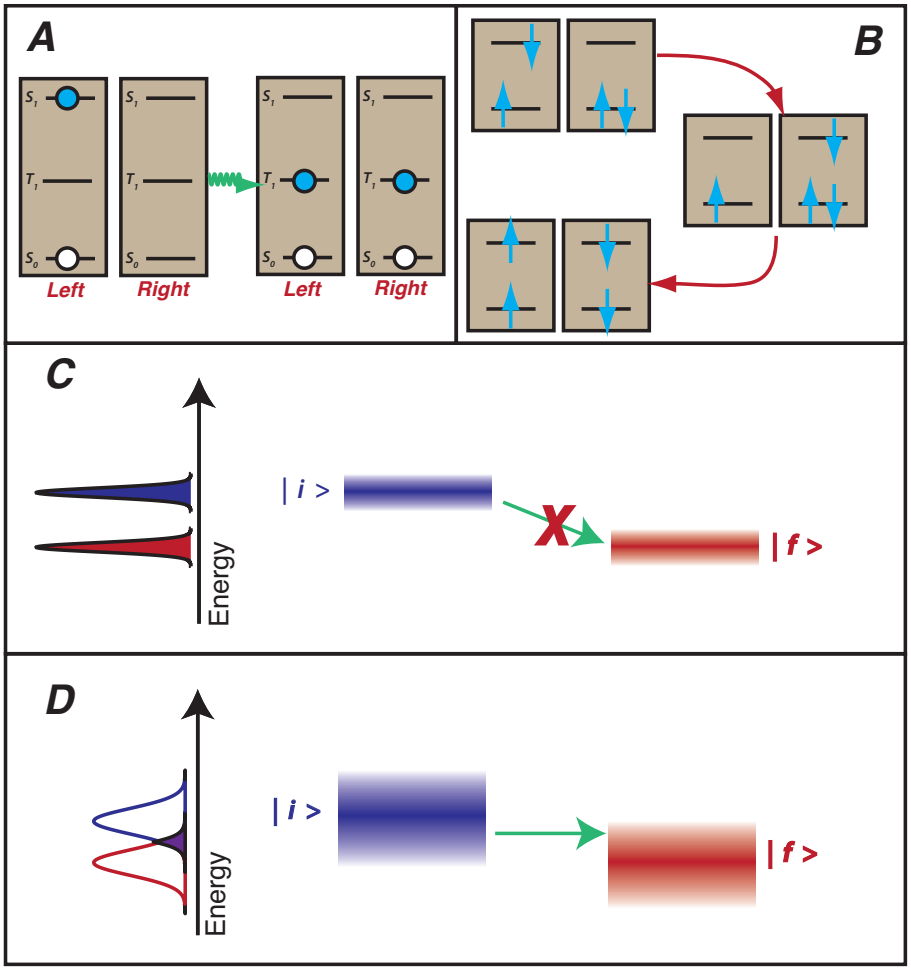

parameters for the theory, we examine the nonMarkovian limit, where the system is prepared in such a way that the solvent is not in thermal equilibrium with the electrons when they are excited. We then analyze the rate theory of a model that separates fluctuations from solvation dynamics and electron transfer kinetics. While phenomenological, the theory is microscopic. As a result, the inputs to the theory can come from a variety of sources: electronic structure calculations, molecular spectroscopy, and molecular dynamics [69, 70, 71, 72].

2.3 Methods

2.3.1 The Electronic Hamiltonian

We begin by discussing a model electronic Hamiltonian. Recent work has suggested that the electronic levels in singlet fission systems can be modeled by considering the frontier molecular orbitals of two chromophores, termed left (L) and right (R). These chromophores could be different molecules, or different chromophores on the same molecule. Each chromophore has HOMO and LUMO energy levels separated by a gap, Δ. For the purposes of illustration, we consider identical chromophores. To construct a fairly general model, we clamp the nuclei at their equilibrium configuration and propose the following semiempirical electronic Hamiltonian,

$$H_{el} = H_{el}^0 + W_{el} \ ,$$

with

$$H_{el}^0 = \sum_{k,\sigma} \epsilon_k n_{k,\sigma} + \mathcal{V} \sum_{\sigma,\sigma'} \left[n_{h_L,\sigma} n_{l_L,\sigma'} + n_{h_R,\sigma} n_{l_R,\sigma'} \right] + U \sum_{k,\sigma} n_{k,\sigma} n_{k,-\sigma} - X \sum_{\sigma} \left[n_{h_L,\sigma} n_{l_L,\sigma} + n_{h_R,\sigma} n_{l_R,\sigma} \right] , \tag{2.1}$$

and

$$W_{el} = - \sum_{j \neq k,\sigma} J_{jk} c_{j,\sigma}^{\dagger} c_{k,\sigma} \ . \tag{2.2}$$

The fermionic creation and destruction operators, $c_{k,\sigma}^{\dagger}$ and $c_{k,\sigma}$ respectively, create or destroy an electron in orbital k with spin σ. The fermionic number operator is $n_{k,\sigma} = c_{k,\sigma}^{\dagger} c_{k,\sigma}$. The ground state is a closed shell, and electrons can reside in the four frontier orbitals $\{h_L, l_L; h_R, l_R\}$ in either

the spin up ($\sigma =\uparrow$) state or spin down ($\sigma =\downarrow$) state. The HOMO and LUMO basis functions are physically-motivated and mutually orthogonal, but do not necessarily represent the result of the real and virtual orbitals in an electronic structure calculation. ϵ_k is the "bare" energy of an electron in orbital k, U is the "Hubbard" on-site Coulomb integral of electrons in the same orbital, $\mathcal{V}$ the off-site Coulomb matrix element, and X is the exchange energy. Note that none of the terms in H^0_{el} couple different orbitals on different chromophores. The coupling matrix elements J_{jk}, do. They are two-center "resonance" integrals that do couple orbitals between R and L chromophores. The resonance integrals represent the electron kinetic energy, and allow electrons to move between orbitals by one-electron hops. The energy levels of H^0_{el} may be split by as much as 1 - 10 eV, while J has been calculated to be in the range of about 0.01 to 0.1 eV [54, 48, 49]. Solute-solvent energy scales, as quantified through the solvent-induced Stokes shift or electron transfer reorganization energies can be on the scale of 0.1 eV. These energy scales suggest that one can approach the singlet fission problem, at least for some of the chromophores in which these parameters are known, in the weak electronic-coupling limit.

2.2 is an energy level diagram of some of the electronic configurations present in the representation of the electronic Hamiltonian in the frontier molecular orbital basis. The electronic interaction parameters can be computed from first principles simulations, but here they are model parameters. In arriving at the model Hamiltonian for the electronic degrees of freedom, we drop all integrals in the Hamiltonian that are three-center and higher. Physically, we suppose that the states are localized enough that three or more **different** orbitals have negligible overlap in space. This is a standard assumption that leads, for example, to the PPP Hamiltonian when atomic orbitals are the assumed basis set [73, 74, 75]. Examples of terms missing from the model electronic Hamiltonian are the Davydov splitting and the direct coupling between singlets and the doubly-excited state [18]. When these are important, 2.1 is probably not a good model Hamiltonian. But when the direct coupling term between singlets and doubly-excited states is dominant, the theory may also be much simpler because the system essentially becomes a two-level system, for which any number of sophisticated theories are applicable. Detailed calculations [54] show that only three

Figure 2.2: Energy level diagrams for electron-electron interactions in 2.1. Each panel represents an electronic state of a chromophore. When two electrons are in the same molecular orbital, they experience an "onsite" Coulomb repulsion U, while two electrons on the same chromophore but in different orbitals experience an "offsite" Coulomb repulsion $\mathcal{V}$. The HOMO-LUMO gap is Δ, and the exchange energy is X. The coupling, J, allows electrons to move between chromophores in one-electron steps, or hops.

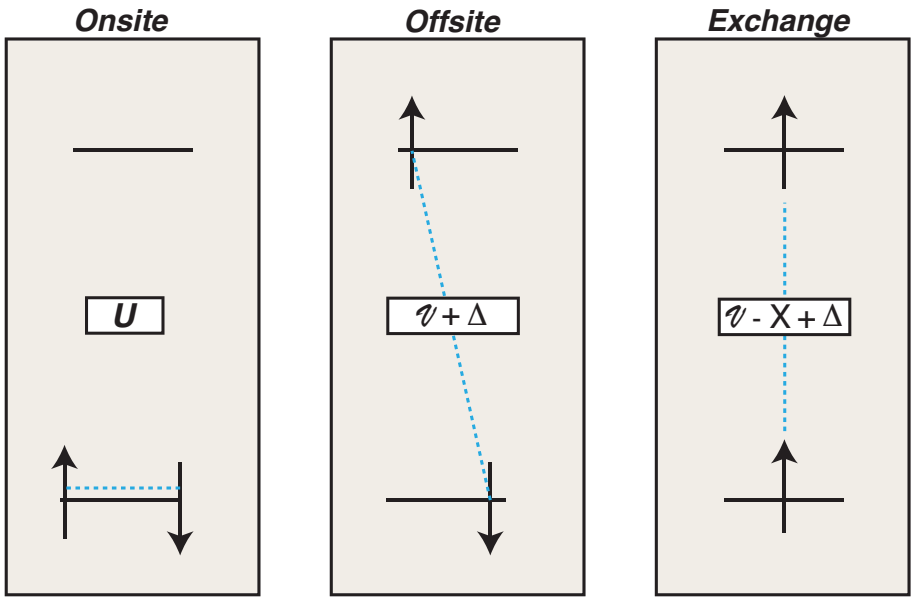

classes of states are close to the energy of the singlet monomer with the total spin angular momentum projection, $\mathcal{S}_z = 0$, diagrammed in 2.2: the singly excited singlets, charge transfer states with three electrons on one chromophore, and doubly-excited states. Guided by the results for a number of organic chromophores that exhibit singlet fission, we ignore spin-orbit coupling [18, 54]. In the absence of spin-orbit coupling, the total electron spin operators $\mathcal{S}^2$ and $\mathcal{S}_z$ both commute with the Hamiltonian and are conserved. As a result of the conservation law, the states must then satisfy selection rules, which in the space of singlet excited states, means that the total electron multiplicity must always remain a singlet[18]. This also implies that $\mathcal{S}_z \mid \Phi \rangle = 0$ for any state $\mid \Phi \rangle$ in the singlet manifold. The spin-adapted linear combinations (SALC) are unitary transforms of the singlet, charge transfer, and doubly-excited electronic configurations that are simultaneous eigenstates of $\mathcal{S}^2$ and $\mathcal{S}_z$ with eigenvalue 0. Note that the $\mid TT \rangle$ is not a two-triplet state, but is a SALC that contains doubly-excited singlet character. There are only six SALC that we consider. They are the ground state, $\mid 0 \rangle$, the singlet state localized on the left chromophore, $\mid S \rangle$, the singlet state localized on the right chromophore, $\mid \overline{S} \rangle$, the charge transfer states localized on the left, $\mid CT \rangle$, and right, $\mid \overline{CT} \rangle$, and the doubly-excited state, $\mid TT \rangle$. This choice is not unique. Indeed, one could, for example, seek linear combinations that are delocalized across each chromophore. We choose these states rather than other linear combinations because they are consistent with weak coupling between chromophores. This choice will be important in 2.4 where we couple the electronic system to a polar solvent bath. Setting the energy of the ground state to zero, and using Δ to denote the HOMO-LUMO gap, the electronic Hamiltonian in the SALC basis is diagonal with energies $E_S = E_{\overline{S}} = \Delta + \mathcal{V} - U$, $E_{CT} = E_{\overline{CT}} = \Delta + 2\mathcal{V} - U - X$, and $E_{TT} = 2(\Delta + \mathcal{V} - U) - 4/3X$. Note that the energy of the $\mid TT \rangle$ state is higher than the energy of the isolated triplet states by 2/3 the exchange energy, $\frac{2X}{3}$. Had we not insisted on total spin angular momentum conservation, we would predict a lower threshold for singlet fission.

Figure 2.3: Spin-adapted linear combinations in the total singlet manifold. Red and blue levels belong to left and right chromophores, respectively. The levels are physically-motivated, mutually orthogonal molecular orbitals, for which the matrix elements in 2.1 are evaluated. Only five singly and doubly-excited states in this system will be simultaneous eigenstates of the total electron spin operators $\mathcal{S}^2$ and $\mathcal{S}_z$ with eigenvalue zero. We denote the many-body electronic states in the number occupation basis as $\mid h_L, l_L; h_R, l_R \rangle$, where, for example, h_L is the HOMO on the left chromophore and l_R is the LUMO on the right chromophore. As an example, the singlet excited state localized on the left chromophore in the number occupation basis is $\mid \mathrm{S} \rangle = \frac{1}{\sqrt{2}} (\mid \downarrow, \uparrow; \uparrow\downarrow, 0 \rangle - \mid \uparrow, \downarrow; \uparrow\downarrow, 0 \rangle)$.

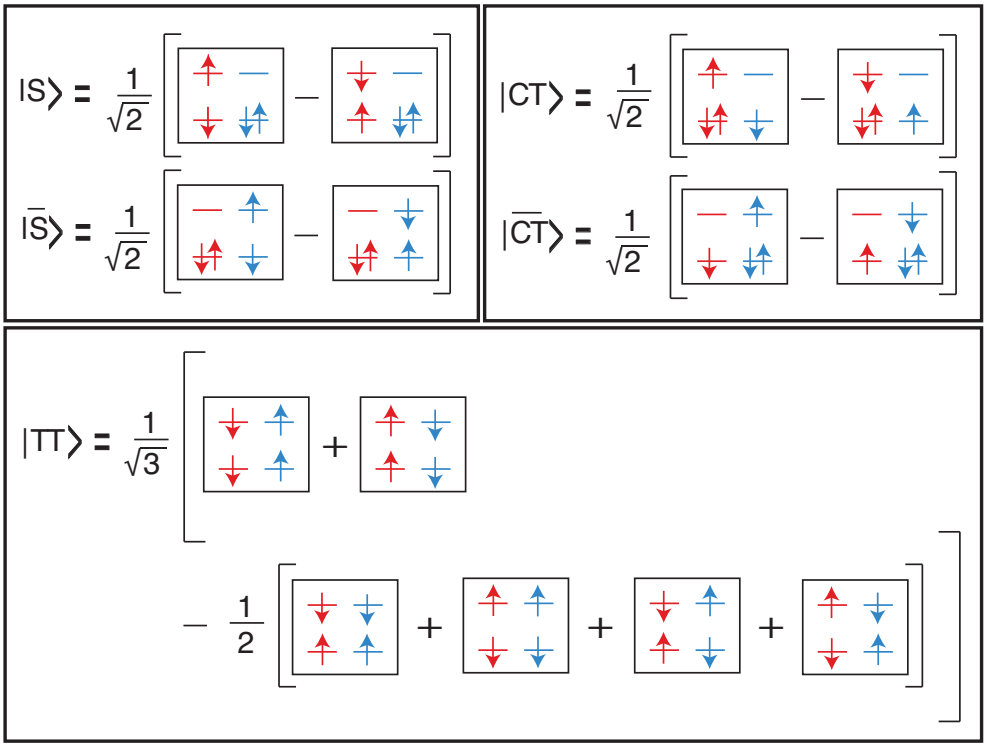

The nonzero off-diagonal matrix elements of W_{el} in the SALC basis are

$$\begin{aligned}
\langle\ S\ |W_{el}|\ CT\ \rangle &= -J_{h_R h_L}\ ,\ \langle\ \overline{S}\ |W_{el}|\ CT\ \rangle = J_{l_R l_L}\ , \\
\langle\ S\ |W_{el}|\ \overline{CT}\ \rangle &= J_{l_L l_R}\ ,\ \langle\ \overline{S}\ |W_{el}|\ \overline{CT}\ \rangle = -J_{h_L h_R}\ , \\
\langle\ CT\ |W_{el}|\ TT\ \rangle &= -\sqrt{\frac{2}{3}} J_{h_L l_R}\ ,\ \langle\ \overline{CT}\ |W_{el}|\ TT\ \rangle = \sqrt{\frac{2}{3}} J_{h_R l_L}\ ,
\end{aligned}$$

with the remaining terms following from the Hermitian conjugate of W_{el}. The SALC, $|\ 0\ \rangle$, $|\ S\ \rangle$, $|\ \overline{S}\ \rangle$, $|\ CT\ \rangle$, $|\ \overline{CT}\ \rangle$, and $|\ TT\ \rangle$ are the diabatic states of the problem (2.3). When all resonance integrals J_{jk} are small and the initial excitation is localized, they are the physically relevant states of the system. This is the limit in which we present the current work. Because we have neglected three-center and higher integrals, singlets do not couple to $|\ TT\ \rangle$ states directly, but rather pass through intermediate charge transfer states via electron or hole transfer [18]. For example, electron transfer couples $|\ S\ \rangle$ to $|\ \overline{CT}\ \rangle$ and hole transfer couples $|\ S\ \rangle$ to $|\ CT\ \rangle$.

2.3.2 Hamiltonian of the Dissipative System

Having specified the electronic states that couple to one another and satisfy spin selection rules, we now derive the equations of motion of the populations of the diabatic states. Experience from small polaron transport [76], electron and energy transfer [77, 78, 79, 80, 7, 8], and spectroscopy shows that one can model the effects of the environment with the Hamiltonian,

$$H = \sum_k |\ k\ \rangle H_k \langle\ k\ | + \epsilon \sum_{k,l \neq k} |\ k\ \rangle J \langle\ l\ |\ . \tag{2.3}$$

2.3 is a generic linear response Hamiltonian. The sum is over diabatic states, $|\ k\ \rangle$, J is a constant in the Condon approximation and ϵ is a parameter whose numerical value is 1, but will order a perturbation expansion for weak coupling. Though evidently nonessential, for simplicity we assume that all couplings between diabatic states are equal, which sets all off-diagonal matrix elements of $W_{el} = J$. Assuming that the environment responds linearly when the system enters diabatic state $|\ k\ \rangle$, H_k can be modeled as a set of quantum-mechanical displaced harmonic oscillators,

$$H_k = E_k + \frac{1}{2} \sum_\nu \omega_\nu \left(p_\nu^2 + (q_\nu + \chi_\nu^k)^2 \right)\ . \tag{2.4}$$

E_k is the bare energy of diabatic state $\mid k \rangle$ (e.g. E_S, E_{CT}, E_{TT}, etc.). The equilibrium position of bath mode ν occurs at -χ_ν^k when the electronic system is in state $\mid k \rangle$. Setting $E_0 = \chi_\nu^0 = 0$ uses the ground state as a reference, so that all energy levels and fluctuations are now with respect to the ground state, $\mid 0 \rangle$. The sum is over all bath modes ν, each with frequency ω_ν, that represent the polarization fluctuations of the solvent. p_ν and q_ν are mass-weighted bath momenta and coordinates, respectively. The spectra of coupling constants between system and bath, or spectral densities,

$$\mathcal{J}_k(\omega) = \frac{\pi}{2} \sum_\nu (\omega_\nu \ \chi_\nu^k)^2 \ \delta(\omega - \omega_\nu) \ ,$$

completely specifies the behavior of the system. While in this work, we specialize the environment to include only solvent polarization fluctuations, it is straightforward to include molecular vibrations and phonons [80] in 2.4.

2.3.3 Equation of Motion for the Populations of the Diabatic States

In Hilbert space, the density matrix obeys the Heisenberg equation of motion, where the Hamiltonian acts on both the right and left of the density matrix. It is convenient to work in Liouville space where one orders the density matrix elements into a vector, $\rho \rightarrow \mid \rho \rangle\rangle$ [81]. The equation of motion can now be written in the form, $\frac{d\mid \rho \rangle\rangle}{dt} = -i\mathscr{L} \mid \rho \rangle\rangle$, and the Liouvillian $\mathscr{L}$ acts only on the left side of the density matrix. In Liouville space inner products are defined as $\langle\langle \ A \mid B \ \rangle\rangle = Tr_S Tr_B \left(A^\dagger B\right)$. Tr_S is a trace over the diabatic states and Tr_B is a trace over the bath states. Choosing $H_0 = \sum_k \mid k \rangle H_k \langle \ k \mid$, $\hbar = 1$, and $V = \sum_{k,l \neq k} \mid k \rangle J \langle \ l \mid$, the full density matrix, $\mid \rho(t) \rangle\rangle$ obeys the quantum Liouville equation in the interaction picture,

$$\frac{d}{dt} \mid \hat{\rho}(t) \rangle\rangle \quad = \quad -i\epsilon \hat{\mathscr{L}}_V(t) \mid \hat{\rho}(t) \rangle\rangle \ ,$$

where $\hat{\mathscr{L}}_V(t) = e^{i\mathscr{L}_0 t} \mathscr{L}_V e^{-i\mathscr{L}_0 t}$ and $\mid \hat{\rho}(t) \rangle\rangle = e^{i\mathscr{L}_0 t} \mid \rho(t) \rangle\rangle$. One can go between the two spaces by using dual relationships between Hilbert and Liouville space in the interaction picture, such as $\hat{\mathscr{L}}_V(t) A \leftrightarrow \left[\hat{V}(t), A\right]$, $\mathscr{L}_0 A \leftrightarrow \left[H_0, A\right]$.

The electronic population is the reduced density matrix element at time t. For state $\mid k \rangle$ it

is $\sigma_k(t) = \langle\langle\ k\ |\ \rho(t)\ \rangle\rangle = Tr_B\big[\langle\ k\ |\rho(t)|\ k\ \rangle\big]$. Motivated by the work of Reichman and Golosov, we isolate the populations of the diabatic states using the projection operator $P = \sum_k\ |\ k\rho_k\ \rangle\rangle\langle\langle\ k\ |$ where ρ_k is an arbitrary, normalized, nuclear density matrix [11, 81]. With the aid of the projection operator, one arrives at the formally exact (time-local) equation of motion for the populations. The equation of motion takes the form of a nonMarkovian quantum master equation [82],

$$\frac{d}{dt}\hat{\sigma}_j(t) = -\sum_k R_{j,k}(t)\hat{\sigma}_k(t) + I_j(t)\ . \tag{2.5}$$

$R_{j,k}(t)$ is an element of the relaxation matrix and $I_j(t)$ is the quantum inhomogeneous term that depends on the initial value of the density matrix in the complementary space, $(1-P)|\ \hat{\rho}(0)\ \rangle\rangle$. This term is often either zero, or it decays quickly [83]. The derivation of 2.5, including the forms of the relaxation operator and inhomogeneous term, are in the Appendix. Because 2.5 is exact, it is a convenient starting point for analysis of the electronic population dynamics. Methods for analyzing it include explicit quantum simulation via path integral and semiclassical methods [84, 85, 86], perturbation expansions [82, 12], and asymptotic approximations [11, 81].

We expand the relaxation operator to second order in perturbation theory with respect to ϵ to find the approximate quantum master equation in the weak-coupling limit. Assuming that the initial state is a product state so that $(1-P)|\ \hat{\rho}(0)\ \rangle\rangle = 0$, the inhomogeneous term disappears entirely. This assumption simplifies analysis considerably, but will be re-assessed when more details about the initial conditions from experiments become available. In singlet fission, systems are necessarily multilevel, and electronic states in these systems can undergo rapid internal conversion. The initial conditions are likely to be subtle and highly system-dependent.

Expanding 2.5 to second order in ϵ, inserting complete sets of diabatic states, and coming out of the interaction picture yields tractable expressions for the populations [82, 87],

$$\frac{d}{dt}\sigma_j(t) = \sum_k\ \big[W_{k\to j}(t)\sigma_k(t) - W_{j\to k}(t)\sigma_j(t)\big] + \mathscr{O}(\epsilon^3)\ . \tag{2.6}$$

$W_{j\to k}(t)$ is a time-dependent rate,

$$W_{j\to k}(t) = 2J^2\int_0^t d\tau \mathrm{Re}\left[Tr_B\left\{e^{-iH_k\tau}e^{iH_j\tau}\rho_j(t)\right\}\right]\ . \tag{2.7}$$

2.7 is the nonMarkovian generalization of Fermi's golden rule to a multilevel dissipative system. When t is long relative to the energy equilibration time in state $\mid k \rangle$, one can make the ergodic hypothesis, $\rho_j(t) \approx \rho_j^{(eq)}$, where $\rho_j^{(eq)} = \exp(-\beta H_j)/Z_j$, and $Z_j = Tr_B\left[\exp(-\beta H_j)\right]$. Extending the integral to infinity is equivalent to making the Markov approximation and results in Fermi's golden rule,

$$W_{j\to k} = J^2 \int_{-\infty}^{\infty} d\tau \, \langle \exp(-iH_k\tau)\exp(iH_j\tau)\rangle_j \ , \tag{2.8}$$

where $\langle\cdot\rangle_j$ is an equilibrium ensemble average with respect to state $\mid j \rangle$, $\langle A\rangle_j = Tr_B(A\rho_j^{(eq)})$. The nonMarkovian effects appear as transients, manifest at early times, but converge to the (time-independent) golden rule rates at long times. An example illustrating this convergence appears in 2.4. The prefactor J^2 controls the distance dependence of the rates. Because it is a resonance integral, rates should have an approximately exponential dependence on the distance between the chromophores.

2.3.4 Rate Theories

Assuming that each diabatic state is statistically independent [12] implies that the coupling matrix elements in 2.4 obey $\chi_\nu^k \, \chi_\mu^l = 0$ for $k \neq l$. After performing a cumulant expansion of 2.8, taking the trace over the bath, and using Parseval's theorem, 2.8 becomes the multilevel generalization of Förster/Dexter theory applied to singlet fission,

$$W_{j\to k} = \frac{J^2}{2\pi} \int_{-\infty}^{\infty} d\omega \ A_k(\omega) I_j(\omega) \ .$$

$A_k(\omega)$ and $I_j(\omega)$ are envelope functions related to the strength of solvent-induced fluctuations about diabatic states $\mid k \rangle$ and $\mid j \rangle$. If both states are bright, the envelope functions can be cast in terms of the absorption spectrum of state $\mid k \rangle$ and the emission spectrum of state $\mid j \rangle$. The envelope functions can be written as

$$\begin{aligned} I_j(\omega) &= \int_{-\infty}^{\infty} dt \exp(i\omega t) \exp\left[-i\left(E_j - \lambda_j\right)t - g_j^*(t)\right] , \\ A_k(\omega) &= \int_{-\infty}^{\infty} dt \exp(i\omega t) \exp\left[-i\left(E_k + \lambda_k\right)t - g_k(t)\right] \ . \end{aligned} \tag{2.9}$$

$\lambda_j = \frac{1}{2}\sum_\nu \omega_\nu (\chi_\nu^j)^2$ is the reversible work done by the solvent to equilibrate state $\mid j \rangle$ from the ground state and $g_j(t)$ is a lineshape function for the energy level fluctuations in state $\mid j \rangle$. It can be related to the spectral density, $\mathcal{J}_j(\omega)$,

$$g_j(t) = \frac{1}{\pi}\int_0^\infty d\omega \, \frac{\mathcal{J}_j(\omega)}{\omega^2}\left[\coth(\beta\omega/2)(1-\cos(\omega t)) - i\left(\omega t - \sin(\omega t)\right)\right] \ . \tag{2.10}$$

Dipole selection rules forbid emission or absorption to any state other than $\mid S \rangle$ and $\mid \overline{S} \rangle$, so envelope functions and associated spectral densities cannot be inferred from linear emission and absorption spectra as they can be in Förster theory. They must be fit from experimental data, computed from molecular dynamics trajectories, or calculated with a given model for the spectral densities. In this chapter we use model spectral densities.

2.4 Results and Discussion

Golden rule rates depend on the spectral densities associated with their energy level fluctuations with respect to the ground state for each level. For simplicity, we assume that fluctuations in all levels are identical. For a model spectral density, we take

$$\mathcal{J}(\omega) = 2\gamma\frac{\omega\Gamma}{\omega^2+\Gamma^2} \ , \tag{2.11}$$

which is a model spectral density applied broadly to electronic spectroscopy in polar solvents. γ is an energy scale that controls the coupling strength between the electronic states and the bath. In the high temperature limit the time correlation function for energy level fluctuations decays exponentially with a time constant of $1/\Gamma$ [88]. When the timescale of energy level fluctuations is slow with respect to $1/\gamma$, each chromophore is in a static environment and the lineshape function is quadratic in time,

$$g^{\text{Slow}}(t) = k_B T\gamma t^2 \ . \tag{2.12}$$

The golden rule rate from $\mid j \rangle$ to $\mid k \rangle$ is the overlap of two Gaussians, evaluated by integrating 2.9 using the lineshape functions in 2.12,

$$W_{j\to k}^{\text{Slow}} = J^2\sqrt{\frac{\pi}{2k_BT\gamma}}\exp\left[-\frac{(E_k - E_j + 2\gamma)^2}{8k_BT\gamma}\right] \ . \tag{2.13}$$

If one identifies the solvent reorganization energy with 2γ, 2.13 has precisely the same form as the nonadiabatic Marcus electron transfer rate. The static limit implies inhomogeneously broadened fluctuation spectra. In the inhomogeneous limit, the envelope functions are probability distributions of a state having a given energy in the ensemble [82]. What 2.13 says is that only a subset of chromophores in the ensemble have the same energy in state $\mid k \rangle$ and $\mid j \rangle$, and only they can conserve energy. Because 2.13 is essentially a weak-coupling high temperature approximation to the rate, it is not surprising that the result is reminiscent of the Marcus theory. The role of fluctuations is evident from 2.13. The rate is not maximal when the bare energies E_k and E_j are equivalent, but instead when their energy difference matches the strength of environmental fluctuations, 2γ.

Outside the slow modulation and high temperature limits, we evaluate the lineshape functions $g_j(t)$ and $g_k(t)$ by expressing the hyperbolic cotangent function in 2.10 as a sum over Matsubara frequencies and performing contour integrals [89, 90, 6]. 2.4 shows the results as a function of the coupling strength, γ for off-resonant bare energies, $E_k - E_j$ = -0.1 eV at T = 300 K, and $1/\Gamma$ = 100 fs. When the energies are off-resonant, fluctuations increase the rate of transfer from $\mid j \rangle$ to $\mid k \rangle$, up to a point. Above a critical threshold, the rate decreases with increasing γ. If the coupling strength to fluctuations far exceeds $\mid J \mid$, fluctuations stabilize the diabatic states too much and thermal activation is increasingly difficult. The system becomes self-trapped [6]. This behavior is qualitatively similar to that predicted by 2.13 in the high-temperature static limit. 2.5 shows the results for the time-dependent rate of going from state $\mid j \rangle$ to state $\mid k \rangle$ as a function of time for physically reasonable values of the model parameters: $1/\Gamma$ = 100 fs, T = 300 K, γ = 0.1 eV and $E_k - E_j$ = -0.05 eV. We assume that the system has entered electronic $\mid j \rangle$ on a timescale much faster than the solvent or nuclei can equilibrate to that state. This can happen, for example, in a rapid interconversion process from an excited state above S_1 that was prepared with an ultrafast laser pulse. The time-dependent nuclear density matrix in 2.7 is then $\exp(-iH_j t)\rho_g \exp(iH_j t)$, where ρ_g is the nuclear density operator for the ground state. We have evaluated this rate by making a polaron transformation, cumulant expansion and trace over the bath, and a stationary phase approximation to the integral over τ in 2.7 using the spectral density in 2.11. It is convenient

Figure 2.4: The golden rule rate from state $\mid j \rangle$ to $\mid k \rangle$ as a function of the system-bath coupling energy γ. $E_k - E_j$ = -0.1 eV at T = 300 K, and $1/\Gamma$ = 100 fs (See text). The energy levels are off resonance and fluctuations enhance the rate of transfer until the system enters the self-trapping regime [6].

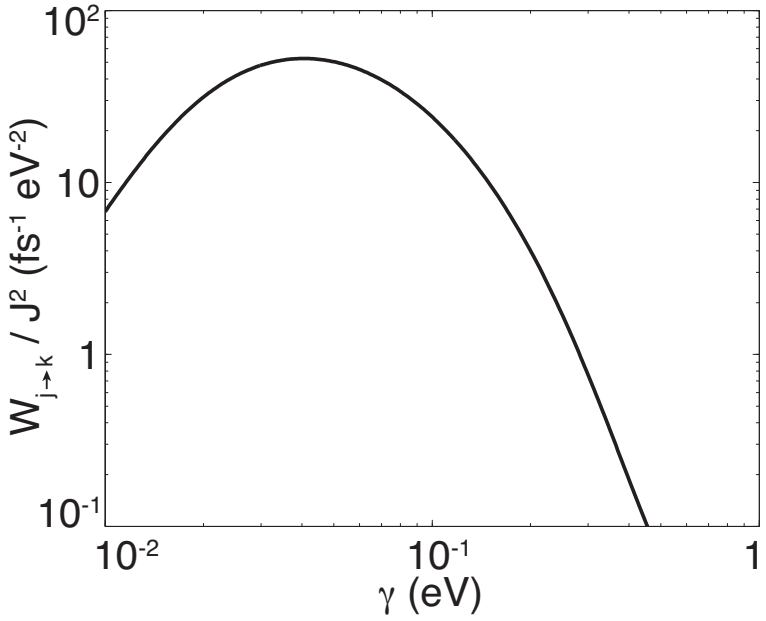

to use the approximation, $\cot(x) \approx 1+\exp(-x)/x$, which is good in the temperature range in which we study. Details of this procedure can be found in Refs. [83, 12]. In the parameter range studied, the approximation to the time-dependent rate,

$$W_{j\to k}(t) \approx J^2\sqrt{\frac{2\pi}{D(\beta)}}\exp\left[-\frac{(E_k - E_j - 2\gamma + 2C(t))^2}{2D(\beta)}\right] , \tag{2.14}$$

where $C(t) = \gamma\exp(-\Gamma t)$ is the time-dependent reorganization energy, $\beta = 1/(k_B T)$, and $D(\beta) = \frac{2}{\pi}\int_0^\infty d\omega \mathcal{J}(\omega)\left[1 + \frac{2}{\beta\omega}\exp(-\beta\omega/2)\right]$, is rather accurate. This approximation makes the role of non-Markovian effects physically transparent, and accompanies the stationary-phase result in 2.5. While the specific values for the model parameters studied here are not yet known for singlet fission experiments, the parameters used in 2.5 are realistic for solvation dynamics in polar solvents [72]. The fact that the time-dependent rate only converges to the golden rule rate for t greater than about 600 femtoseconds should give one pause. Because singlet fission has been reported to occur on sub-picosecond timescales, these results indicate that electronic dynamics in singlet fission may fall outside the scope of a rate theory based on the golden rule even in the weak-coupling limit, and that a proper description in systems that interconvert on sub-picosecond timescales should include real-time quantum dynamics. Finally, we comment on the multistate character of the theory, and model the polarization fluctuations from microscopic considerations. 2.6 is a coarse-grained view, from the solvent's perspective, of the diabatic states in the problem. The singlet states experience a solvochromatic shift relative to the ground state, provided that the electron distribution is different in the excited state than in the ground state. This shift is a solvent response to an **intramolecular** dipole moment that occurs when the chromophore enters the electronically excited state. An **intermolecular**, or more precisely interchromophoric, dipole moment relative to the ground state characterizes the charge transfer states. These states experience an outer sphere reorganization energy from the solvent in the Marcus sense. If only singlets and charge transfer states were involved, one could simply apply the theories of photoinduced electron transfer. But the charge transfer states are intermediates between the singlets and the $\mid TT \rangle$ state. Relative to the charge transfer states, the solvent must relax an intermolecular dipole moment **and** accommodate

Figure 2.5: The nonMarkovian rate and golden rule rate from state $\mid j \rangle$ to $\mid k \rangle$ as a function of time. $E_k - E_j$ = -0.05 eV at T = 300 K, $1/\Gamma$ = 100 fs and γ = 0.1 eV (See text). The stationary phase approximation (SPA) to the nonMarkovian rate shows good agreement with the approximate form in 2.14. The nonMarkovian rate converges to the golden rule rate, but only for times greater than about 600 fs.

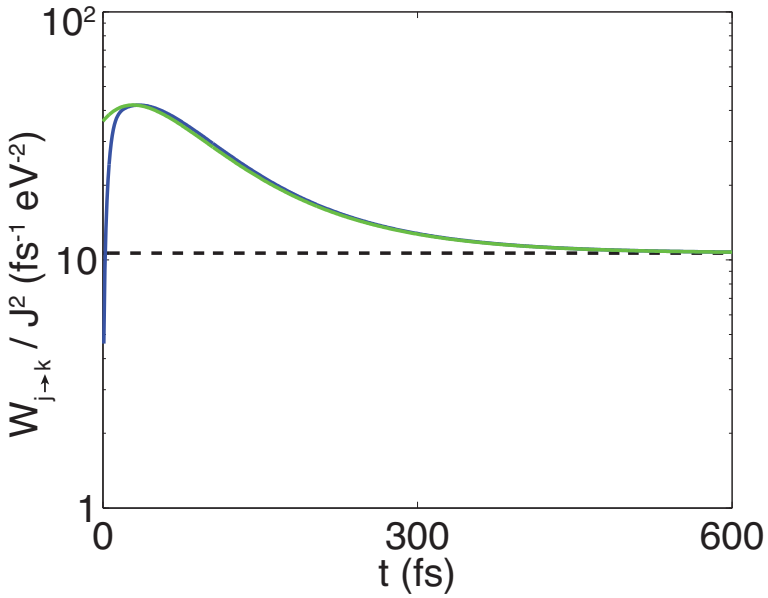

Figure 2.6: Schematic of the charge distribution on each chromophore in the $\mid S \rangle$, $\mid \overline{CT} \rangle$, and $\mid TT \rangle$ states. Blue and red colors denote charge differences relative to the ground state. The SALC states are linear combinations of states of the same polarization, only with different spin configurations. The solvent responds to the charge, not the spin. If the system starts with the solvent equilibrated in the $\mid S \rangle$ state, an electron transfer event brings the $\mid S \rangle$ state to $\mid \overline{CT} \rangle$, while **both** an electron transfer and an intramolecular charge redistribution must occur in the $\mid TT \rangle$ state when coming from the $\mid \overline{CT} \rangle$ state. The model system-bath Hamiltonian in 2.15 takes these considerations into account.

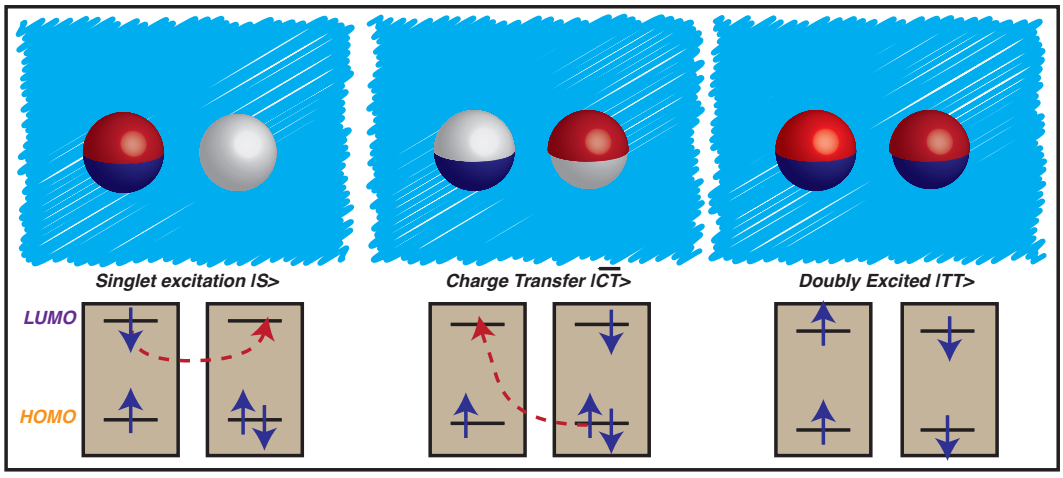

Figure 2.7: (**A**) The "mediated" two electron process as a function of energy level stagger for E_S and E_{TT} fixed with $E_{\overline{CT}}$ varying. The orange rectangle signifies the region where $E_{\overline{CT}} > E_S$, the green rectangle denotes the region where $E_{\overline{CT}} < E_{TT}$, and the blue region is where $E_S > E_{\overline{CT}} > E_{TT}$. Schematic configurations in the top right panel illustrate one-electron electron transfer events. (**B**) Marcus rates in the high temperature limit for $T = 300K$, $\Lambda = \lambda = 0.1$ eV, $E_{TT} = -0.1eV$. The extra reorganization energy for the $\mid \overline{CT} \rangle \rightarrow \mid TT \rangle$ increases the width of the $W_{\overline{CT}\rightarrow TT}$ rate relative to that of the $W_{S\rightarrow\overline{CT}}$ rate. Forward rates are solid lines and back transfer rates are dashed. The dotted vertical light blue lines represent the "window of opportunity" for singlet fission, where $E_S > E_{\overline{CT}} > E_{TT}$, and terminate on the black dots where forward and back transfer rates are equivalent. In the window of opportunity, all forward transfer rates are larger than the back transfer rates.

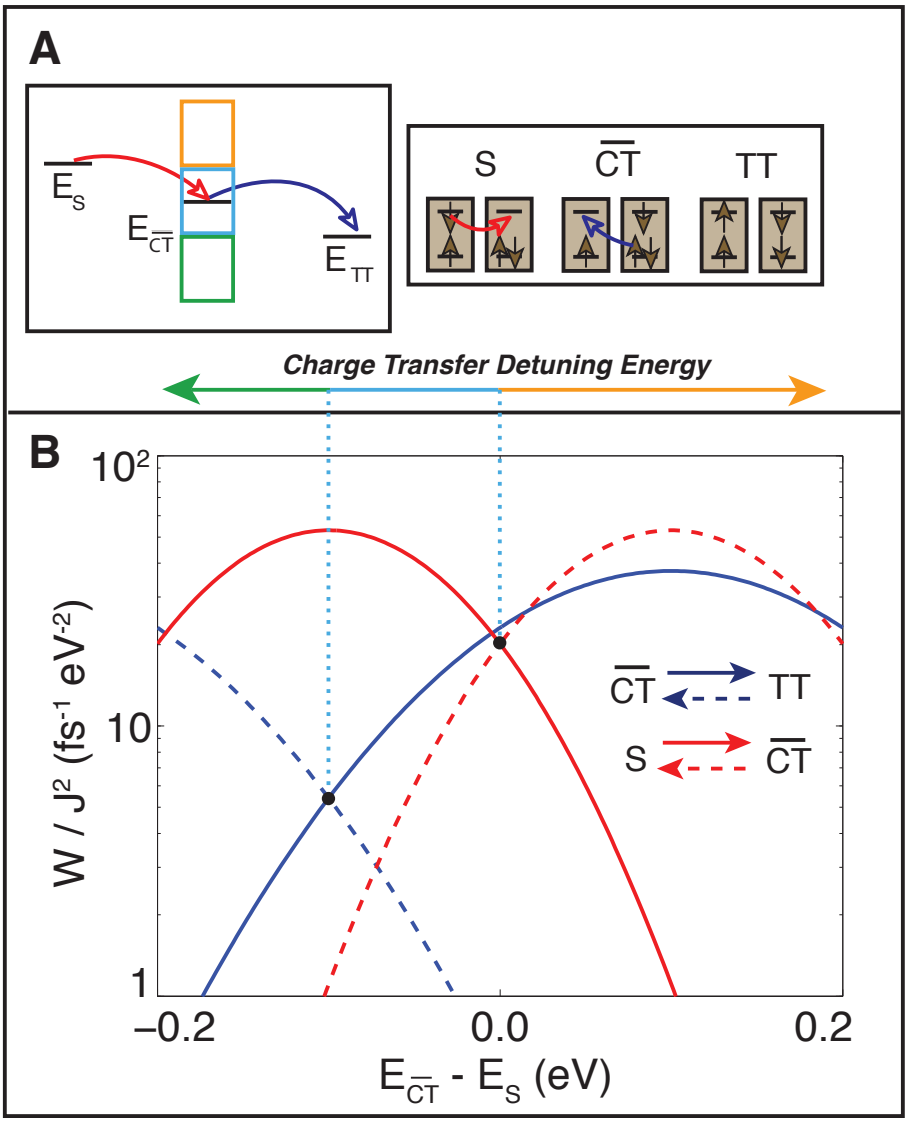

an additional electronic excitation in the $\mid TT \rangle$ state. To model these phenomena, we assume that the system begins in state $\mid S \rangle$, and the solvent has equilibrated to that electronic charge distribution. To make progress in this direction, we rewrite H_0 in the canonical "system plus bath" form, $H_0 = H_S + H_{SB} + H_B$. H_0 is still diagonal in the diabatic basis but we propose that H_{SB} should be

$$H_{SB} = (n_R - n_L) \sum_\nu \omega_\nu \Lambda_\nu q_\nu + (n^* - 1) \sum_\nu \omega_\nu \lambda_\nu q_\nu \ . \tag{2.15}$$

$n_R - n_L$ is the total number of electrons on the right chromophore minus the number of electrons on the left chromophore, while n^* is the number of electrons in the LUMO orbitals. The form of 2.15 ensures that the bath responds **linearly** to the change in the dipole moments relative to state $\mid S \rangle$. For simplicity, we assume that intermolecular and intramolecular polarization fluctuations are uncorrelated by imposing $\lambda_\nu \Lambda_\nu = 0$. In the high-temperature limit, the transfer rates between $\mid S \rangle$ and $\mid \overline{CT} \rangle$, and from $\mid \overline{CT} \rangle$ to $\mid TT \rangle$ assume the form of a Marcus rate,

$$W_{S \to \overline{CT}} = J^2 \sqrt{\frac{\pi\beta}{\Lambda}} \exp\left[-\frac{\beta}{4\Lambda} \left(E_{\overline{CT}} - E_S + \Lambda \right)^2 \right] , \tag{2.16}$$

$$W_{\overline{CT} \to TT} = J^2 \sqrt{\frac{\pi\beta}{\lambda + \Lambda}} \exp\left[-\frac{\beta}{4(\lambda + \Lambda)} \left(E_{TT} - E_{\overline{CT}} + \lambda + \Lambda \right)^2 \right] .$$

$\Lambda = \frac{1}{2} \sum_\nu \omega_\nu \Lambda_\nu^2$ is the reorganization energy associated with interchromophoric electron transfer and $\lambda = \frac{1}{2} \sum_\nu \omega_\nu \lambda_\nu^2$ is the reorganization energy for intramolecular charge redistribution in the excited state. It is related to the Stokes shift. Because the solvent must do more work to accommodate the charge distribution in the $\mid TT \rangle$ state, the rates in 2.16 indicate that the inverted regime occurs at higher energies for the $W_{\overline{CT} \to TT}$ than for $W_{S \to \overline{CT}}$. 2.7 (B) is a plot for the forward transfer rates, $W_{S \to \overline{CT}}$ and $W_{\overline{CT} \to TT}$ compared to the back transfer rates $W_{\overline{CT} \to S}$ and $W_{TT \to \overline{CT}}$ for the energy level stagger between $\mid S \rangle$ and $\mid TT \rangle$ fixed as a function of the energy for the charge transfer intermediate $\mid \overline{CT} \rangle$. The specific parameters appear in the figure caption. 2.7 indicates a region where $E_S > E_{\overline{CT}} > E_{TT}$ (between the dotted blue lines), where the forward rates exceed the back transfer rates. The weak-coupling, high-temperature result predicts the non-Arrhenius behavior characteristic of Marcus electron transfer. While this is not particularly surprising, 2.4

illustrates the interplay between energy level spacings and solvent fluctuations as a design principle for maximizing singlet fission yields. Even if the bare energy levels are not resonant, environmental fluctuations make the rates nonzero.

We have presented a model for singlet fission in the presence of solvation-induced energy level fluctuations and analyzed it using model parameters for electronic energy levels, electronic-coupling, and spectral densities in the weak electronic-coupling limit. The model electronic Hamiltonian employed allowed us to identify selection rules and approximate energies of electronic configurations. Enforcing total angular momentum spin conservation predicts that degeneracy between the singly excited singlet states and the doubly-excited $\mid TT \rangle$ state should occur at a slightly higher energy than that of the isolated triplets. This is because one needs to include the doubly-excited spin singlets to satisfy total spin angular momentum conservation. This is vaguely reminiscent of theories of MEG in nanocrystals and carbon nanotubes, where selection rules delay the onset of MEG, although the matrix elements evaluated there are different. It would be interesting to check this prediction against more detailed electronic structure calculations. Though we did not follow this route for reasons of consistency, if the $\mid S \rangle$ and $\mid TT \rangle$ states are directly coupled, as some have suggested for molecules like pentacene [18], it is simple to redefine the diabatic states and extend the results of 2.3.3 to describe this case. Using a reasonable initial density matrix and model parameters for energy level splittings and solvent reorganization energies, we find that the nonMarkovian aspects of electron dynamics in singlet fission may be significant on sub-picosecond timescales. One should apply the golden rule with caution when dynamics occur on timescales of less than a picosecond, even in the limit of weak coupling. Finally, while we have assumed the weak electronic-coupling limit in this work, this assumption is probably marginal in some cases. Recent work has found coupling matrix elements that range between 0.02 to 0.1 eV. If the reorganization energy is not larger than this energy scale, the weak electronic-coupling limit is not valid. If the electronic-coupling matrix elements are larger than the reorganization energies, then one should analyze the density matrix dynamics with Redfield theory or one of its variants [88, 91]. If the reorganization energies and electronic-coupling matrix elements are of the same size, which may

be the case in some systems, perturbative approaches are not trustworthy [92]. While there is still much theoretical and experimental work that needs to be done to understand what controls electronic energy levels and coupling, we hope the current work will help empower the sophisticated tools of condensed phase chemical physics: nonlinear spectroscopy, molecular dynamics simulations, and quantum dynamical theory, to build a comprehensive picture of singlet fission.

2.5 Appendix 2A - Quantum Master Equations

We can solve the Liouville equation in the complementary space by defining $Q = 1 - P$ and solving for $Q|\ \hat{\rho}(t)\ \rangle\rangle$, which is given by

$$Q|\ \hat{\rho}(t)\ \rangle\rangle = \mathscr{G}_Q^+(t,0)Q|\ \hat{\rho}(0)\ \rangle\rangle - i\epsilon \int_0^t d\tau \mathscr{G}_Q^+(t,\tau)Q\hat{\mathscr{L}}_V(\tau)P|\ \hat{\rho}(\tau)\ \rangle\rangle$$

using the time evolution operators

$$g_-(t,\tau) = \hat{T}_- \exp\left[i\epsilon \int_\tau^t ds\hat{\mathscr{L}}_V(s)\right]$$
$$\mathscr{G}_Q^+(t,\tau) = \hat{T}_+ \exp\left[-i\epsilon Q \int_\tau^t ds\hat{\mathscr{L}}_V(s)\right]$$

where $\hat{T}_+$ and $\hat{T}_-$ denote forward and backward time evolution, respectively. This solution can be recast as

$$Q|\ \hat{\rho}(t)\ \rangle\rangle = \left[1 - \Sigma(t)\right]^{-1}\left[\mathscr{G}_Q^+(t,0)Q|\ \hat{\rho}(0)\ \rangle\rangle + \Sigma(t)P|\ \hat{\rho(t)}\ \rangle\rangle\right]\ , \tag{2.17}$$

where the $\Sigma(t)$ operator is given by [82]

$$\Sigma(t) = -i\epsilon \int_0^t d\tau \mathscr{G}_Q^+(t,\tau)Q\hat{\mathscr{L}}_V(\tau)Pg_-(t,\tau)\ .$$

When 2.17 is introduced into our reduced space we get the exact solution

$$\frac{d}{dt}P|\ \hat{\rho}(t)\ \rangle\rangle = -i\epsilon P\hat{\mathscr{L}}_V(t)P|\ \hat{\rho}(t)\ \rangle\rangle - i\epsilon P\hat{\mathscr{L}}_V(t)\left[1 - \Sigma(t)\right]^{-1}\left[\mathscr{G}_Q^+(t,0)Q|\ \hat{\rho}(0)\ \rangle\rangle + \Sigma(t)P|\ \hat{\rho}(t)\ \rangle\rangle\right]\ . \tag{2.18}$$

Operating from the left with $\langle\langle\ j\ |$ on 2.18 we get

$$\frac{d}{dt}\hat{\sigma}_j(t) = -\sum_k R_{j,k}(t)\hat{\sigma}_k(t) + I_j(t) \tag{2.19}$$

where the relaxation matrix and inhomogeneous terms are

$$R_{j,k}(t) = i\epsilon\langle\langle\ j\ |\hat{\mathscr{L}}_V(t)\big[1-\Sigma(t)\big]^{-1}|\ k\rho_k\ \rangle\rangle$$
$$I_j(t) = -i\epsilon\langle\langle\ j\ |\hat{\mathscr{L}}_V(t)\big[1-\Sigma(t)\big]^{-1}\mathscr{G}_Q^+(t,0)Q|\ \hat{\rho}(0)\ \rangle\rangle\ .$$

Using the simplification that $P\hat{\mathscr{L}}_V P = 0$ we expand 2.19 to $\mathscr{O}(\epsilon^2)$ which leads to 2.6 and 2.7.

2.6 Appendix 2B - Biexciton Interactions and Spin Relaxation Measured using Magnetic Fields

The multiexciton singlet state, $|\ TT\ \rangle$, is a linear combination of Slater determinants with triplet character each weighted by Clebsch-Gordon coefficients. There are 2^2 one-triplet (two electron) Slater determinants and 4^2 two-triplet (four electron) Slater determinants: 2 singlets, 9 triplets, and 5 quintets. If the two triplets born out of singlet fission do not interact, there are 3^2 degenerate two-triplet states in the absence of an external magnetic field, 3 of which have singlet character. The zero-field states for each molecule of a dimer are $|\ x\ \rangle = \frac{1}{\sqrt{2}}\big(|\ \beta,\beta\ \rangle - |\ \alpha,\alpha\ \rangle\big)$, $|\ y\ \rangle = \frac{i}{\sqrt{2}}\big(|\ \beta,\beta\ \rangle + |\ \alpha,\alpha\ \rangle\big)$, and $|\ z\ \rangle = \frac{1}{\sqrt{2}}\big(|\ \alpha,\beta\ \rangle + |\ \beta,\alpha\ \rangle\big)$. The dimer Hilbert space for independent chromophores is then the direct product space:

$$\{\ |\ x\ \rangle,|\ y\ \rangle,|\ z\ \rangle\ \}\otimes\{\ |\ x\ \rangle,|\ y\ \rangle,|\ z\ \rangle\ \}\quad . \tag{2.20}$$

In a strong magnetic field, the monomer magnetic states are $|\ 0\ \rangle = |\ z\ \rangle$, $|\ +\ \rangle = |\ \alpha,\alpha\ \rangle$, and $|\ -\ \rangle = |\ \beta,\beta\ \rangle$, with the corresponding to the dimer product basis:

$$\{\ |\ 0\ \rangle,|\ +\ \rangle,|\ -\ \rangle\ \}\otimes\{\ |\ 0\ \rangle,|\ +\ \rangle,|\ -\ \rangle\ \}\quad . \tag{2.21}$$

When local spins are allowed to interact, the character of the $|\ TT\ \rangle$ state changes such that fluorescence decay changes in a strong magnetic field. Burdett *et al.*[93] and Piland *et al.*[94] have extended Johnson and Merrifield's theory,[28] including the dipole-dipole interactions between triplets that reduce the singlet character of two-triplet states in a high magnetic field, to polycrystalline films and amorphous solids. This is the most direct way to differentiate interacting triplet

pairs from independent triplets using magnetic fields. In Fig. 2.8 we illustrate the change in two-triplet character of the $\mid TT \rangle$ state when a magnetic field is applied.

Figure 2.8: The multiexciton singlet state in the absence of a magnetic field (a) and in the presence of a strong magnetic field (b), illustrated using uncertainty cones in the $\hat{x}\hat{y}$ plane. In a strong magnetic field, the number of nonzero Clebsch-Gordon coefficients is reduced from 3 to 2, with the $\mid T_+ \rangle = \frac{1}{\sqrt{2}}(\mid +,- \rangle + \mid -,+ \rangle)$ Slater determinant selected rather than the zero-field states, $\mid x,x \rangle$ and $\mid y,y \rangle$.

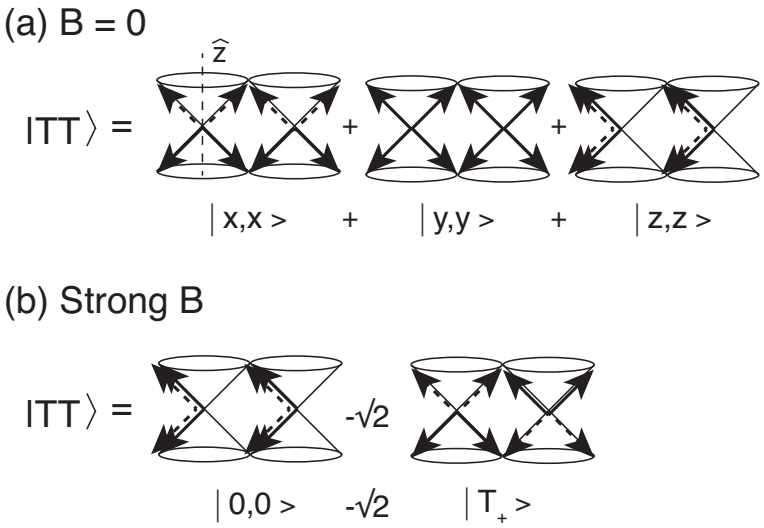

Spin-spin interactions break the degeneracy of $\mid +,- \rangle$ and $\mid -,+ \rangle$ in the strong-field representation of $\mid TT \rangle$, shown in Fig. 2.8, leading to changes in the prompt and delayed fluorescence.[93, 94] If fission is to enhance photocurrent in multijunction devices, the triplet excitons born out of singlet fission must be separated. This $\mid TT \rangle$ to $\mid T \rangle \otimes \mid T \rangle$ transition is spin-forbidden, occuring on nanosecond timescales over which the doubly excited state equilibrates across the 3^2 zero-field spin states.[93] Work is currently underway by Burdett, Bardeen, and coworkers to measure and better describe spin relaxation in singlet fission.

Chapter 3

Collective Aspects of Singlet Fission in Molecular Crystals

3.1 Abstract

We present a model to describe collective features of singlet fission in molecular crystals and analyze the model using many-body theory. The model we develop allows excitonic states to delocalize over several chromophores and is consistent with the character of the excited states in many molecular crystals, such as the acenes, where singlet fission occurs. As singlet states become more delocalized and triplet states more localized, the rate of singlet fission increases. We also determine whether or not the two triplets resulting from fission are correlated. Using the Bethe Ansatz and an entanglement measure for indistinguishable bipartite systems, we calculate the triplet-triplet entanglement as a function of the biexciton interaction strength. The biexciton interaction can produce bound biexciton states and provides a source of entanglement between the two triplets. Significant entanglement between the triplet pair occurs well below the threshold for bound pair formation. Our results paint a dynamical picture that helps explain why fission has been observed to be more efficient in molecular crystals than in their covalent dimer analogues, and have consequences for photovoltaic efficiency models that assume that the two triplets can be extracted independently.

3.2 Introduction.

Singlet fission (SF) is an internal conversion process that can take place in organic molecules and crystals where one photon produces two triplet excitons. While the observation of SF in

organic chromophores is decades old, Hanna and Nozik's proposal[14] that dye-sensitized solar cells incorporating SF chromophores can break the Shockley-Queisser limit[13] has reignited interest in the phenomenon of singlet fission.[95, 96, 97, 93, 98, 99, 48, 100, 101, 102, 94, 103, 47, 104, 105, 20, 21, 22, 23, 24, 25, 26, 106, 107, 108] While these photovoltaic applications are important, SF presents several fundamentally challenging problems in condensed phase chemical physics.

One might argue that we remain in the observational phase of fission research.[18, 19] There are a handful of chromophores that undergo SF, and the reasons that some do and others do not remain poorly understood.[18, 19, 20, 21, 22, 23, 24, 25, 26] Moreover, the guiding principles that are in place, like the energy matching condition, which says that fast fission can occur if it is exoergic or nearly isoergic, are mostly empirical and perhaps overly simplistic.[98, 99, 107, 108, 109] Indeed, recent experiments on tetracene call into question how general this requirement really is, particularly in crystals where the density of two-triplet states is large.[99, 101, 95, 97, 103] While the majority of SF systems investigated experimentally are condensed, often solid phases of molecular crystals, theory has primarily focused on SF in isolated dimers.[18, 19, 110, 111, 112, 26, 53, 105, 113, 114, 115, 116, 24, 107, 108, 117] While these studies are insightful, a complete and comprehensive theoretical picture of SF must describe fission in crystals, which are qualitatively different than dimers.

In the most conceptually simple picture of SF, one considers fission between a pair of chromophores.[18, 19, 106, 108] While tractable, this local viewpoint misses important details about the nature of the electronically excited states in crystals.[118, 119, 120, 121, 122, 107] Experiments[123, 124, 97, 125] and several calculations[126, 49, 127, 128, 108] provide evidence that the electronic wavefunction of the optically bright singlet in acene molecular crystals is delocalized across several chromophores. The triplet states, in contrast, localize to individual molecules.[18, 129, 117, 130, 122] If one thinks of a molecular crystal as a dense array of chromophores, the singlets can couple to one another through electronic dipole-dipole coupling, while the triplet states, which are dark, can not.[49, 117] This leads to a band-narrowing and localization effect for the triplets relative to the singlets, which has measurable consequences for singlet and triplet ex-

citon transport mechanisms in acene crystals.[49, 18] The first part of this manuscript addresses how differences between localization and delocalization can influence fission yields. SF can be a dominant decay pathway for singlet excited states in pentacene and tetracene molecular crystals, and in pentacene crystals, for example, some have reported near unit quantum yield.[131, 132, 133, 21] In covalent dimer analogues of tetracene and pentacene crystals, however, fission yields are typically an order of magnitude less efficient than their crystalline counterparts.[18, 19, 95, 108] One potential reason is that the electronic couplings in the dimer analogues simply aren't big enough to enable SF rates that out-compete other relaxation processes.[108] It could also be the case that collective characteristics of the excited states, like exciton delocalization that has no parallel in dimers, play an important role.[134, 135, 136] These are much more difficult to describe and understand, and are a principal focus of this work.

The singlet fission process we study appears is [18, 19]

$$S_1 \leftrightarrow {}^1(TT) \rightarrow T_1 + T_1 \quad . \tag{3.1}$$

The photon prepares an initial singlet state, S_1, that decays into a doubly-excited state, ${}^1(TT)$, which is a superposition of triplet excitons. There are nine spin states that result from adding the angular momentum for a pair of triplets, but only the singlet within this manifold, designated with the ^{1} superscript, connects to the initial singlet, S_1, through spin selection rules.[18] While Eq. 3.1 has the form of a chemical rate equation, one should refrain from interpreting it in this way because the mechanism may involve both electronic populations and coherences.[18, 19] As recent detailed work on acenes has shown, the interconversion events, shown in Eq. 3.1, are not stepwise in those systems. SF occurs through a mechanism reminiscent of "superexchange", where a superposition of the S_1 and ${}^1(TT)$ states decohere into ${}^1(TT)$.[101, 95, 93, 98, 99, 48, 102, 47, 104, 105, 28, 135] Theoretical calculations of spectral features, such as the Davydov splitting, have shown that the initial excitation possesses significant charge transfer character not shown in Eq. 3.1.[49] In some of the acenes, a consistent picture for the first step is emerging, but is still under debate.[105, 104, 109, 114, 108, 137, 98] The second step, ${}^1(TT) \rightarrow T_1 + T_1$, is less well understood. While

the $^1(TT)$ state is an approximate eigenstate of the electronic Hamiltonian, it is not an eigenstate of the spin-dipole operator, which splits the levels of the $^1(TT)$ state.[28, 29, 18, 19] Burdett and Bardeen's time-resolved fluorescence experiments have resolved the quantum beats that result from this splitting and their measurements provide some timescales for the transition from the $^1(TT)$ state to $T_1 + T_1$.[96, 93, 138] This transition may require spin-lattice relaxation that occurs on nanosecond (ns) timescales.[96, 93, 138, 139]

Many optical experiments that measure SF yields do so indirectly,[95, 97, 98, 99, 48, 100] so estimates of SF yields from these measurements must be interpreted with some care. The spectra are often broad and congested, with linewidths exceeding the laser bandwidth.[48] Pump-probe experiments, for example, attribute the SF yield to the amplitude of the induced absorption from the S_1 to the putative T_1 state. But without an external magnetic field these experiments cannot reliably distinguish between the $^1(TT)$ and the $T_1 + T_1$ state.[98, 99, 48] If both states contribute to the induced absorption then both the intermediate and final states contribute to the transient absorption signature, and so estimates of the SF yield, along with assignments of the dynamics from these measurements, will be inaccurate.[93] In addition, the molecular crystals and aggregates that undergo SF exhibit a high degree of polymorphism, which not only changes with temperature, but also implies that samples prepared using different methods or under different conditions can have different morphologies, intermolecular electronic couplings, and SF yields.[140, 64, 102, 141, 115, 100, 21] These factors have all likely contributed to variations in estimates of SF timescales, which can range from 0.1 picoseconds (ps) to 100 ps in solid phases of tetracene.[142, 103, 101, 96, 98, 99]

In theoretical descriptions of SF in crystals, one should describe exciton delocalization and recognize that, in contrast to the electron and exciton transfer work that has dominated the literature in the last few decades, SF is a multielectron process. Many theories of electron and energy transfer dynamics in the condensed phase can be phrased as an effective one-body problem.[76] A concrete example is the Holstein small polaron model,[143, 144, 145, 76] which underpins both the Marcus theory of electron transfer [7] and the Förster/Dexter theory of energy transfer,[67] and is a model that our group has generalized to describe SF in dimers when the weak electronic coupling

limit applies.[106] In the Marcus scenario, the electron distorts the nuclei and solvent polarization as it moves between electronic states so that the reaction coordinates are massive and can be treated classically.[69, 70] While the electron is a fermion, its spin statistics are immaterial in the single particle problem. In the case of energy transfer in molecular crystals, the Coulomb interaction between the electron and the hole in the excited state binds them into an exciton.[120, 126, 65] So while an exciton is formally a two-particle state, the electron and hole move together and function, in many ways, as a single particle. In both cases, the electron (or hole) in electron transfer or the exciton in energy transfer, the relevant electronic states behaves as quasiparticles; in many ways like an elementary particle, but with an energy shift and lifetime inherited from the interactions between the particle and the other degrees of freedom.[146] Making the quasiparticle notion quantitative is a frontier area in electronic structure theory first pioneered in condensed matter physics, but one that has seen recent application in molecular systems.[147, 148, 126, 128, 149] To connect our work to this nascent framework and make quasiparticle notions precise, we employ the methods of many-body and Green's Function Theory in this manuscript.[150]

By analogy, SF is at least a two quasiparticle problem, where one must understand not only how these effective excitons interact with the environment, but how they interact with each other. Many-body electron-electron interactions and entanglement between pairs of excitons, not present in one-body problems, are manifest in fission. The model presented here captures essential features of SF in periodic molecular crystals, but allows questions about particle-particle entanglement to be addressed clearly. In particular, for photovoltaic applications, it is natural to expect that maximum extraction efficiency occurs when the $T_1 + T_1$ state is composed of distinct and independent excitons. Our criteria for "distinct" and "independent" come from quantum information theory and move beyond the preliminary classifications of triplet-triplet independence, which hypothesized that triplets that are "well-separated" are independent.[135, 151] Pairs of quantum particles born under selection rules can exhibit quantum entanglement, where even though they are well-separated spatially, they are not independent; a measurement on one of the particles affects the state of the other. In analogy to spin-entangled pairs produced in Bell test experiments,[152] the $^1(TT)$ state,

born from an optically bright singlet, is certainly spin-entangled even if the excitons are spatially well-separated. One might suppose still that thermal fluctuations destroy any kind of quantum entanglement, but there are theoretical models for which this is not true where thermal fluctuations can produce or reinforce entanglement.[153, 154, 155, 156, 157, 158, 159, 160]

While a dimer picture cannot describe excitons that span more than two molecules, we draw on it to construct a molecular level description for SF in a crystal that allows for delocalization amongst several chromophores. We present a model Hamiltonian that builds on empirical evidence for SF in both experiments and theory.[117, 161, 145, 162, 49, 127, 124, 95, 163, 164] When parameterized from microscopic simulations, the exciton model we employ for the excitonic states gives a quantitative description of the electronically excited states in acene molecular crystals,[145, 49, 127] with the largest electron correlation energy coming from the interaction between the electron and hole on the same molecule.[120] At this level of detail, excitonic states are particles, and the exciton model shares similarities with tight binding models of electronic band structure. Just like electrons and holes have band structure, so do excitons.[145] The exciton resonance integrals, J_S and J_T play the role of the electronic tunneling matrix elements in tight binding models and are proportional to the excitonic bandwidth. In this work we use the resonance integral for triplets as a surrogate for delocalization: the larger the resonance integral, the larger the degree of delocalization. This is not entirely rigorous because we do not include explicit localization mechanisms for triplet states other than the biexciton interaction. Rather than saying the resonance integral is large or small, one must instead compare the size of these resonance integrals to another energy scale responsible for localization, like the electron-phonon coupling strength. While two-particle excited states are somewhat of a novelty in electron and energy transfer, they occur naturally in nonlinear spectroscopies, and we draw upon these studies to understand SF.[165, 166, 167, 168, 169] Models akin to the one we develop can capture essential spectral features of exciton-exciton interactions in pump-probe spectroscopy of linear and cylindrical molecular aggregates.[170, 171, 165, 166, 172, 169] Importantly, these studies show that, in collective systems like aggregates and crystals, one needs to include the biexciton interaction or else the bleach and induced absorption signals in pump probe spectra will

cancel one another and produce no signal.[173]

In this work we develop and solve the exciton model Hamiltonian in one dimension and do not include dissipation via electron phonon or spin lattice relaxation. While exciton dynamics in some molecular crystals and aggregates do occur in dimensions less than three,[49, 126, 128] these choices are made for technical reasons. First, in one dimension the exciton model for SF transforms into a quantum lattice model of interacting fermions, a procedure detailed in Section 3.3, which dramatically simplifies the analysis of the two-triplet state. Second, the Bethe Ansatz, which is thought to be exact for fermions in one dimension, provides solutions for these two particle states.[174, 175] We do not include dissipation because quantifying bipartite (two-triplet) entanglement on a quantum lattice in a dissipative environment is not straightforward.[176, 177, 178, 153] Quantum dissipation through the electron-phonon interaction and loss of spin coherence through spin-lattice relaxation are certainly important phenomena for singlet fission in crystals, but these features are even more poorly understood than the ones addressed here. We therefore defer their study to later work.

The outline of the manuscript is as follows: In Sec. 3.3, we describe the model for fission, calculate the eigenstates in the noninteracting case, and write the translationally invariant representation of all excitonic states on the periodic lattice. The periodicity of the crystal leads to momentum selection rules which state that the center of mass momentum for the triplet pair born from fission must have the same momentum as the singlet. For N chromophores in a lattice, there are $\sim N^2$ two-exciton states, but Pauli exclusion for the two-exciton states, in addition to optical and momentum selection rules, reduce the size of the Hilbert space considerably. In a periodic lattice, only one singlet state is bright and only $\sim N/2$ two-triplet states couple to that singlet. In Sec. 3.4, we use many-body Green's functions to describe SF in the case where the biexciton interaction is zero, which yields an exactly solvable result, vis-a-vis the quasiparticle interpretation. This scenario reduces to the Fano-Anderson model that describes how a quantum impurity, here the bright singlet state, interacts with a continuum formed by the two-triplet states. The singlet fission rate comes directly from the singlet self-energy and reduces to the Golden Rule, which predicts that the singlet fission rate increases with increasing triplet localization. While the optical selection rules

in perfectly periodic lattices preclude a formal analysis of how singlet localization impacts the rate of singlet fission, we show, using a variational solution for a localized singlet state, that the rate of singlet fission, W, depends on the delocalization length, ℓ, strongly, as $W \sim \exp(-1/\ell^2)$. In Sec. 3.6 we use scattering theory to study the system for nonvanishing biexciton interaction strength, χ, and in Sec. 3.7 we characterize the two-triplet states using the Bethe Ansatz . The size of χ/J_T determines whether or not the two-triplet states are bound to one another or are unbound, and in Sec. 3.8, we compute triplet-triplet entanglement using the Slater decomposition. We conclude by discussing our results in the context of recent and past work on singlet fission, including that of Suna and Merrifield.[135, 28, 29, 134, 119]

3.3 A Model Hamiltonian for Fission.

Molecular crystals are ordered, periodic, and dense arrays of chromophores that can be modeled using quantum lattices.[143, 144] In the diabatic picture of the crystal lattice the nuclei are fixed, each molecule becomes a site, and each site can support one exciton. The excited state wavefunctions are product states, similar to the Heitler-London approximation for electronic states of molecules.[172, 179, 180, 181, 182, 183] The many-body ground state is $\mid 0 \rangle = \prod_n (S_0)_n$ and the excited state with a singlet localized on site n is $\mid n \rangle_S = (S_1)_n \prod_{m \neq n} (S_0)_m$, where $(S_0)_n$ is a singlet ground state on site n and $(S_1)_n$ is the first excited state of site n. The excited state with a triplet localized on molecule n is $\mid n \rangle_T = (T_1)_n \prod_{m \neq n} (S_0)_m$, where $(T_1)_n$ is the triplet excited state wavefunction of site n. We pass to a second-quantized formalism by introducing the singlet and triplet excitation operators, $\mathcal{P}_n^\dagger \equiv \mid n \rangle_S \langle 0 \mid$ and $\mathcal{T}_n^\dagger \equiv \mid n \rangle_T \langle 0 \mid$, respectively, and the singlet and triplet de-excitation operators, $\mathcal{P}_n \equiv \mid 0 \rangle_S \langle n \mid$ and $\mathcal{T}_n \equiv \mid 0 \rangle_T \langle n \mid$, respectively.[173]

The exciton basis describes particles called paulions that obey a mixed Bose-Fermi commutation algebra. Like fermions, paulions forbid double singlet and double triplet excitons localized on the same molecule,

$$\mathcal{P}_n^\dagger \mathcal{P}_n^\dagger = 0 \quad , \quad \mathcal{T}_n^\dagger \mathcal{T}_n^\dagger = 0 \quad , \tag{3.2}$$

and also forbid the singlet-triplet composite exciton,

$$\mathcal{P}_n^\dagger \mathcal{T}_{n'}^\dagger = \mathcal{T}_{n'}^\dagger \mathcal{P}_n^\dagger = 0 \quad . \tag{3.3}$$

The total Hamiltonian, $\mathscr{H}$, is the sum of the exciton Hamiltonian, H, and the light-matter interaction in the dipole approximation, $-ME(t)$,

$$\mathscr{H} = H - ME(t) \quad . \tag{3.4}$$

The dipole operator, M is $M = \mu \sum_n (\mathcal{P}_n^\dagger + \mathcal{P}_n)$ for identical molecules, μ is the molecular transition dipole moment, and $E(t)$ is the time-dependent electric field that drives transitions. In the product basis, M is

$$M = \mu^* \sum_n \mid n \rangle_S \langle\, 0 \mid + \mu \sum_n \mid 0 \rangle_S \langle\, n \mid \quad . \tag{3.5}$$

The exciton Hamiltonian, H, spans the Hilbert space of singlet and triplet excitons, H_S and H_T, respectively. H also couples singlets and triplets through V and $V^\dagger$, operators that correspond to singlet fission and triplet-triplet annihilation, respectively,

$$H = H_S + H_T + V + V^\dagger \quad . \tag{3.6}$$

Each term in the exciton Hamiltonian in Eq. 3.6 appears in Eq. 3.7 – Eq. 3.9

$$H_S = \epsilon_S \sum_n \mathcal{P}_n^\dagger \mathcal{P}_n - J_S \sum_n \left[\mathcal{P}_n^\dagger \mathcal{P}_{n+1} + \mathcal{P}_{n+1}^\dagger \mathcal{P}_n\right] \tag{3.7}$$

$$\begin{aligned} H_T = \epsilon_T \sum_n \mathcal{T}_n^\dagger \mathcal{T}_n - J_T \sum_n \left[\mathcal{T}_n^\dagger \mathcal{T}_{n+1} + \mathcal{T}_{n+1}^\dagger \mathcal{T}_n\right] \\ -\chi \sum_n \mathcal{T}_n^\dagger \mathcal{T}_{n+1}^\dagger \mathcal{T}_{n+1} \mathcal{T}_n \end{aligned} \tag{3.8}$$

$$V = \frac{\gamma}{4} \sum_n \left[\mathcal{T}_n^\dagger \mathcal{T}_{n+1}^\dagger + \mathcal{T}_{n-1}^\dagger \mathcal{T}_n^\dagger\right] \mathcal{P}_n \tag{3.9}$$

Fig. 3.1 illustrates the terms in the Hamiltonian. The energies ϵ_S and ϵ_T are the "on-site" singlet and triplet exciton energies, the energies of the individual molecular excited states in the effective field of the crystal. The singlet and triplet resonance integrals are J_S and J_T, respectively, and χ is the biexciton interaction strength. All of the model parameters in this study are positive. Singlet

resonance integrals are available from quantum chemistry calculations,[49, 127, 128, 108] but few calculations of J_T and χ have been published.[117, 129, 184, 185] In acene crystals that exhibit fission, there is evidence that singlet exciton transport is bandlike while triplet exciton transport occurs via hopping diffusion.[123, 124, 97, 125, 126, 49, 127, 128, 108, 18, 129, 117, 130, 122] On physical grounds, the singlet excitons, which are optically bright, can couple to one another through-bond and through-space via transition dipole coupling, while triplet excitons, which are dark, only couple from one molecule to another with through-bond interactions. In either case, one expects that $|J_S|/|J_T| >> 1$.[186, 187, 188, 189, 129] The exciton resonance integral can even change signs for different polarization directions in the same crystal,[145, 167, 190] but in this paper, we choose $J_S > 0$ and $J_T > 0$, so that both bands run up from the Γ-point in the Brillouin zone. We also work in units where $\hbar = 1$. Because the Hamiltonian is periodic, the eigenstates of the Hamiltonian must remain unchanged under translation. This symmetry gives rise to a crystal momentum quantum number, k. The Fourier transform, $\hat{\mathcal{P}}_k^\dagger = \frac{1}{\sqrt{N}} \sum_n e^{ikna} \mathcal{P}_n^\dagger$ and $\hat{\mathcal{P}}_k = \frac{1}{\sqrt{N}} \sum_n e^{-ikna} \mathcal{P}_n$, diagonalizes Eq. 3.7, $H_S = \sum_k | \ k \ \rangle E_S(k) \langle \ k \ |$, where $| \ k \ \rangle = \hat{\mathcal{P}}_k^\dagger | \ 0 \ \rangle$, and the energy spectrum of all singlet excitons is

$$E_S(k) = \epsilon_S - 2J_S cos(ka), \tag{3.10}$$

where a is the lattice spacing between sites, $k = (1-N)\pi/L, (3-N)\pi/L, \cdots, 0, 2\pi/L, \cdots, (N-1)\pi/L$, and $L = Na$ is the total length of the lattice. The dipole operator is particularly simple in the $| \ k \ \rangle$ basis, $M = \mu^* \hat{\mathcal{P}}_{k=0}^\dagger + \mu \hat{\mathcal{P}}_{k=0}$, and therefore only the $k = 0$ mode is optically bright in a periodic lattice. We designate the optically bright singlet $| \ S \ \rangle \equiv | \ k = 0 \ \rangle$. It has energy

$$E_S = \epsilon_S - 2J_S \tag{3.11}$$

relative to the ground state. Because the fields used in experiments are weak, we assume that the role of the electric field is simply to prepare the system in state $| \ S \ \rangle$. Dynamics then follow from the decay of $| \ S \ \rangle$ into two-triplet states, which we compute using many-body theory.

Figure 3.1: Dynamics of singlet and triplet excitons. A singlet localized at site n, $\mid n \rangle_S$, may relax to two triplets with one triplet at site n and one to the left or to the right of it. $\mid n \rangle_S$ may not relax to next nearest-neighbor triplets. The singlet and triplet resonance integrals, J_S and J_T, are related to exciton energy transport in a crystal and are proportional to exciton bandwidths. The local triplet-triplet interaction strength, χ, is a measure of the mutual attraction between nearest-neighbor triplets. γ is the quantum amplitude for singlet fission, coupling a singlet localized at site n to two triplets, one triplet localized at site n and the other triplet localized at either site $n-1$ or $n+1$. Singlet and triplet excitons are denoted by circles and x's, respectively. The matrix elements, J_S, J_T, and χ account for intermolecular electron-electron interactions and all have expressions in terms of many-body repulsion integrals over the appropriate wavefunctions.[76, 107]

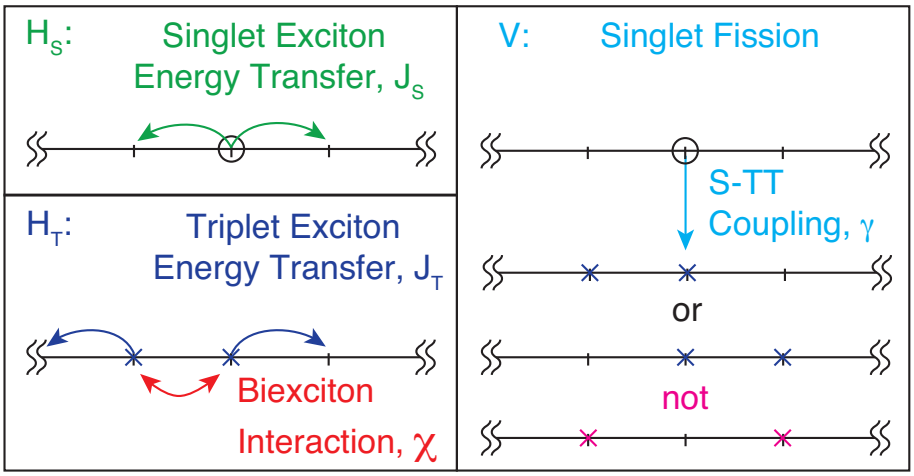

3.3.1 The Jordan-Wigner Transformation and Matrix Representations

While the exciton basis is convenient for constructing a model, there are many complications one encounters when trying to represent the exciton Hamiltonian in matrix form for practical calculations.[191, 170, 119, 118] To alleviate these problems, we use the Jordan-Wigner transformation to turn the paulions into fermions. The Jordan-Wigner transformation is exact in one dimension and is a standard method of attack for quantum lattice problems. The Jordan-Wigner string operator, $\Theta_n = e^{\pi i \sum_{n'<n} t^\dagger_{n'} t_{n'}}$, provides a relationship between the paulion and fermion creation operators, $\mathcal{T}^\dagger_n = t^\dagger_n \Theta^\dagger_n$, and a relationship between the paulion and fermion annihilation operators, $\mathcal{T}_n = \Theta_n t_n$. Physically, $t^\dagger_n$ creates an fermion at the same lattice site as $\mathcal{T}^\dagger_n$ creates a paulion, but with a phase that is -1 for each excitation to the left of site n. Unlike the paulions, the Jordan-Wigner particles obey fermionic anticommutation algebra,

$$\{t_n, t^\dagger_{n'}\} = \delta_{n,n'} \quad , \quad \{t_n, t_{n'}\} = \{t^\dagger_n, t^\dagger_{n'}\} = 0 \quad . \tag{3.12}$$

It is convenient to separate the two-particle states into their center of mass and relative separation, $R = \frac{m+n}{2}$ and $r = n - m$ respectively. The two-triplet state with one Jordan-Wigner fermion localized at site $R+r/2$ and the other triplet localized at site $R-r/2$ is $\mid R, r \rangle = t^\dagger_{R-r/2} t^\dagger_{R+r/2} \mid 0 \rangle$. The translationally invariant two-particle states are [190, 167]:

$$\mid Q, r \rangle = \frac{1}{\sqrt{N}} \sum_R e^{iQRa} \mid R, r \rangle \quad , \tag{3.13}$$

with the sum running over $R = 0, \frac{1}{2}, \cdots, \frac{N-1}{2}$. The momenta conjugate to the center of mass and relative two-triplet separation are $Q/2$ and q, respectively, so that one triplet has momentum $q_1 = Q/2 + q$ and the other has momentum $q_2 = Q/2 - q$. The center of mass momentum is enumerated by [170, 192]

$$Q = 0, 4\pi/L, \cdots, 4(N-1)\pi/L \tag{3.14}$$

Two-particle states in the momentum basis that satisfy Pauli exclusion are sine transforms of the position-space two-triplet wavefunctions,[190, 167]

$$\mid Q,q \rangle \;\; = \;\; \frac{2}{N}\sum_{R}\sum_{r} e^{iQRa} sin(qra) \mid R,r \rangle \;\; , \tag{3.15}$$

where the summation over the relative separation runs over $r = 1, 2, \cdots, \frac{N-1}{2}$, and the relative momentum conjugate to r goes over the range $q = \pi/L, 3\pi/L, \cdots, (N-2)\pi/L$. Importantly, Pauli exclusion forbids states with $q = 0$.

By inserting a complete set of states on both sides for both the singlet and two-triplet states we can express the exciton Hamiltonian as

$$H_S \;\; \equiv \;\; \sum_{k} \mid k \rangle E_S(k) \langle \; k \mid, \tag{3.16}$$

$$H_{TT} \;\; \equiv \;\; \sum_{Q}\sum_{q,q'} \mid Q,q \rangle \left[\delta_{q,q'} E_{TT}(Q,q) + \chi\, \zeta(q,q')\right] \langle \; Q,q' \mid, \tag{3.17}$$

$$V_{TT,S} \;\; \equiv \;\; \sum_{k}\sum_{Q}\sum_{q} \mid Q,q \rangle \delta_{Q,k} F(Q,q) \langle \; k \mid, \tag{3.18}$$

which takes the form of a partitioned matrix,

$$H := \begin{pmatrix} H_S & V^{\dagger}_{TT,S} \\ V_{TT,S} & H_{TT} \end{pmatrix} \;\; , \tag{3.19}$$

where Eq. 3.19 shows how we partition the Hamiltonian matrix and the := sign denotes the representation of the Hamiltonian in the chosen basis. Provided that the lattice is large enough (Appendix 3.11)[191, 170, 119], matrix elements follow from the application of Wick's theorem, with the bare two-triplet energies corresponding to the energies of two noninteracting triplet excitons,

$$E_{TT}(Q,q) = 2\epsilon_T - 4J_T cos(Qa/2) cos(qa) \;\; . \tag{3.20}$$

The biexciton interaction couples triplet states with the same center of mass momentum, Q,

$$\zeta(q,q') = -\frac{4}{N} sin(qa) sin(q'a) \;\; . \tag{3.21}$$

Singlets couple to two-triplet states with a strength governed by a momentum form factor,[193]

$$F(Q,q) = \frac{\gamma}{\sqrt{N}} cos(Qa/2) sin(qa) \;\; . \tag{3.22}$$

Appendix 3.11 contains the derivation of all matrix elements.

In the case that all fission occurs from the zero momentum singlet, $\mid S \rangle$, the two-triplet state must have a zero center of mass. $\mid q \rangle \equiv \mid 0, q \rangle$. In this case we abbreviate the two-triplet energies and form factor as

$$E_{TT}(q) = E_{TT}(0, q) \tag{3.23}$$

and

$$F(q) = F(0, q) \quad , \tag{3.24}$$

respectively. The energy-level diagram of the singlet fission model appears in Fig. 3.2.

3.4 The Singlet Self-Energy and the Rate of Singlet Fission.

In Sec. 3.3 we showed that the center of mass momentum is a constant of the motion and that the model's invariance under translations results in a simple momentum form factor for the singlet-two-triplet couplings. These two facts constitute the momentum selection rules of ultrafast fission in molecular crystals. In Fig. 3.3 we sketch the singlet fission phenomenon as a scattering process and plot the energies of triplet pairs within the first Brillouin zone, taking an example where the center of the two-triplet band at $2\epsilon_T = 0$ and the triplet bandwidth at $4J_T/\gamma = 5$. In Fig. 3.3 (b) the triplet pair dispersion along q is equivalent to that of a one-dimensional tight-binding model, thus reducing the two-body problem to an effective one-body problem.

The dynamics, in principle, proceed by solving for the time-dependence of the wavefunction from the initial condition $\mid \psi(0) \rangle = \mid S \rangle$. The solution to the time dependent Schrödinger equation, written as an initial value problem is $\mid \psi(t) \rangle = U(t) \mid S \rangle$ with the time evolution operator $U(t)$ $(t > 0)$, related to the retarded Green's function, $G(E)$, by the inverse Laplace transform,

$$U(t) = \Theta(t) e^{-iHt} \tag{3.25}$$

$$= \frac{i}{2\pi} \int_{-\infty}^{\infty} dE \; e^{-iEt} \; G(E) \quad . \tag{3.26}$$

Figure 3.2: Schematic of ground state absorption and singlet fission, shown in green and light blue, respectively. Ground state absorption accesses the zero momentum singlet that then relaxes, via fission, to two triplet excitons. In the diagram the triplet bandwidth increases from left to right. If the triplets are spatially localized, the density of states is very large but also narrow. SF to these states will be rapid, but will not be tolerant to any energy fluctuations in either the singlet or two-triplet states. As the triplet bandwidth increases (left to right in the figure), the two-triplet density of states widens. In our one-dimensional model, the two-triplet density of states has Van Hove singularities at the band edges. The detuning parameter, Δ, is the energy difference between the bottom of the singlet band and the bottom of the two-triplet band, $\Delta = E_S - 2E_T$, where the bottom of the two-triplet band is $2E_T = 2\epsilon_T - 4J_T$. Triplet-triplet interactions cause two-triplet density to shift and form satellite peaks. The center of the two-triplet band is twice the energy of a localized triplet, ϵ_T.

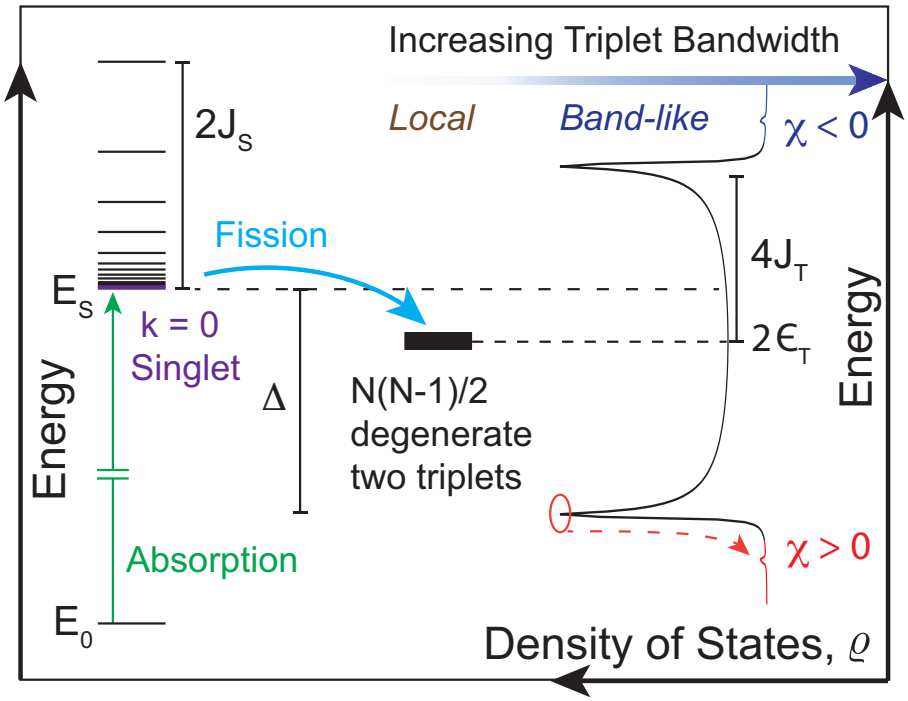

Figure 3.3: (a) Singlet fission as a scattering process. By analogy to optical mixing in nonlinear crystals, where one must phase match, singlet fission in a periodic system conserves both energy and momentum. The energy of the initial state therefore decides both the energy and the relative momentum of the two-triplet state. The singlet, shown in purple, scatters to two triplets with relative momentum $2q$. The momentum in the center of mass of the triplet pair is zero. (b) Energy of triplet pairs as a function of the relative momentum, $E_{TT}(q) = 2\epsilon_T - 4J_T cos(qa)$. A singlet of energy E_S produces a triplet pair at the same energy and with a definite relative momentum, $E_S = E_{TT}(q^*)$, thus simultaneously conserving both energy and momentum.

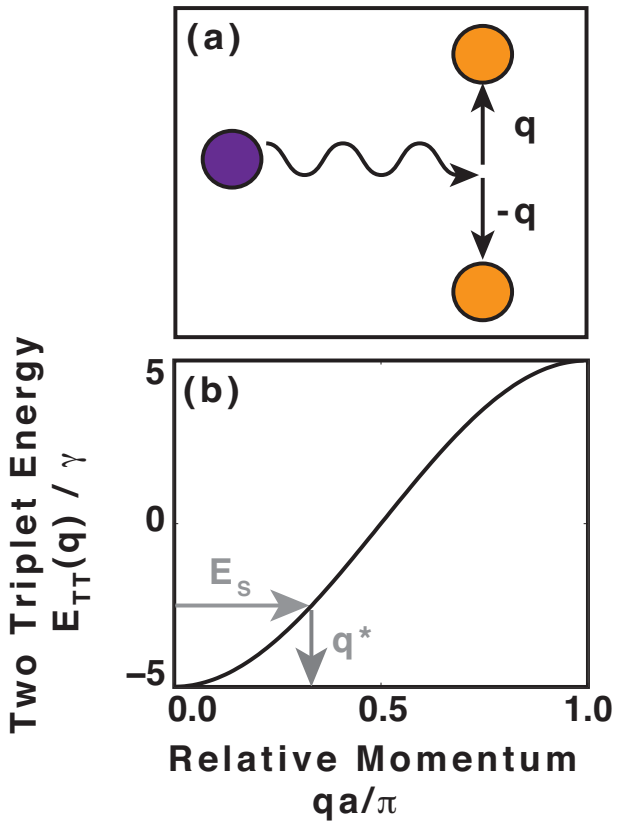

In systems with many degrees of freedom, it is often impossible to solve or even approximate the full wavefunction. But in the many-body theory of condensed phase systems with dense spectra, $G(E)$ plays a similar role as the wavefunction. $G(E)$ has poles at the eigenvalues of the fully interacting Hamiltonian. Many useful properties, like the density of states, come directly from $G(E)$, and the Green's function approach is invaluable in theories of transport and spectroscopy.[194] Even though it is called a Green's "function", like $U(t)$, $G(E)$ is an operator. Eq. 3.26 can be rewritten as the resolvent equation for $G(E)$,

$$\left[E - H + i0^+\right] G(E) = \mathbf{1}, \tag{3.27}$$

where 0^+ is shorthand for $\lim_{\epsilon \to 0^+} \epsilon$. $\mathbf{1} = \mid S \rangle\langle S \mid + \sum_q \mid q \rangle\langle q \mid$ expresses completeness of the Hilbert space in the singlet and two-triplet sectors, and $z = E + i0^+$ is the Laplace variable conjugate to time.[194]

To calculate the projection of $G(E)$ onto the singlet and two-triplet sectors, we represent the resolvent equation, Eq. 3.27, in matrix form and then partition the matrix, [192, 195, 86] as in Eq. 3.19,

$$\begin{pmatrix} E + i0^+ - E_S & -V^\dagger_{TT,S} \\ -V_{TT,S} & E + i0^+ - H_{TT} \end{pmatrix} \begin{pmatrix} G_S & G_{S,TT} \\ G_{TT,S} & G_{TT} \end{pmatrix} = \mathbf{1} \quad . \tag{3.28}$$

The singlet and two-triplet Green's functions are $G_S = \mid S \rangle\langle S \mid G \mid S \rangle\langle S \mid$ and $G_{TT} = \sum_{q,q'} \mid q \rangle\langle q \mid G \mid q' \rangle\langle q' \mid$. By algebraically solving Eq. 3.28 for the partitioned Green's functions, we have, for example,

$$G_S(E) = \frac{1}{E - E_S - \Sigma_S(E) + i0^+}, \tag{3.29}$$

where the singlet self-energy is

$$\Sigma_S(E) = V^\dagger_{TT,S}[E - H_{TT} + i0^+]^{-1} V_{TT,S} \quad . \tag{3.30}$$

The self-energy describes the interaction of the optically bright singlet with the two-triplet manifold. In the limit that $\gamma \to 0$, the singlet decouples, $\Sigma_S(E) = 0$ and there is only one pole for $G_S(E)$ at $E = E_S$. When $\gamma \neq 0$, $\Sigma_S(E)$, describes how this pole, or resonance, shifts and broadens. In the

quasiparticle picture, the singlet acquires a finite lifetime, inversely proportional to the imaginary part of the self-energy, when it undergoes fission to a dense set of triplet states. Because the singlet only interacts with the two-triplet states, the self-energy describes the dynamics of the SF process in frequency (E) space.

Analyzing the self-energy when the biexciton interaction is zero leads to an interesting result that forms a basic picture of SF in molecular crystals. When the triplet-triplet interaction is zero ($\chi = 0$) the self-energy of the singlet is equivalent to the self-energy of a quantum impurity in the Fano-Anderson model,[27, 196]

$$\Sigma_S^{\chi=0}(E) = \sum_q \frac{|F(q)|^2}{E - E_{TT}(q) + i0^+}. \tag{3.31}$$

In a large quantum lattice, the spectrum becomes continuous and the sum from the matrix product in Eq. 3.30 becomes an integral, [194, 190]

$$\frac{1}{N}\sum_q f(qa) \to \frac{1}{2\pi}\int_0^\pi d\theta f(\theta) \quad , \tag{3.32}$$

The self-energy for $\chi = 0$, $\Sigma_S^{\chi=0}$ becomes

$$\Sigma_S^{\chi=0}(E) = \frac{\gamma^2}{2\pi}\int_0^\pi d\theta \frac{\sin^2(\theta)}{E - 2\epsilon_T + 4J_T\cos(\theta) + i0^+}. \tag{3.33}$$

One can evaluate the integral directly, or use the identity $\frac{1}{x+i0^+} = Pr.(1/x) - i\pi\delta(x)$. In the latter case, it is easy to see that the imaginary part of the self-energy is equivalent to the rate from Fermi's Golden Rule,[192]

$$W_0 \equiv -2Im\left[\Sigma_S^{\chi=0}(E = E_S)\right]. \tag{3.34}$$

giving the result,

$$W_0 = \frac{\gamma^2}{4J_T}\sqrt{1 - \left(\Delta/4J_T - 1\right)^2} \quad , \tag{3.35}$$

where W_0 is the SF rate when $\chi = 0$. The detuning, $\Delta = E_S - 2E_T$ is the energy of the singlet relative to the bottom of the two-triplet band (Fig. 3.2), and for every value of the detuning there is a critical wavevector, q^*, that satisfies both energy and momentum conservation rules (Fig. 3.3). The Golden Rule rate is usually a product of the density of states and the square of

the coupling matrix element, and both factors have different physical interpretations that provide insight into what controls the rate. The density of two-triplet states per site, $\varrho(E)$, also comes from the imaginary part of the two-triplet Green's function,

$$\begin{aligned} \varrho(E) &= -\frac{1}{N\pi} Im[G_{TT}(E)] && (3.36) \\ &= -\frac{1}{2\pi^2} Im\left[\int_0^\pi d\theta \frac{1}{E - 2\epsilon_T + 4J_T cos(\theta) + i0^+}\right], \\ &= \frac{1}{8\pi J_T} \frac{1}{\sqrt{1 - \left(\frac{E-2\epsilon_T}{4J_T}\right)^2}} \quad . && (3.37) \end{aligned}$$

Equipped with the density of states, Eq. 3.35 can be written as a canonical Golden Rule formula,

$$W_0 = 2\pi |V|^2(E_S)\varrho(E_S), \tag{3.38}$$

where the square of the coupling matrix element is $|V|^2(E) = \gamma^2[1 - (E - 2\epsilon_T)^2/(4J_T)^2]$. While the density of states peaks sharply near the band edges, corresponding to the van Hove singularities, the square of the coupling matrix element goes to zero at these points to satisfy Pauli exclusion for the two-triplet states. Thus the rate of fission is not maximal where the density of states is the largest, but instead where the density of states is flat, which occurs in the middle of the two-triplet band. Fig. 3.4 shows plots of the singlet fission rate, the density of states, and the square of the coupling matrix element. The maximal SF rate scales as $1/J_T$ for Δ/J_T fixed. Consistent with recent calculations and empirical observations,[126, 65] fission is therefore fastest when J_T is small. The reason for this is that a small value of J_T increases the density of states in the middle of the triplet band, where the coupling matrix element is the largest. While a narrow triplet bandwidth implies fast fission, there is a trade-off. Fig. 3.4 shows that the rate is a more sensitive function to the detuning energy as J_T decreases, meaning that the SF rate is faster, but less robust to energy level fluctuations in either the singlet or two-triplet energies.

3.4.1 SF from a Localized Singlet State

The preceding analysis showed that the SF rate decreases with increasing triplet bandwidth. We now comment on how the extent of localization in the singlet state affects the rate of SF. The

Figure 3.4: The rate of singlet fission as a function of the detuning and triplet resonance integral. The singlet-two-triplet coupling matrix element squared (a) and density of two-triplet states (b) as a function of detuning, Δ, and the triplet resonance integral, J_T. As the triplet bandwidth increases, the maximum rate of SF decreases, but SF can also occur over a broader range of energies. In this sense, there appears to be a trade-off between a fast rate of SF and one that is tolerant of energy level fluctuations.

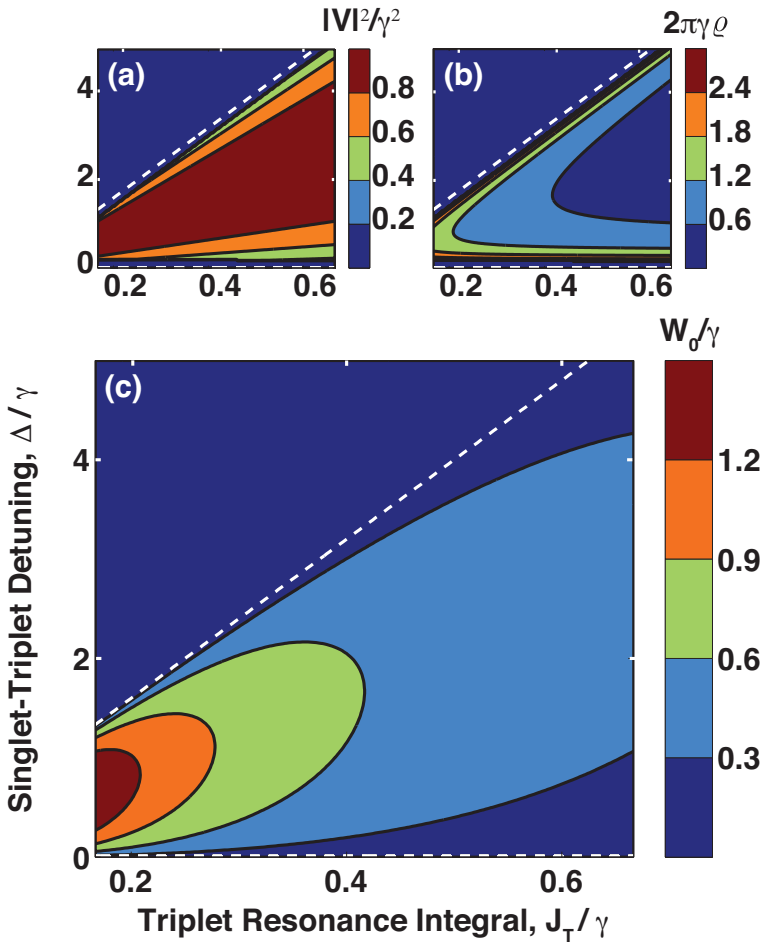

optical selection rules for singlets on a perfectly periodic lattice, discussed in Sec. 3.3, imply that the optically bright singlet state is completely delocalized. Evidence, from both experiments and simulations,[126, 49, 127] shows that while the singlet states are more delocalized than the triplets are, they span on the order of 10 molecules. Quantitatively, singlet excitons can scatter off of phonons, crystal impurities, or couple to localized charge transfer states. Any of these interactions lead to an initial singlet state that is not a pure $\mid k = 0 \rangle$ state, but is instead a superposition state, $\mid I \rangle = \frac{1}{\sqrt{N}} \sum_k A(ka) \hat{\mathcal{P}}_k^\dagger \mid 0 \rangle$. This state is a zero-order eigenstate of some Hamiltonian, with energy E_i. While this Hamiltonian acts to localize the singlet, its details are, in fact, not essential for the analysis presented here. If it is not too different from H_S, the coefficients $A(ka)$ will be sharply peaked near zero. The Golden Rule rate of singlet fission from this variational initial state, $\tilde{W}$, is

$$\tilde{W} = 2\pi \sum_{k,k'} \sum_{Q,q} \frac{1}{N} A^*(k'a) A(ka) \langle\ k' \mid V \mid\ Q, q\ \rangle \langle\ Q, q \mid V \mid\ k\ \rangle \delta(E_i - E_f) \tag{3.39}$$

$$\approx 2\pi \sum_{k} \sum_{Q,q} \frac{1}{N} |A(ka)|^2 |\langle\ k \mid V \mid\ Q, q\ \rangle|^2 \delta(E_i - E_f) \quad . \tag{3.40}$$

$$\approx \frac{1}{\sqrt{2\pi}} \frac{\rho\gamma^2}{\sigma} \frac{1}{4J_T} \int_{-\pi}^{\pi} d\Theta e^{-(\rho\Theta)^2/2\sigma^2} cos(\Theta/2) \tag{3.41}$$

$$\approx W^* \exp\left(-\frac{\sigma^2}{8\rho^2} \right) \quad , \tag{3.42}$$

where $\rho = N/L$ is the linear density of the lattice and W^* is the maximum singlet fission rate along the energy detuning coordinate. In moving from the first equation to the last, we assume that $A(ka)$ is so sharply peaked about $k = 0$, that $A^*(ka)A(k'a)$ is zero unless $k \approx k'$, replace $|A(ka)|^2$ with its second cumulant (Gaussian) approximation and evaluate the singlet fission rate at the maximum with respect to the detuning between the initial and final states, $E_i - 2E_T = 4J_T$. The exciton delocalization length in real space, ℓ, is inversely related to σ, which leads to the relationship

$$\ln\left(\frac{\tilde{W}}{W^*} \right) \sim -\frac{1}{\ell^2} \quad , \tag{3.43}$$

so that the fission rate decreases very strongly with the degree of localization in the singlet state.

3.5 Biexciton Interactions

Density functional theory calculations[117, 129] have shown that triplet resonance integrals for the acenes span nearly four orders of magnitude, 0.01 to 10 wavenumbers. In analogy to the spectroscopy of molecular aggregates, some have proposed using pump-probe spectroscopy to measure the biexciton interactions. When biexciton interactions are nonzero, $\chi \neq 0$, we must calculate a diagonal representation of H_{TT}. With $H_{TT}|\ \alpha\ \rangle = E_\alpha|\ \alpha\ \rangle$, the singlet self-energy is

$$\begin{aligned} \Sigma_S(E) &= \\ &= \sum_\alpha \langle\ S\ |V^\dagger|\ \alpha\ \rangle [E - E_\alpha + i0^+]^{-1} \langle\ \alpha\ |V|\ S\ \rangle \quad . \end{aligned} \tag{3.44}$$

In the absence of biexciton interactions, the inverse lifetime of $|\ S\ \rangle$ depends on only two energy scales, Δ/γ and J_T/γ. For nonzero χ, the lifetime depends on all three energy scales, J_T/γ, Δ/γ, and χ/γ. The fission rate for interacting triplets appears in Fig. 3.5 with respect to χ/γ and J_T/γ, and with the detuning parameterΔ fixed to 3γ. In Fig. 3.5 the singlet-two-triplet resonance ranges from the center of the triplet pair band at $4J_T/\gamma = 3$ to 3γ away from the bottom of the triplet pair band at $4J_T/\gamma = 10$. We can see from Fig. 3.5 that fission is fastest when the triplets are noninteracting only when $4J_T/\gamma < 3$. Even when χ is nonzero, the SF rate increases with decreasing J_T, which leaves the qualitative conclusions deduced from the $\chi = 0$ case unchanged. We emphasize that, although χ and J_T are likely to be smaller than the singlet bandwidth, the ratio χ/J_T has yet to be calculated or measured.

3.6 Characterizing the Fission Product: Structure Functions.

To characterize the two-triplet states, we start by considering the two-triplet density correlation function, written in terms of the center of mass and relative coordinates for an eigenstate of H_{TT}, $|\ \Psi\ \rangle$, measured in units of the lattice density in Eq. 3.45.

$$\rho_2(R,r) = \langle\ \Psi\ |\ R,r\ \rangle \langle\ R,r\ |\ \Psi\ \rangle \tag{3.45}$$

Figure 3.5: The fission rate described in the text as a function of χ and $\Delta/\gamma = 3$, computed numerically using a lattice of 2001 sites. The dashed black line indicates the direction for which the rate decreases most slowly. A dashed white line along $\chi/\gamma = 0$ emphasizes that for $4J_T/\gamma > 3$ fission is fastest when the singlet relaxes to an interacting two-triplet system. Even with the biexciton interaction nonzero, the SF rate still increases when J_T decreases.

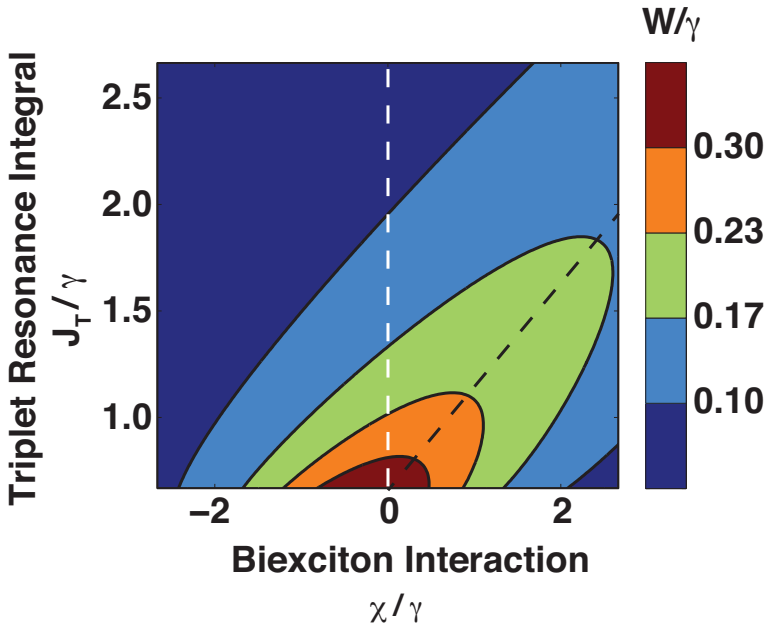

To satisfy Pauli exclusion and parity, $r > 0$ and the average is over the fully interacting states of the triplet Hamiltonian. The radial distribution function for the exciton pair, $g(r)$, is

$$c^2 g(r) = \rho \int d(aR)\ \rho_2(R, r) \quad , \tag{3.46}$$

where c is the bulk exciton density. The pair distribution function is related to the static structure factor, $S(\theta)$, through

$$g(r) - 1 = \frac{2}{\pi} \int_0^\pi d\theta\ sin(\theta r)\big(S(\theta) - 1\big) \quad . \tag{3.47}$$

The Lippmann-Schwinger equation provides a convenient connection between the wave function of the total Hamiltonian, $\mid \Psi \rangle$, and the singlet state,

$$\mid \Psi \rangle = \mid S \rangle + G_0 T \mid S \rangle \quad . \tag{3.48}$$

G_0 is the unperturbed Green's function of singlet and triplet excitons corresponding to $H_0 = H_S + H_{TT}$, with $V = H - H_0$ corresponding to the SF and triplet-triplet annihilation processes.[194, 197] The T-matrix is $T = V[1 - G_0 V]^{-1}$. In terms of the T-matrix, the two-triplet density is

$$\rho_2(R, r) = \big|\langle\ R, r\ |G_0 T|\ S\ \rangle\big|^2 \quad . \tag{3.49}$$

Calculations of both the pair distribution function and $S(\theta)$ appear in Appendix 3.12. By solving the Lippmann-Schwinger equation for a fixed detuning, we find that the static structure factor is sharply peaked at the resonant momentum, $q^* a = cos^{-1}\big[1 - \Delta/4J_T\big]$, similar to the momentum selection rules we found in the $\chi = 0$ case. In Fig. 3.6 we show the static structure factor with the triplet bandwidth fixed at $4J_T/\gamma = 10$.

While both J_T and χ may be small, the ratio χ/J_T could have a profound effect on the character of the two-triplet states that participate in SF.

3.7 Bound States from the Bethe Ansatz.

If a singlet relaxes to a composite two-triplet state, the triplet pair may behave as one entity if it is strongly correlated. In linear spectroscopies no such correlations can be observed.

Figure 3.6: The static structure factor described in the text, illustrating scattering from the singlet state to classes of unbound and bound states. The structure factor follows the momentum selection rules for the unbound two-triplet states (a,b), but shows the emergence of candidate bound states (c,d) when $\chi/J_T > 2$. In Sec. 3.7, we show using the Bethe Ansatz that the satellite peaks do indeed correspond to bound two-triplet states. We have fixed the bulk triplet density at $c = 10/L$. Points where $S(qa) \neq 1$ are shown in black.

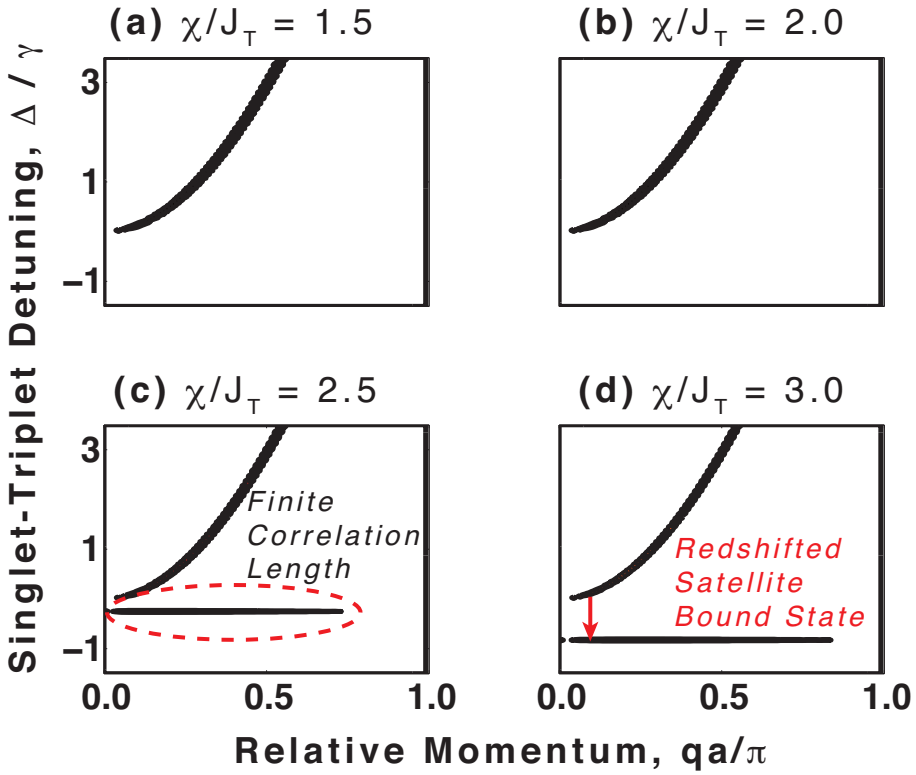

In nonlinear spectroscopies the triplet-triplet interactions that distort one triplet momenta may exhibit correlated spectral features that register as off-diagonal cross peaks.[198]

Recently Feng *et al.*[104] computed the number of unpaired electrons in the singly and doubly excited states of a dimer model using one-particle transition density matrices. While their technique can elucidate one-electron character of nonadiabatic transitions it cannot quantify spatial entanglement of multiple triplet excitons. Any entanglement measure computed from a one-particle density matrix assigns the same degree of correlation to all two-particle density matrices.[199] In this section we decouple the singlet from the two triplets, $\gamma \to 0$, and discuss how biexciton interactions acting in concert with triplet hopping lead to a nontrivial entanglement. For nonzero triplet-triplet interactions the triplet momenta are correlated through the Bethe Ansatz phase even if that phase is entirely real.[30] This correlation may seem surprising, since the two-triplet density of states is relatively insensitive to such local interactions, but it is an intrinsic property of the composite pair.

When triplet-triplet interactions are included, the momentum basis no longer diagonalizes the triplet Hamiltonian. The Bethe Ansatz is a physically motivated parameterization of eigenvectors most commonly used to build the eigenspace of spin Hamiltonians through a series of spin flip operations. Two spin flips are analogous to creating two fermionic triplets in our model. The Bethe Ansatz provides insight into the emergence of bound two-triplets and triplet-triplet entanglement. We start by writing the arbitrary singlet fission product state as some combination of composite two-triplet states,

$$| \psi \rangle = \sum_{m} \sum_{n>m} A_{m,n} t_m^\dagger t_n^\dagger | 0 \rangle \quad , \tag{3.50}$$

where $H_{TT}| \psi \rangle = E| \psi \rangle$. The Bethe Ansatz is a form of eigenstate,[200, 201, 202]

$$A_{m,n} = a_{1,2} z_1^m z_2^n + a_{2,1} z_2^m z_1^n \quad , \tag{3.51}$$

having abbreviated $z_1 = e^{iq_1 a}$ and $z_2 = e^{iq_2 a}$. These Bethe Ansatz coefficients are not antisymmetric

and are defined only for $r = n - m \geq 1$. Wick's theorem tells us that for $r = n - m > 1$,

$$(E - 2\epsilon_T)A_{m,n} = -J_T\big(\quad A \quad _{m,n-1} + A_{m-1,n} \\ + \quad A_{m,n+1} + A_{m+1,n}\big) \quad , \tag{3.52}$$

and for the $r = 1$ case,

$$(E + \chi - 2\epsilon_T)A_{m,m+1} = -J_T\big(A_{m-1,m+1} + A_{m,m+2}\big) \quad . \tag{3.53}$$

Eqs. 3.52 and 3.53 do not apply to the $r < 1$ case. From Eq. 3.52 we calculate the energy spectrum:

$$E = 2\epsilon_T - 2J_T cos(q_1 a) - 2J_T cos(q_2 a) \quad . \tag{3.54}$$

Although Eq. 3.54 is of the same form as two independent triplet excitons, the biexciton interactions induce momentum shifts that in general are complex.[30] By solving Eq. 3.53 using Eqs. 3.54 and 3.51, we find

$$a_{1,2}/a_{2,1} = \frac{1 + z_1 z_2 - z_1(\chi/J_T)}{z_2(\chi/J_T) - 1 - z_1 z_2} \tag{3.55}$$

If $\chi = 0$ then $a_{1,2}/a_{2,1} = -1$, and $A_{m,n} = z_1^m z_2^n - z_2^m z_1^n$. Periodic boundary conditions require $A_{R,r} = A_{R+N/2,r}$, consistent with our spectrum of total two-triplet momentum.[190] Periodic boundary conditions also require that $A_{m,n} = A_{m,n+N}$, and therefore

$$q_1 = Q/2 + q - i \ \ln[a_{1,2}/a_{2,1}]/Na \tag{3.56}$$

$$q_2 = Q/2 - q + i \ \ln[a_{1,2}/a_{2,1}]/Na \quad , \tag{3.57}$$

Eqs. 3.55, 3.56, and 3.57 form a set of nonlinear equations that, for each of the $N(N-1)/2$ triplet pairs, provides a phase through which the mixing coefficients can be calculated,[30] $\phi = -i \ \ln[a_{1,2}/a_{2,1}]$.

The Bethe Ansatz phase correlates each of the one triplet momenta and indicates the emergence of bound states when it becomes complex and the magnitude of the two terms in Eq. 3.51 are no longer unity. For complex ϕ, the magnitude of the two terms in Eq. 3.51 are proportional

to $e^{(r/N-1/2)\mathrm{Im}\phi}$ and $e^{-(r/N-1/2)\mathrm{Im}\phi}$, so as $r \to \infty$ one term diverges as the other tends to 0. If $\mathrm{Im}[\phi] > 0$, then $e^{i\phi/2} = 0$ such that as $r \to \infty$ the Ansatz is well behaved, $A_{m,m+r} \to 0$. Similarly, if $\mathrm{Im}[\phi] < 0$, then $e^{-i\phi/2} = 0$.

One of the earliest theories of biexciton interactions between doubly excited states in a one-dimensional crystal was made in 1959 by R. E. Merrifield, who calculated bound biexcitons when doubly excited states reside on a single molecule.[134] Smith and Michl[18, 19] proposed that bound biexcitons are stable for $\chi/k_BT > 1$. Others have used simulated pump-probe spectra [170] to calculate a threshold of $\chi/J_T = 2$. To determine when attractive triplet-triplet interactions lead to bound biexcitons we first calculate the distortions of the triplet pair density of states caused by the biexciton interactions, $\Delta\varrho(E) = |\varrho(E;\chi) - \varrho(E;\chi=0)|/\varrho(E,\chi=0)$. In Fig. 3.7 we plot $\Delta\varrho(E)$ (a), having fixed the triplet bandwidth at $4J_T/\gamma = 10$. We also compute the complex phase in the Bethe Ansatz in Fig. 3.7 (b). We see from Fig. 3.7 (a) that unless biexciton interactions are roughly greater than $\chi/J_T \approx 2$ no bound states can be resolved from the continuum. This is confirmed by the Bethe Ansatz in Fig. 3.7 (b) that indicates bound states may occur for $\chi/J_T > 2$, or half the triplet bandwidth, similar to the threshold that Juzeliūnas and Reineker calculated for singlets.[170] As we have discussed, the meaning of "bound states" in the Bethe Ansatz is asymptotic and is to be understood in the limit that the triplet-triplet separation approaches infinity.

The two-triplet density of states, the Bethe Ansatz, and the static structure factor all identify a threshold for bound states at approximately the same ratio of χ/J_T. The Bethe Ansatz suggests that even below this threshold there may be appreciable triplet-triplet entanglement. We can only speculate as to the magnitude of the biexciton interaction and we see no reason at this date to exclude the possibility of bound states. In acenes, the singlet-two-triplet resonance may fall within the triplet pair density of states or well outside of it. The initial singlet may relax quickly, but the relative motion of the two-triplets born out of fission also depends on J_T and Δ.

Figure 3.7: (a) Distortions of the two-triplet density of states described in the text for $\chi/J_T = 2.0$, 2.5, and 3.0, shown in blue, green, and red, respectively. The small differences for $\chi/J_T \leq 2$ near the Van Hove singularity at $E/4J_T = -1$ indicate the absence of bound states. (b) Domain where the Bethe Ansatz phase is complex and bound states may occur in the plane spanned by the ratio χ/J_T and the noninteracting relative momentum, $2q$. 2001 lattice sites were used and all resonances were broadened by $\gamma/10$. The dashed color lines emphasize the points of correspondence with the distortions shown in (a). Complex phases for $\chi/J_T < 2$ may indicate quasi bound two-triplet states.

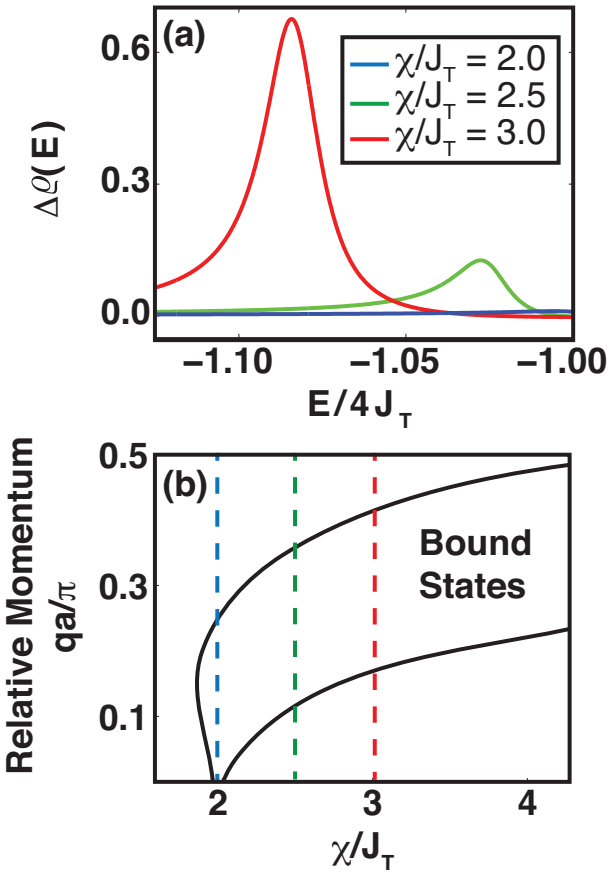

3.8 Triplet-Triplet Entanglement and the Slater Decomposition

Johnson and Merrifield[28, 29] were first to consider a spin-dipole interaction that broke the symmetry of spin angular momentum and entangled pure spin states. This spin correlation leads to a decoherence of the S_1 and $^1(TT)$ singlets. As the initial singlet excitation relaxes, it scatters to some distribution of triplet pairs that may possess a finite and spatial triplet-triplet entanglement. In Suna's original work,[135] the triplets were local, and if two triplets diffused to some critical separation they were considered correlated. Although Suna speculated that band effects could be important and even wrote equations of motion in reciprocal space, the general solution including both biexciton interactions and band effects was relegated to later work.

The interpretation of separability and many-body entanglement in the context of measurements can be challenging.[203, 176, 177] Measurement causes quantum discord, and it is not yet clear whether the measurement of one triplet born out of fission affects the measurement of the second. In the limiting case that each triplet is statistically independent, the two-triplet state can be written as a product of one triplet states. To measure triplet-triplet entanglement we will search for a decomposition of the eigenstate, $\mid \psi \rangle$, characterized as a mixture of plane waves and local triplets when $\chi \sim J_T$. Although we choose to study the spatial component of the electronic wavefunction a similar analysis can be developed for the spin dynamics on nanosecond timescales.[96, 93]

To measure entanglement between two triplets, we ask whether or not the two-particle density matrix can be formed from a product state in *any basis*. We will compute a Slater rank,[204, 205] analogous to the Schmidt number, or the number of nonzero singular values in the singular-value decomposition of the density matrix for distinguishable particles. The two-triplet eigenstate, $\mid \psi \rangle$, is

$$\mid \psi \rangle \;\; = \;\; \sum_{m,n} A_{m,n} t_m^\dagger t_n^\dagger \mid 0 \rangle \;\; , \tag{3.58}$$

where the A-matrix is antisymmetric ($A_{m,n} = -A_{n,m}$) unlike Eq. 3.51, and the A-matrix is normalized such that $Tr\left[A^\dagger A\right] = 1/2$. For the real normal A-matrix, a unitary congruence transformation

reduces to an ordinary similarity transformation [206, 205]

$$\tilde{A} = U^{\dagger} A U^{*} = \mathrm{diag}\big[Z_0, Z_1, \cdots, Z_M\big] \quad , \tag{3.59}$$

where each block is defined by $Z_i = \begin{pmatrix} 0 & z_i \\ -z_i & 0 \end{pmatrix}$, with eigenvalues $\pm i z_i$. Z_0 is an $(N-2M)$ by $(N-2M)$ null matrix and M is the number of nonzero eigenvalues, referred to in this manuscript as the Slater rank. In this manuscript we set a threshold of $1/N$ below which eigenvalues are considered zero.

We represent the composite two-fermion system in a basis of one-fermion states using the Slater decomposition,

$$\mid \psi \rangle = 2 \sum_{i=1}^{\leq N/2} z_i \mid 2i-1 \rangle \otimes \mid 2i \rangle \quad . \tag{3.60}$$

Notice that the sum is not running over the lattice index but instead runs over the Slater states defined by $\mid i \rangle = \tilde{t}_i^{\dagger} \mid 0 \rangle$ with $\tilde{t}_i^{\dagger} = \sum_j U_{i,j}^{\dagger} t_j^{\dagger}$. In this manuscript we use Wimmer's algorithm for speed and efficiency.[206] Here, a series of Householder transformations defines the similarity transform. The partial trace with respect to one of the two triplets,

$$4 \sum_{i=1}^{\leq N/2} |z_i|^2 \mid 2i-1 \rangle\langle 2i-1 \mid \tag{3.61}$$

is itself mixed rather than pure if $\mid \psi \rangle$ is entangled.[207] The prefactor of 2 in Eq. 3.60 accounts for the parity of the two triplets.

When $M = 1$, the two-triplet wavefunction is a single Slater determinant. By definition, $M = 1$ for $N = 2$ and $N = 3$ although there may exist classical correlation in either case.[204] When the Slater number is greater than one, the pair state is considered nonseparable with respect to pure one triplet subsystems. There are $(N-1)/2$ lattice sites to the left of $N/2$ and therefore the point of maximum entanglement occurs when $|z|^2 = 1/2(N-1)$.

When $\chi \sim J_T$ a quasibound resonance is embedded in the triplet pair energy band and neither the local nor the momentum basis approximately diagonalize the triplet Hamiltonian. In Fig. 3.8 we calculate the Slater decomposition with the triplet bandwidth fixed at $4J_T/\gamma = 10$. It is clear

Figure 3.8: The Slater rank, relative to unity measured in units of the maximum rank, for a lattice of $N = 1001$ sites. We average our entanglement measure over 50 triplet pairs nearly resonant with the singlet energy, which is J_T away from the bottom Van Hove singularity, at the center of the two-triplet band, and J_T away from the upper Van Hove singularity in the blue, green, and red lines, respectively. The energy of the singlet is shown in the inset corresponding to the blue, green, and red entanglement calculations. The Bethe Ansatz predicts a threshold for bound two-triplets at approximately $\chi/J_T \approx 2.0$ (Fig. 3.7). Bound states emerge between $\chi/J_T = 1.5$ and 2.0, illustrated with a dashed black line and a dashed blue line, respectively.

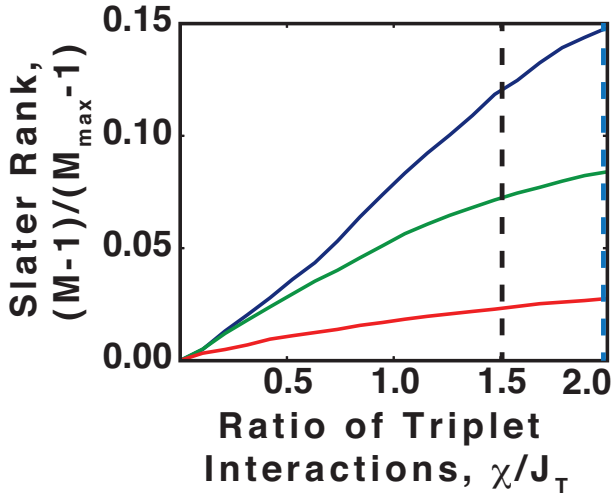

from Fig. 3.8 that for $\chi = 0$ the Slater rank is one ($M = 1$). Independent of how far apart the two triplets are from each other, each triplet will behave more independently the weaker the triplet-triplet interactions are. As the triplet-triplet interaction strength increases, so too does the Slater rank. Provided $\chi/J_T \neq 0$, there exists finite triplet-triplet entanglement that can be on the order of 10% of the maximal entanglement before the threshold for bound states is reached. Recall that the upper entanglement limit corresponds to the maximum number of Slater determinants that could be needed to represent any two-triplet state. Broader averaging and larger lattices can improve the smoothness of the Slater rank, but qualitative and quantitative trends remain the same. We have not pursued an extensive analysis of the bipartite entanglement, but have highlighted key aspects of triplet-triplet entanglement not discussed in the literature. Our calculation not only associates biexciton interactions with triplet-triplet entanglement, but also illustrates that the energy of the singlet-two-triplet resonance will also tune the triplet-triplet correlation. Our theory is unique in this way— rules that govern singlet to two-triplet scattering rates may also steer the system towards entangled two-triplets and even bound two-triplets if the triplet resonance integral is finite.

Our entanglement measure does not, alone, distinguish between classical and quantum correlation. To make such a distinction, one needs a somewhat detailed model for the triplet extraction process, which is beyond the scope of the current work.[208, 209, 210] Future work is needed to quantify the relative entropy of entanglement for triplets born out of singlet fission.

3.9 Conclusions.

To summarize, we have constructed a model of singlet fission in molecular crystals that is consistent with known characteristics of the excited states in acene crystals and singlet fission. In this model, excitations are confined to a periodic one-dimensional quantum lattice where each site corresponds to a molecule that can support either a singlet or a triplet excited state. Singlets and triplets on individual molecules couple to one another with exciton resonance integrals, J_S and J_T, corresponding to the bandwidth of singlet and triplet excitons, respectively. In accordance with both calculations and electron-pushing mechanisms,[18, 19, 76, 106, 108] we model singlet fission as

a process that occurs between adjacent chromophores. In the absence of lattice disorder, the crystal periodicity leads to momentum selection rules that accompany the energy matching condition of SF. Using Green's functions and many-body theory, we analyzed the dynamics of SF from an initially excited singlet state. In the limit of a perfectly periodic lattice and when the two-triplet biexciton interaction, χ, is zero, the singlet excited state becomes a quantum impurity, coupled to a dense set of two-triplet states. Our model for SF then maps onto the Fano-Anderson model.[27, 196] The SF rate, taken from the imaginary part of the singlet self-energy of the singlet Green's function reduces to Fermi's Golden rule, a product of the coupling matrix element squared and the two-triplet density of states. While the two-triplet density of states is largest near its band edges, no molecule can support two triplet excitons, and formally, the Pauli exclusion principle sends the coupling matrix element to zero at the band edges. Thus, the singlet fission rate is largest when the singlet decays to the middle of the two-triplet band. When J_T is small, the band is narrow and more two-triplet states appear in the middle of the band. As a result, the rate of SF is largest when J_T is small. Using the magnitude of J_T as a surrogate for triplet localization, this result implies that the SF rate is large when the singlet relaxes to localized two-triplet states. Lattice disorder, impurity or phonon scattering, and, importantly, coupling to charge transfer states, localizes the singlet exciton. To gauge the importance of exciton delocalization in the singlet state, we used a variational calculation to argue that, as the singlet state becomes more localized, the SF rate decreases precipitously. The excitonic states of the acene crystals that exhibit fast SF are consistent with these characteristics. In both pentacene and tetracene,[123, 124, 97, 125, 126, 49, 127, 128, 108] the singlet state is delocalized and the triplet states are nearly localized to individual molecules (vanishingly small J_T).

For singlet excitations in periodic molecular aggregates, nonlinear spectra can measure the singlet-singlet biexciton interaction strength. This work includes the biexciton interaction in SF dynamics and finds that it plays an important role here too. The energy shift that the biexciton interactions cause may not strongly affect fluorescence quantum beating, but if its magnitude is close to the triplet resonance integral, J_T, then the triplets will be entangled with one another,

even before the threshold where χ generates bound two-triplet states. This result has consequences for photovoltaic efficiency models that assume triplets can be extracted independently. This work takes some important first steps in constructing a theoretical understanding of SF in molecular crystals, but it is not a full and comprehensive picture of SF. To gain a tractable model, we have not included some important features in SF. Exciton dynamics in crystals occur in more than one dimension. Phonon and spin dynamics at finite temperatures are important, particularly when assessing the two-triplet entanglement and modeling the final step of SF, ${}^1(TT) \rightarrow T_1 + T_1$. Our model does, however, allow for these features to be included systematically. In addition to the density of states and coupling arguments presented above, our model and results suggest a physical picture that can help explain how exciton localization and delocalization contribute to the difference in SF yields between crystals and analogous dimers. If, as in dimers, the singlet were localized to one molecule, the two-triplet state would correspond to a triplet exciton on adjacent chromophores. The likelihood that these triplets would undergo geminate recombination back to the singlet is high. As the singlet becomes more delocalized in a crystal, the singlet has some some quantum amplitude on each chromophore and singlet fission can produce triplet pairs that are separated by more one or more chromophores. These states are less likely to annihilate one another and reform the singlet.

3.10 Acknowledgements

Paul Teichen would like to thank Mark Sweeney and the participants of Josef Michl's singlet fission workshops for many interesting conversations.

3.11 Appendix 3A - Triplet Hamiltonian Matrix Elements.

For a one-dimensional quantum lattice, the triplet Hamiltonian can be expressed with Jordan-Wigner operators as

$$H_T = \epsilon_T \sum_{n=0}^{N-1} t_n^\dagger t_n - J_T \sum_{n=0}^{N-2} \left(t_n^\dagger t_{n+1} + t_{n+1}^\dagger t_n \right) + J_T \left(t_{N-1}^\dagger t_0 + t_0^\dagger t_{N-1} \right) \Theta_N - \chi \sum_{n=0}^{N-1} t_n^\dagger t_{n+1}^\dagger t_{n+1} t_n \quad . \tag{3.62}$$

The Jordan-Wigner creation operator $t_n^\dagger$ creates a Jordan-Wigner fermion at position n. To calculate the matrix elements of the Hamiltonian in the basis of momentum states we use Wick's theorem. Here, an expectation value is expressed as a sum over all possible contractions, each which becomes a commutator (anticommutator) for bosons (fermions). Using the series representation of Θ_N, one can show that the matrix elements of the triplet Hamiltonian, with all boundary terms included, are [190, 167]

$$\begin{aligned} &\langle\, Q, r \,|H_T|\, Q', r' \,\rangle = \\ &= \frac{1}{N} \sum_{R,R'} e^{-iQRa + iQ'R'a} \langle\, R, r \,|H_T|\, R', r' \,\rangle \qquad (3.63) \\ &= 2\epsilon_T \delta_{Q,Q'} \left(\delta_{r,r'} - \delta_{r,-r'} \right) \\ &\quad - \chi\, \delta_{Q,Q'} \left(\delta_{r,1}\delta_{r,r'} - \delta_{r,1}\delta_{r,-r'} - \delta_{r,-1}\delta_{r,-r'} + \delta_{r,-1}\delta_{r,r'} \right) \\ &\quad - 2J_T \delta_{Q,Q'} cos\left(Qa/2\right) \left(\delta_{r+1,r'} + \delta_{r-1,r'} \right. \\ &\quad \left. - \delta_{r+1,-r'} - \delta_{r-1,-r'} \right) \quad , \qquad (3.64) \end{aligned}$$

and matrix elements in the basis of momentum states are

$$\begin{aligned} &\langle\, Q, q \,|H_T|\, Q', q' \,\rangle = \\ &= \frac{4}{N} \sum_{r,r'} sin\left(qra\right) sin\left(q'r'a\right) \langle\, Q, r \,|H_T|\, Q', r' \,\rangle \\ &= \delta_{Q,Q'}\delta_{q,q'} E_{TT}(Q,q) + \delta_{Q,Q'} \chi\, \zeta(q,q') \quad , \qquad (3.65) \end{aligned}$$

where the two-triplet energies and the couplings between triplet pairs, one pair with relative momentum $2q$ and one pair with relative momentum $2q'$ but each with the same center of mass

momentum, are Eqs. 3.66 and 3.67, respectively.

$$E_{TT}(Q,q) = 2\epsilon_T - 4J_T cos\big(Qa/2\big)cos(qa) \tag{3.66}$$

$$\zeta(q,q') = -\frac{4}{N} sin(qa) sin(q'a) \tag{3.67}$$

The matrix elements of the singlet fission operator are calculated in the same way, first expressing V in terms of the Jordan-Wigner operators:

$$\begin{aligned} V = &\frac{\gamma}{4}\sum_{n=1}^{N-2}\big(t_n^\dagger t_{n+1}^\dagger - t_n^\dagger t_{n-1}^\dagger\big)\mathcal{P}_n \\ &+\frac{\gamma}{4}\big[\big(t_0^\dagger t_{N-1}^\dagger + t_{N-2}^\dagger t_{N-1}^\dagger\big)\mathcal{P}_{N-1} + \big(t_0^\dagger t_1^\dagger + t_0^\dagger t_{N-1}^\dagger\big)\mathcal{P}_0\big] \quad . \end{aligned} \tag{3.68}$$

The boundary terms of the singlet-two-triplet interaction cannot be regrouped with the bulk terms and therefore the Jordan-Wigner string operators break the translational symmetry of the full electronic Hamiltonian at the boundaries of the lattice.[191, 170] As we increase the number of lattice sites the effect of this symmetry breaking decreases,[119] and matrix elements coupling a singlet with momentum k to a translationally invariant two-triplet states are

$$\begin{aligned} &\langle\ Q,r\ |V|\ k\ \rangle = \\ &= \frac{1}{\sqrt{N}}\sum_R e^{-iQRa}\langle\ R,r\ |V|\ k\ \rangle \\ &\approx \frac{\gamma}{4N}\sum_R e^{-iQRa}\sum_{m,n=0}^{N-1} e^{ikma}\langle\ 0\ |t_{R+r/2}t_{R-r/2}\cdots \\ &\qquad \cdots\big(t_n^\dagger t_{n+1}^\dagger - t_n^\dagger t_{n-1}^\dagger\big)\mathcal{P}_n\mathcal{P}_m^\dagger|\ 0\ \rangle \\ &= \frac{\gamma}{2N}\sum_R e^{-iQRa}\big(\delta_{r,1}e^{ik(R-1/2)a} - \delta_{r,-1}e^{ik(R+1/2)a}\big) \quad . \end{aligned} \tag{3.69}$$

Matrix elements in the basis of momentum states are

$$\begin{aligned} &\langle\ Q,q\ |V|\ k\ \rangle = \\ &= \frac{2}{\sqrt{N}}\sum_r sin\big(qra\big)\langle\ Q,r\ |V|\ k\ \rangle \approx \delta_{Q,k}F(Q,q) \quad , \end{aligned} \tag{3.70}$$

with the momentum form factor,

$$F(Q,q) = \frac{\gamma}{\sqrt{N}} cos\big(Qa/2\big)sin\big(qa\big) \quad . \tag{3.71}$$

For a single optically bright singlet, $\mid S \rangle$, we have

$$F(q) = \frac{\gamma}{\sqrt{N}} sin\big(qa\big) \quad . \tag{3.72}$$

For the superposition singlet state, $\mid I \rangle$, matrix elements that couple $\mid I \rangle$ to the translationally invariant two-triplet states are

$$\begin{aligned} \langle\, Q, r \,|V|\, I \,\rangle \approx \frac{\gamma}{4\sqrt{N}} \sum_R e^{-iQRa} \big[\delta_{r,1} - \delta_{r,-1}\big] \cdots \\ \cdots \big[A(R - r/2) + A(R + r/2)\big] \quad , \end{aligned} \tag{3.73}$$

with $A(n) = \sum_k A(k) e^{ikna}/\sqrt{N}$, and matrix elements that couple $\mid I \rangle$ to the momentum two-triplet states are

$$\begin{aligned} \langle\, Q, q \,|V|\, I \,\rangle \approx \frac{\gamma}{2N} sin(qa) \sum_R e^{-iQRa} \cdots \\ \cdots \big[A(R - r/2) + A(R + r/2)\big] \quad . \end{aligned} \tag{3.74}$$

3.12 Appendix 3B - Pair Distribution Functions

Using the Lippmann-Schwinger equation one can show that the two-triplet density is $\rho_2(R, r) = \big|\langle\, R, r \,|G_0(E_S)T(E_S)|\, S \,\rangle\big|^2$ and therefore the pair distribution function is

$$c^2 g(r) = \rho \int d(aR) \big|\langle\, R, r \,|G_0(E_S)T(E_S)|\, S \,\rangle\big|^2 \quad . \tag{3.75}$$

The quantum amplitude for fission to a triplet pair separated by a distance r can be written as a sum over momentum states,

$$\langle\, R, r \,|G_0 T|\, S \,\rangle \;\; = \;\; \sum_q \langle\, R, r \mid q \,\rangle \langle\, q \,|G_0 T|\, S \,\rangle \tag{3.76}$$

In the absence of biexciton interactions the quantum amplitude for fission to a triplet pair with relative momentum $2q$ is $\langle\, q \,|G_0 T|\, S \,\rangle$, which can be written in terms of the singlet self-energy as

$$\begin{aligned} \langle\, q \,|G_0 T|\, S \,\rangle = \langle\, q \,|G_0 \big[V \;\; + \;\; VG_0V \\ + \;\; VG_0VG_0V \\ + \;\; \cdots \big] |\, S \,\rangle \quad . \end{aligned} \tag{3.77}$$

Eq. 3.77 can be resummed to

$$\begin{aligned} \langle\ q\ |G_0T|\ S\ \rangle &= \\ &= \frac{\gamma}{\sqrt{N}}\frac{sin(\theta)}{E-2\epsilon_T+4J_Tcos(\theta)+i0^+}\frac{1}{1-G_0^{(S)}\Sigma_S}\quad , \end{aligned} \tag{3.78}$$

having defined the zeroth order singlet Green's function, $G_0^{(S)}(E)=[E-E_S+i0^+]^{-1}$. With this resummation we write the real-space amplitude,

$$\langle\ R,r\ |G_0T|\ S\ \rangle = \frac{\gamma}{4J_T}\frac{1}{\pi\sqrt{L}}\frac{1}{1-G_0^{(S)}(E)\Sigma_S(E)}I(r,E)\quad , \tag{3.79}$$

in terms of the integral

$$I(r,E)=\int_0^\pi d\theta\frac{sin(\theta r)sin(\theta)}{(E-2\epsilon_T)/4J_T+cos(\theta)+i0^+}\quad . \tag{3.80}$$

One-dimensional tight-binding integrals of this form have been discussed in the literature,[211, 194] and their solutions can be found using the residue theorem. Start by shifting the complex energy by $z\leftarrow(E-2\epsilon_T)/4J_T$ and make a change of variables, $u=e^{i\theta}$, such that the integral becomes a contour integral along a unit ($a=1$) semicircle in the counter-clockwise direction,

$$I=\frac{i}{4}\oint du\frac{u^{r+1}+u^{-(r+1)}-u^{1-r}-u^{r-1}}{u^2+2zu+1}\quad , \tag{3.81}$$

with two roots at $u_\pm=-z\pm\sqrt{z^2-1}$. If $z\in\mathbb{R}$ and $-1\le z\le 1$ then both roots lie on the unit circle and

$$\begin{aligned} I(r,E_S) &= \frac{\pi}{2}\frac{u_+^{1-r}+u_+^{r-1}-u_+^{r+1}-u_+^{-(r+1)}}{u_--u_+} \\ &= \frac{\pi}{2}\left(-\frac{E_S-2\epsilon_T}{4J_T}+i\sqrt{1-\left(\frac{E_S-2\epsilon_T}{4J_T}\right)^2}\right)^{-r} \\ &\quad -\frac{\pi}{2}\left(-\frac{E_S-2\epsilon_T}{4J_T}+i\sqrt{1-\left(\frac{E_S-2\epsilon_T}{4J_T}\right)^2}\right)^{r}\quad . \end{aligned} \tag{3.82}$$

When biexciton interactions are included we solve for the eigensystem of H_T numerically, and the quantum amplitude for fission to a triplet pair with relative momentum $2q$ becomes

$$\begin{aligned} \langle\ q\ |\ \alpha\ \rangle &= \sum_{\alpha'}\langle\ q\ |\ \alpha'\ \rangle\langle\ \alpha'\ |G_0T|\ S\ \rangle \\ &= \frac{1}{1-G_0^{(S)}\Sigma_S}\sum_{\alpha'}\langle\ q\ |\ \alpha'\ \rangle\frac{\langle\ \alpha'\ |V|\ S\ \rangle}{E-E'_\alpha+i0^+}\quad , \end{aligned} \tag{3.83}$$

with $H_{TT}|\ \alpha\ \rangle = E_\alpha|\ \alpha\ \rangle$.

Having calculated the quantum amplitudes, we can now write the pair distribution function as

$$c^2 g(r) = \frac{1}{2}\left|\frac{\gamma}{4J_T\pi}\frac{I(r,E_S)}{1-G_0^{(S)}(E_S)\Sigma_S(E_S)}\right|^2 \quad , \tag{3.84}$$

and therefore the static structure factor is

$$\begin{aligned} S(\theta) &= 1 + \frac{4}{L}\int d(ar)\ sin(\theta ra)\big(g(r)-1\big) \\ &= 1 + \frac{4}{L}\int d(ar)\ sin(\theta ra)\Bigg(\\ &\qquad \frac{\rho^2}{2c^2}\left|\frac{\gamma}{4J_T\pi}\frac{I(r,E_S)}{1-G_0^{(S)}(E_S)\Sigma_S(E_S)}\right|^2 - 1 \\ &\qquad\qquad \Bigg) \quad , \end{aligned} \tag{3.85}$$

3.13 Appendix 3C - Bosonification on a Square Lattice

The role of biexciton interactions and the thresholds for bound triplet pairs born out of fission have not been analyzed for two-dimensional molecular aggregates. For the larger acenes diffusion may be anisotropic. To extend our analysis to the case of a isotropic and anisotropic diffusion in two dimensions, we propose to study a square lattice model. In a discrete square lattice, the Pauli creation and destruction operators, $\mathcal{T}_{\mathbf{n}}^\dagger$ and $\mathcal{T}_{\mathbf{n}}$, respectively, create or destroy a triplet exciton on lattice site $\mathbf{n} = \big(n_x\ n_y\big)$. The mixed Bose Fermi commutation relations are

$$\big[\mathcal{T}_{\mathbf{n}}, \mathcal{T}_{\mathbf{n}'}^\dagger\big] = \delta_{\mathbf{n},\mathbf{n}'}\big[1 - 2\mathcal{T}_{\mathbf{n}'}^\dagger\mathcal{T}_{\mathbf{n}}\big] \quad , \quad \big[\mathcal{T}_{\mathbf{n}}, \mathcal{T}_{\mathbf{n}'}\big] = 0 \quad . \tag{3.86}$$

In bra-ket notation local one triplet and two triplet states are $|\ \mathbf{n}\ \rangle = \mathcal{T}_{\mathbf{n}}^\dagger|\ 0\ \rangle$, and $|\ \mathbf{m},\mathbf{n}\ \rangle = \mathcal{T}_{\mathbf{m}}^\dagger\mathcal{T}_{\mathbf{n}}^\dagger|\ 0\ \rangle$, respectively. The triplet Hamiltonian for diffusion and biexciton interactions in two dimensions is Eq. 3.87.

$$H_T = \epsilon_T\sum_{\mathbf{n}}\mathcal{T}_{\mathbf{n}}^\dagger\mathcal{T}_{\mathbf{n}} - \sum_{\langle\mathbf{m},\mathbf{n}\rangle}J(\mathbf{m},\mathbf{n})\mathcal{T}_{\mathbf{m}}^\dagger\mathcal{T}_{\mathbf{n}} - \sum_{\langle\mathbf{m},\mathbf{n}\rangle}\chi(\mathbf{m},\mathbf{n})\mathcal{T}_{\mathbf{m}}^\dagger\mathcal{T}_{\mathbf{n}}^\dagger\mathcal{T}_{\mathbf{n}}\mathcal{T}_{\mathbf{m}} \tag{3.87}$$

The hopping matrix elements and triplet-triplet interactions in the nearest-neighbor approximation are

$$J(\mathbf{m},\mathbf{n}) = J_x\delta_{m_y,n_y}\delta_{m_x,n_x\pm1} + J_y\delta_{m_y,n_y\pm1}\delta_{m_x,n_x} \tag{3.88}$$

$$\chi(\mathbf{m},\mathbf{n}) = \chi_x\delta_{m_y,n_y}\delta_{m_x,n_x\pm1} + \chi_y\delta_{m_y,n_y\pm1}\delta_{m_x,n_x} \tag{3.89}$$

The periodic boundary conditions for the triplet operators are $\mathcal{T}_{n_x,N+1} = \mathcal{T}_{n_x,1}$, $\mathcal{T}_{N+1,n_y} = \mathcal{T}_{1,n_y}$, $\mathcal{T}^\dagger_{n_x,N+1} = \mathcal{T}^\dagger_{n_x,1}$, and $\mathcal{T}^\dagger_{N+1,n_y} = \mathcal{T}^\dagger_{1,n_y}$. The energy of singlet bound states relative to the two-exciton continuum has been shown to be dependent on the orientation of the molecular dipole moments in two-dimensional aggregates. Quantum lattices of molecular dipole moments oriented either parallel to or perpendicular to the plane are used to model J and H aggregates, respectively.[190] Although the two-triplet states are dark we can classify anisotropy with J and H type lattice models. For the J type lattice we set $J_x = -J_y/2$ and $\chi_x = -\chi_y/2$ whereas for the H type lattice we set $J_x = J_y$ and $\chi_x = \chi_y$.

Paulions are hard-core bosons, and mixed Bose-Fermi commutation relations are not preserved under unitary transformations, leading to nonphysical particle statistics. Juzeli$\bar{u}$nas and Knoester[172] show that the many-boson interactions arising from the Agranovich-Toshich transformation can be approximated by a hard-core interaction. We write the triplet Pauli operators in terms of Bose operators using the Holstein-Primakov transformation for one- and two- exciton states:

$$\mathcal{T}^\dagger_{\mathbf{n}} = s^\dagger_{\mathbf{n}}\big(1 - s^\dagger_{\mathbf{n}}s_{\mathbf{n}}\big) \quad , \tag{3.90}$$

which obey the commutation relations

$$\big[s_{\mathbf{m}}, s^\dagger_{\mathbf{n}}\big] = \delta_{\mathbf{m},\mathbf{n}} \quad , \quad \big[s_{\mathbf{m}}, s_{\mathbf{n}}\big] = 0 \quad . \tag{3.91}$$

This transformation is sometimes referred to as Bosonification. After Bosonification, the triplet Hamiltonian H_T becomes $H_T = H_0 + V_{kin}$ with

$$H_0 = \epsilon_T \sum_{\mathbf{n}} s^\dagger_{\mathbf{n}}s_{\mathbf{n}} - \sum_{\langle\mathbf{m},\mathbf{n}\rangle} J(\mathbf{m},\mathbf{n})s^\dagger_{\mathbf{m}}s_{\mathbf{n}} - \sum_{\langle\mathbf{m},\mathbf{n}\rangle} \chi(\mathbf{m},\mathbf{n})s^\dagger_{\mathbf{m}}s^\dagger_{\mathbf{n}}s_{\mathbf{n}}s_{\mathbf{m}} \tag{3.92}$$

and

$$V_{kin} = -\epsilon_T \sum_{\mathbf{n}} s^\dagger_{\mathbf{n}} s^\dagger_{\mathbf{n}} s_{\mathbf{n}} s_{\mathbf{n}} + \sum_{\langle \mathbf{m},\mathbf{n} \rangle} J(\mathbf{m},\mathbf{n}) \left(s^\dagger_{\mathbf{m}} s^\dagger_{\mathbf{m}} s_{\mathbf{m}} s_{\mathbf{n}} + s^\dagger_{\mathbf{m}} s^\dagger_{\mathbf{n}} s_{\mathbf{n}} s_{\mathbf{n}} \right) \quad . \tag{3.93}$$

Juzeliūnas and Knoester have shown that, without exciton-exciton interactions, the model Hamiltonian in Eq. 3.87 is equivalent to the hard-core Boson model. Their proof involves adding large kinematic interactions to enforce the Pauli exclusion principle. The same arguments apply with the exciton-exciton interactions included, so we take

$$H_T \to H_0 + \frac{A}{2} \sum_{\mathbf{n}} s^\dagger_{\mathbf{n}} s^\dagger_{\mathbf{n}} s_{\mathbf{n}} s_{\mathbf{n}} \tag{3.94}$$

for $A \to \pm\infty$.

Chapter 4

Dynamic Fluctuations Facilitate Vibronic Energy Transfer in Light-Harvesting Antennas

4.1 Introduction

Energy that is harvested by close to a million bacteriochlorophylls (BChls) in the chlorosome of photoantennas in green sulfur bacteria is efficiently transported to a reaction center. This phenomenon has motivated research on the quantum dynamics that occur within pigment aggregates.[212] Evidence for energy transfer on subpicosecond timescales has been found in many organisms like *Chlorobium Tepidum*[213, 214] where the Fenna-Matthews-Olson (FMO) complex acts as a bridge between the chlorosome and the reaction center. The FMO complex is a trimer with each monomer composed of seven BChl molecules, shown in Fig. 4.1.

Recently, it was proposed that this ultrafast energy transfer involved purely electronic coherence between localized pigment excited states. Pigments are strongly bound to protein scaffolding,[212] and quantum dynamics simulations show that localized vibrations have prolonged coherent oscillations.[215] In the last decade there have been numerous claims that two-dimensional electronic spectroscopy (2DES) exhibits signatures of electronic coherence. Turner *et al.* modeled coherence between a ground state and one electronic excited state, each capable of supporting one quantum of vibrational energy.[216] They found that vibrational coherence displayed unique nonrephasing signatures and that coherence dephasing times are approximately 150 fs. Butkus *et al.*[217] identified pure electronic coherence not involved in energy transport with static diagonal peaks and oscillatory off-diagonal peaks, allowing for up to two quanta of vibrational energy. In 2013, Tiwari, Peters,

Figure 4.1: Diagram of a photoantenna, described in the text. The simplified composition of each constituent is shown in the dashed boxes. In the integral membrane proteins (PscA) electrons are shuffled from a primary electron acceptor derived from BChla to iron-sulfur centers. In the peripheral protein (PscB), electrons are transferred from the iron-sulfur centers to a mobile ferredoxin.

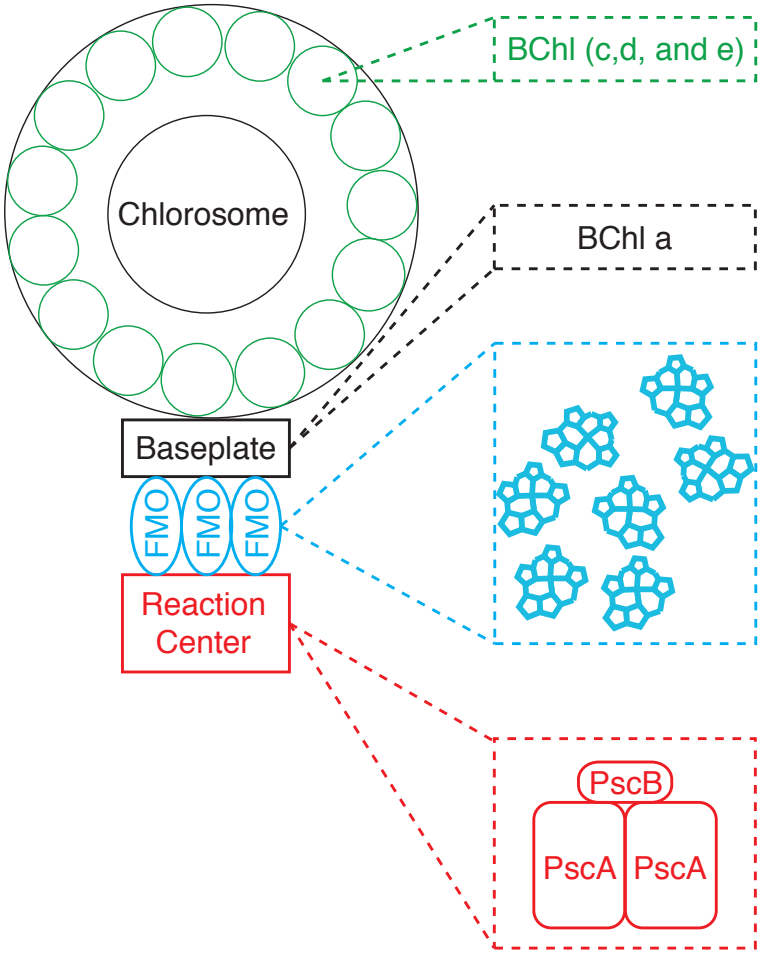

and Jonas [32] showed that a vibronic energy matching enhances pulsed laser excitation of coherence between intra-pigment vibrations. Their basic energy level diagram is shown in Fig. 4.2. The energies of electronic excitations localized at individual pigments are modulated by intra-pigment vibrations and also by fluctuations of protein scaffolding within the photoantenna. Tiwari, Peters, and Jonas[32] showed that it is only the anticorrelated linear combination of donor and acceptor intra-pigment vibrations that directly participates in the transfer of electronic energy in a static protein environment. We will refer to these vibrations hereafter as the anticorrelated vibrations. Their nonadiabatic treatment defines local potentials of each pigment by fixing the local electronic excitation and equilibrating the remaining nuclear degrees of freedom. In this chapter we consider dynamic exciton vibronic transition frequencies, and show that nonadiabatic vibrational mixing that is in phase with intra-pigment vibrations does not couple to the transfer of electronic excitation energy.

Quantum dynamics of reduced degrees of freedom can be calculated exactly for simple model spectral densities using the hierarchical equations of motion (HEOM). In Sec. 4.3 we compare non-perturbative dynamics obtained using HEOM with solutions of the Redfield equation. The HEOM does not require the secular approximation and is exact at all values of the Kubo parameter.[218] S. Jesenko *et al.* compared the HEOM and Redfield dynamics for a dimer and trimer in the presence of a thermal reservoir,[219] but did not include the anticorrelated vibrations in their quantum master equation.

Dynamic fluctuations of the protein scaffolding, which can be measured using optical anisotropy,[220, 221] can modulate the nonadiabatic coupling between electronic excitations, J, the exciton splitting between the donor and acceptor vibronic manifolds, Δ, and the stabilization energy of the intra-pigment vibrations, E_s. We model the protein scaffold as a thermal reservoir which introduces a stochastic distortion of the stabilization energy. Correlated fluctuations, where the random fluctuation of transition frequencies of one pigment depend on the transition frequencies of a neighboring pigment,[218, 221] have been simulated using molecular dynamics.[222]

The outline of the chapter is as follows: In Sec. 4.2, we define a model Hamiltonian for a

Figure 4.2: One-exciton diabatic and adiabatic energies of a dimer.[32] Donor and acceptor electronic surfaces, shown in blue and green, respectively, can support up to 2 quanta of anticorrelated vibrational energy. The bias between the donor and acceptor electronic states has been fixed at $\Delta = 150\ cm^{-1}$ with an electronic interaction between the donor and acceptor diabats of $J = 66\ cm^{-1}$. J couples the undisplaced donor and acceptor states with equivalent quanta of vibrational energy. The vibrational frequency and stabilization energy are $\omega = 200\ cm^{-1}$ and $E_s = 5\ cm^{-1}$, respectively.

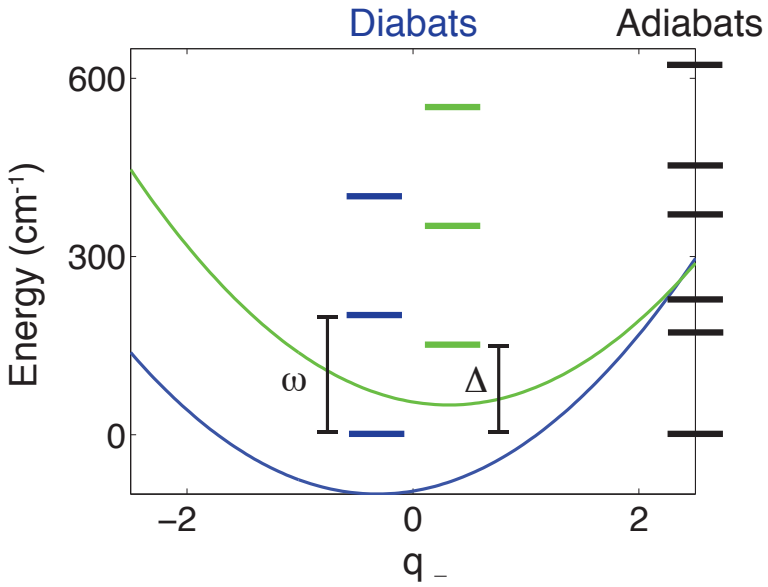

dimer of two pigments where the electronic excitation can localize on either pigment, and intra-pigment vibrations can be either correlated or uncorrelated across the dimer. We use the polaron transformation to dress the electronic coupling with the anticorrelated momentum and show that, in the polaron representation, the correlated vibration does not couple to the transfer of electronic energy. To simulate dynamic vibronic transition frequencies, we introduce a thermal reservoir that linearly couples to the electronic degrees of freedom. We show that thermal fluctuations correlated across both pigments do not activate the correlated vibration. In Sec. 4.3 we calculate coherent dynamics using the HEOM and the Redfield equation, and demonstrate that perturbation theory in the system-bath coupling well approximates the exact dynamics over a wide range of values for the Kubo parameter. In Sec. 4.4 we simulate the transfer of electronic energy from the FMO complex to the reaction center by adding an anti-Hermitian Hamiltonian that "pulls" population out of the acceptor pigment.

4.2 A Model for Photosynthetic Antennas

To model the electronic energies of a dimer of two pigments, we first localize the excitation on the donor pigment, $\mid e, g \rangle$, and equilibrate all the nuclear degrees of freedom about $\mid e, g \rangle$. The energy minimum in this diabatic configuration is E_D. Likewise, the optical transition and Franck-Condon energy of the acceptor pigment is E_A.[223] These two electronic excitations comprise a Hilbert space for the bare electronic Hamiltonian. In this basis, the electronic Hamiltonian takes the matrix form:

$$H_S := -(\Delta/2)\sigma_z + J\sigma_x \quad , \tag{4.1}$$

where Δ is the bare exciton energy gap, $\Delta = E_D - E_A$, and J is an electronic coupling attributed to Coulombic interactions between BChl pigments.[218] σ_x and σ_z are the first and third Pauli matrices. Eq. 4.1 is the generic Hamiltonian of a two-level system. We will show that anticorrelated vibrations couple to the electronic degrees of freedom as in the spin-boson model.

Correlated $(+)$ and anticorrelated $(-)$ vibrational displacements are defined in this chapter by

$q_+ = (b_+^\dagger + b_+)/\sqrt{2m\omega}$ and $q_- = (b_-^\dagger + b_-)/\sqrt{2m\omega}$, respectively, assuming each localized vibration has equivalent frequencies and stabilization energies. The total vibronic Hamiltonian that governs the energetics of the two localized electronic excitations coupled to correlated and anticorrelated vibrations is a sum of the electronic Hamiltonian with the renormalized vibrational frequencies and the electron-vibration interaction, $H_{vibronic} = H_S + H_{vib} + H_{S-vib}$, with

$$H_{vib} = \omega\big(b_-^\dagger b_- + 1/2\big) + \omega\big(b_+^\dagger b_+ + 1/2\big) + d^2/m\omega^2 \tag{4.2}$$

and

$$H_{S-vib} := -d\left(q_+\mathbf{1} + q_-\sigma_z\right) \quad . \tag{4.3}$$

$\mathbf{1}$ is the identity operator, $b_\pm$ are the vibration annihilation operators, $b_\pm = \sqrt{\frac{m\omega}{2}}\big(q_\pm + ip_\pm/m\omega\big)$, and $b_\pm^\dagger$ are their Hermitian conjugates. Tiwari, Peters, and Jonas[32] showed that it is only the anticorrelated vibrations that couples to the transfer of electronic energy. Define a Polaron transformation for the vibronic system as, $\tilde{H}_{vibronic} = e^S H_{vibronic} e^{-S}$, with

$$S := \big(i\alpha/2\big)\left(p_+\mathbf{1} + p_-\sigma_z\right) \tag{4.4}$$

and $p_\pm = i\sqrt{m\omega/2}(b_\pm^\dagger - b_\pm)$. We have abbreviated $\alpha = 2d/m\omega^2$ in Eq. 4.4. Re-sum the expansion $e^S H_{vibronic} e^{-S} = H_{vibronic} + [S, H_{vibronic}] + \frac{1}{2!}[S,[S, H_{vibronic}]] + \cdots$ to arrive at the transformed vibronic Hamiltonian:

$$\tilde{H}_{vibronic} = -(\Delta/2)\sigma_z + J\sigma_x cos(\alpha p_-) - J\sigma_y sin(\alpha p_-) + H_{vib} \quad . \tag{4.5}$$

Eq. 4.5 is a matrix representation of $\tilde{H}_{vibronic}$ in the dimer basis of electronic excited states, $\{\ |\ e,g\ \rangle, |\ g,e\ \rangle\ \}$. The electronic coupling has been dressed with vibrations,

$$J\sigma_x cos(\alpha p_-) - J\sigma_y sin(\alpha p_-) = J\begin{pmatrix} 0 & e^{i\alpha p_-} \\ e^{-i\alpha p_-} & 0 \end{pmatrix} \quad , \tag{4.6}$$

but the exciton splitting between the donor and acceptor is unchanged. We can see from Eq. 4.5 that the correlated inter-pigment vibration does not couple to the electronic degrees of freedom in the polaron representation.

In this chapter, we quantize the canonical position and momentum of the pigment vibrations. Feynman's method for disentangling operators[76] gives the normal ordered polaron operators:

$$e^{i\alpha p_-} = e^{-\alpha b_-^\dagger \sqrt{m\omega/2}}\ e^{\alpha b_- \sqrt{m\omega/2}}\ e^{-m\omega\alpha^2/4} \tag{4.7}$$

$$e^{-i\alpha p_-} = e^{\alpha b_-^\dagger \sqrt{m\omega/2}}\ e^{-\alpha b_- \sqrt{m\omega/2}}\ e^{-m\omega\alpha^2/4} \quad . \tag{4.8}$$

The diagonal elements of the electronic coupling, written in the number basis for the anticorrelated vibrations,

$$|\ \mu_-\ \rangle = \frac{(b_-^\dagger)^{\mu_-}}{\sqrt{\mu_-!}}|\ 0\ \rangle \quad , \tag{4.9}$$

where μ_- is the anticorrelated vibrational quantum number, are the Laguerre polynomials,

$$\langle\ \mu_-\ |\langle\ e,g\ |J_{DA}/J|\ g,e\ \rangle|\ \mu_-\ \rangle = e^{-m\omega\alpha^2/4} L_{\mu_-}(m\omega\alpha^2/2) \quad . \tag{4.10}$$

Eq. 4.10 describes an electronic coupling that is damped by increasing the Franck-Condon displacement of the vibrations for stabilization energies approximately equal to 5 cm^{-1}. The Laguerre polynomials are $L_0(x) = 1$, $L_1(x) = 1 - x$, and $L_2(x) = \frac{1}{2}x^2 - 2x + 1$. The coupling between the electronic degrees of freedom and the inter-pigment vibrations facilitates an energy matching that, in the polaron picture, increases the magnitude of the dressed electronic couplings:

$$\langle\ \mu_-\ |\langle\ e,g\ |J_{DA}/J|\ g,e\ \rangle|\ 0\ \rangle = e^{-m\omega\alpha^2/4}\frac{1}{\sqrt{\mu_-!}}\big(-\sqrt{m\omega/2}\ \alpha\big)^{\mu_-} \tag{4.11}$$

and

$$\begin{aligned}\langle\ \mu_-\ |\langle\ e,g\ |J_{DA}/J|\ g,e\ \rangle|\ 1\ \rangle \quad = \quad & e^{-m\omega\alpha^2/4}\Bigg[\frac{\sqrt{\mu_-!}}{(\mu_- - 1)!}\big(-\sqrt{m\omega/2}\ \alpha\big)^{\mu_- - 1} \\ & -\frac{1}{\sqrt{\mu_-!}}\big(\sqrt{m\omega/2}\ \alpha\big)^{\mu_- + 1}\Bigg] \quad .\end{aligned} \tag{4.12}$$

In Fig. 4.3 we plot the local pigment energy level diagram alongside the polaron energies fixing the stabilization energy at $E_s = 5\ cm^{-1}$ such that $m\omega\alpha^2/2 = 0.1$. We now couple the vibronic system to a thermal reservoir and explore whether or not the thermal fluctuations "activate" the correlated intra-pigment vibration.

Figure 4.3: (a) The dimer (left) and polaron (right) energies for $\Delta = 150\ cm^{-1}$ and $\omega = 200\ cm^{-1}$. (b) The dressed electronic couplings in the polaron representation as a function of the anticorrelated vibrational displacements.

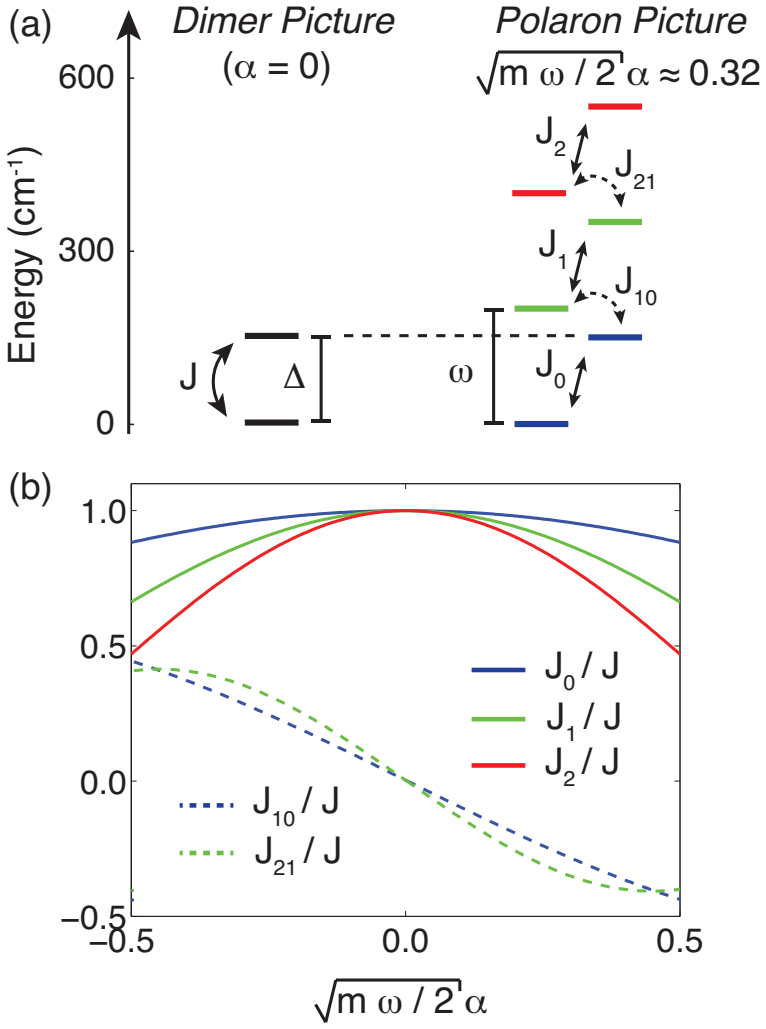

The large protein network in which the pigment dimer is embedded must reorganize when a vibronic transition occurs. If the restoring force to these transitions is approximately linear, then we can model the protein scaffold with a heat bath of harmonic oscillators. In this case, the system-bath model Hamiltonian is the sum of isolated vibronic interactions of the pigment dimer, the renormalized energies of the thermal reservoir, and the interactions between the electronic degrees of freedom and the thermal reservoir, $H = H_{vibronic} + H_B + V$. Fluctuations are correlated for vibronic transition frequencies for each pigment, and therefore two statistically independent thermal reservoirs modulate the pigment energies for a dimer, with the canonical position and momenta: $\{\ q_{j,D/A}\ ,\ p_{j,D/A}\ \}$, such that the j^{th} reservoir mode causes a variation in one of two pigment potentials, $\{\ V_{D/A}\ \}$, through

$$c_{j,D/A} = \left.\frac{\partial V_{D/A}\big(\{q_{k,D/A}\}\big)}{\partial q_{j,D/A}}\right|_{\{q_{k,D/A}\}=\{0\}} \quad , \tag{4.13}$$

abbreviating the equilibrium configuration of the reservoir with $\{0\}$. For small variations about this equilibrium, the interaction Hamiltonian can be written as

$$V = -\sum_j \begin{pmatrix} c_{j,D}q_{j,D} & 0 \\ 0 & c_{j,A}q_{j,A} \end{pmatrix} \quad . \tag{4.14}$$

The renormalized bath frequencies are contained in the bath Hamiltonian, H_B, such that

$$H_B + V = \begin{pmatrix} \sum_j \frac{p_{j,D}^2}{2m_j} + \frac{m_j\omega_j^2}{2}\big(q_{j,D} - \frac{c_{j,D}}{m_j\omega_j^2}\big)^2 & 0 \\ 0 & \sum_j \frac{p_{j,A}^2}{2m_j} + \frac{m_j\omega_j^2}{2}\big(q_{j,A} - \frac{c_{j,A}}{m_j\omega_j^2}\big)^2 \end{pmatrix} \quad , \tag{4.15}$$

which describes a bath in thermal equilibrium. $H_B + V$ is invariant under the polaron transformation:

$$\tilde{H}_B + \tilde{V} = H_B + V \quad . \tag{4.16}$$

The total Hamiltonian in the polaron picture shows that the correlated intra-pigment vibrations decouple from the dynamical picture of vibronic energy transfer,

$$\tilde{H} = -(\Delta/2)\sigma_z + J\sigma_x cos(\alpha p_-) - J\sigma_y sin(\alpha p_-) + H_{vib} + H_B + V \tag{4.17}$$

The spectral density that defines the distribution of couplings between the electronic excitation localized at $\mid e,g \rangle$ and the thermal reservoir is

$$J_D(\omega) = \frac{\pi}{2}\sum_j \frac{\left(c_{j,D}\right)^2}{m_j\omega_j}\delta(\omega-\omega_j) \quad . \tag{4.18}$$

Similarly, for the acceptor pigment we have

$$J_A(\omega) = \frac{\pi}{2}\sum_j \frac{\left(c_{j,A}\right)^2}{m_j\omega_j}\delta(\omega-\omega_j) \quad . \tag{4.19}$$

The reorganization energy for the $D(A)$ pigment renormalizes the local pigment energy of $\mid e,g \rangle(\mid g,e \rangle)$. Each reorganization energy can be calculated from the corresponding spectral density:[223]

$$\lambda_{D/A} = \frac{1}{2}\sum_j \frac{\left(c_{j,D/A}\right)^2}{m_j\omega_j^2} = \frac{1}{\pi}\int_0^\infty d\omega \frac{J_{D/A}(\omega)}{\omega} \quad . \tag{4.20}$$

The time correlation function for harmonic motion equilibrated about the m^{th} pigment is

$$C_m(t) = \left\langle \sum_{j,k} c_{j,m}q_{j,m}(t)c_{k,m}q_{k,m}(0)\right\rangle_B = \frac{\hbar}{\pi}\int_{-\infty}^\infty d\omega J_m(\omega)\big(n(\omega)+1\big)e^{-i\omega t} \quad , \tag{4.21}$$

corresponding to the frequency correlation function,

$$\hat{C}_m[\omega] = \int_0^\infty dt e^{i\omega t}C_m(t) = \hbar J_m(\omega)\big[n(\omega)+1\big] + \frac{i\hbar}{\pi}PP\int_{-\infty}^\infty d\omega' \frac{J_m(\omega')\big[n(\omega')+1\big]}{\omega-\omega'} \tag{4.22}$$

with $n(\omega) = \left(e^{\beta\hbar\omega}-1\right)^{-1}$. A Peierls-like coupling can be written as

$$C_{m,n}(t) = \left\langle \sum_{j,k} c_{j,m}q_{j,m}(t)c_{k,n}q_{k,n}(0)\right\rangle_B = \frac{\hbar}{\pi}\int_{-\infty}^\infty d\omega J_{m,n}(\omega)\big(n(\omega)+1\big)e^{-i\omega t} \quad . \tag{4.23}$$

The imaginary part of $\hat{C}[\omega]$ modifies the vibronic transition frequencies and is essential for correctly accounting for the phonon equilibrium.[88, 224] When the electronic coupling is of the same order of magnitude as typical reorganization energies, it is unclear whether dissipation will be coherent or incoherent, and which energy scale, if any, can be treated perturbatively.

4.3 Vibronic Energy Transfer

4.3.1 The HEOM and Redfield Theory

In this section we review key aspects of the HEOM and Redfield theory in Liouville space, where the elements of the density matrix compose a vector, $\rho \rightarrow \mid \rho \rangle\rangle$, and the density matrix

propagates according to $|\ \rho(t)\ \rangle\rangle = \mathscr{U}(t)|\ \rho(0)\ \rangle\rangle$ with the Liouville space propagator $\mathscr{U}(t) = e^{-i\mathscr{L}t}$. The Liouville operator corresponds to the commutator in Hilbert space, $\mathscr{L}A \leftrightarrow [H, A]$, and dictates the quantum dynamics in the interaction representation through the Liouville equation: $\frac{d}{dt}|\ \hat{\rho}(t)\ \rangle\rangle = -i\epsilon\hat{\mathscr{L}}_V(t)|\ \hat{\rho}(t)\ \rangle\rangle$, where the density matrix in the interaction representation is $|\ \hat{\rho}(t)\ \rangle\rangle = \mathscr{U}_0^\dagger(t)|\ \rho(t)\ \rangle\rangle$. The perturbative Liouville operator is $\hat{\mathscr{L}}_V(t) = \mathscr{U}_0^\dagger(t)\mathscr{L}_V\mathscr{U}_0(t)$ with $\mathscr{U}_0(t) = e^{-i\mathscr{L}_0 t}$. ϵ is a parameter whose numerical value is 1 but will order a perturbation expansion for the coupling between the vibronic system and the thermal reservoir. Inner products in Liouville space correspond to trace operations in Hilbert space: $\langle\langle\ A\ ||\ B\ \rangle\rangle \leftrightarrow Tr[A^\dagger B]$ and $\langle\langle\ i,j\ |\mathscr{L}|\ k,l\ \rangle\rangle \leftrightarrow Tr\big[|\ j\ \rangle\langle\ i\ |[H,|\ k\ \rangle\langle\ l\ |]\big]$.

If the bath dephasing time, $1/2\pi\Lambda$, is fast relative to the energy transfer, we can approximate the initial density matrix with the factorized initial condition,[225, 226, 227] $|\ \rho(t_0)\ \rangle = \rho_B|\ \sigma(t_0)\ \rangle\rangle$, where ρ_B is the canonical ensemble for a bath of harmonic oscillators. In this chapter we use this factorization at all times, $|\ \rho(t)\ \rangle\rangle = \rho_B|\ \sigma(t)\ \rangle\rangle$. Before the pump pulse interacts with the chemical system, $\sigma(t_0) = |\ g,g\ \rangle\langle\ g,g\ |$. In the dipole approximation, the light-matter interaction is $-ME(t)$, where the dipole operator is $M = \mu|\ g,g\ \rangle\langle\ e,g\ | + \mu^*|\ e,g\ \rangle\langle\ g,g\ |$. After an impulsive pump, the first order change to the density matrix is proportional to $|\ e,g\ \rangle\langle\ g,g\ | + |\ g,g\ \rangle\langle\ e,g\ |$, but this would violate positivity to second order. Valkunas[228] uses the augmented density matrix:

$$\sigma(t_0) = \frac{1}{2}\Big(|\ g,g\ \rangle\langle\ g,g\ | + |\ e,g\ \rangle\langle\ e,g\ | + |\ e,g\ \rangle\langle\ g,g\ | + |\ g,g\ \rangle\langle\ e,g\ |\Big)\ . \tag{4.24}$$

Eq. 4.24 is a perfect coherent superposition as achieved by a $\pi/2$ pulse. A typical ad hoc initial condition for simulations of excited state quantum dynamics is[83, 229] $\sigma(t_0) = |\ e,g\ \rangle\langle\ e,g\ |$. In this chapter, we approximate the initial conditions of the system with an incoherent distribution of population, with anywhere from 0 to 2 quanta of anticorrelated vibrational energy. Our simulated dynamics cannot describe phase-controlled interference observed with heterodyne-detection.[230] We are now in a position to directly contrast exact and perturbative simulations of quantum dynamics.

4.3.1.1 The HEOM.

At low temperatures and when $\kappa > 1$, we expect perturbation theory in the coupling between the vibronic system and the thermal reservoir to poorly approximate the true coherent dynamics. To quantify the error in solutions of the Redfield equation, described in the next section, we consider first the HEOM which is exact to an arbitrary level of hierarchy for specific model spectral densities like that of the overdamped Brownian oscillator model. In the absence of dissipation, the vibronic system propagates forward in time through the vibronic propagator $U_{vibronic}(t,t_0) = e^{-i(t-t_0)H_{vibronic}}$,

$$| \psi(t) \rangle = U_{vibronic}(t,t_0)| \psi(0) \rangle \quad , \tag{4.25}$$

having chosen $\hbar = 1$. Following conventional derivations of the HEOM,[231, 232] we define an arbitrary basis of the vibronic system for the path integral representation,[233, 234, 235, 6] x, and write the finite time kernel as a product of short-time kernels:

$$\begin{aligned} U_{vibronic}(x_t,x_0;t-t_0) &= \langle\, x_t \,|U_{vibronic}(t,t_0)|\, x_0 \,\rangle & (4.26)\\ &= \left[\prod_{j=1}^{N-1}\int_{-\infty}^{\infty} dx_j\right]\left[\prod_{j=0}^{N-1} K(x_{j+1},x_j;\Delta t)\right] & (4.27)\\ &= \mathcal{N}\int_{x(t_0)=x_0}^{x(t)=x_t}\mathcal{D}[x(\tau)]\exp\Big[iS[x(\tau);t,t_0]\Big] \quad , & (4.28) \end{aligned}$$

implicitly defining the initial and final points as $x_i = x_0$ and $x_f = x_t$, respectively, and

$$\begin{aligned} \int_{x(t_0)=x_0}^{x(t)=x_t}\mathcal{D}[x(\tau)] &= \lim_{N\to\infty}\left[\prod_{j=1}^{N-1}\int_{-\infty}^{\infty} dx_j\right] & (4.29)\\ \int \mathcal{D}[p(\tau)/2\pi] &= \lim_{N\to\infty}\left[\prod_{j=0}^{N-1}\int_{-\infty}^{\infty} dp_j/2\pi\right] \quad , & (4.30) \end{aligned}$$

where, in the continuum limit, the normalization constant is $\mathcal{N} = \int \mathcal{D}[p(\tau)/2\pi]$.

Define the zeroth order Hamiltonian as the spectrum of reservoir harmonic frequencies, $H_0 = H_B$. The dynamic coupling in the interaction representation is

$$V(t) = e^{iH_Bt}Ve^{-iH_Bt} = -\sum_j \begin{pmatrix} c_{j,D}q_{j,D}(t) & 0 \\ 0 & c_{j,A}q_{j,A}(t) \end{pmatrix} \quad , \tag{4.31}$$

where $q_{j,D/A}(t)$ and $p_{j,D/A}(t)$ are the dynamical position and momentum of the j^{th} bath mode in reservoir (D/A), $q_{j,D/A}(t) = q_{j,D/A}cos(\omega_j t) + \frac{p_{j,D/A}}{m_j\omega_j}sin(\omega_j t)$ and $p_{j,D/A}(t) = p_{j,D/A}cos(\omega_j t) - m_j\omega_j q_{j,D/A}sin(\omega_j t)$, respectively. Eq. 4.31 is often abbreviated as

$$V(t) = \sum_m \mathbf{1}_m F_m(t) \tag{4.32}$$

with $\mathbf{1}_D = \mid e,g \rangle\langle e,g \mid$, $\mathbf{1}_A = \mid g,e \rangle\langle g,e \mid$, and $F_m(t) = -\sum_j c_{j,m}q_{j,m}(t)$. We can approximate the case of fully uncorrelated fluctuations, where the dynamics of each vibronic transition frequency are independent of all others, keeping only the anticorrelated vibrations, and writing

$$V(t) = -\sum_\mu \mid \mu \rangle\langle \mu \mid \sum_j \begin{pmatrix} c_{j,D,\mu}q_{j,D,\mu}(t) & 0 \\ 0 & c_{j,A,\mu}q_{j,A,\mu}(t) \end{pmatrix} \tag{4.33}$$

Eq. 4.33 is an ad hoc form of the interaction, and we have not yet determined whether or not fully uncorrelated fluctuations activate the correlated intra-pigment vibration.

The density matrix in the interaction representation, defined by $\mathscr{L}_V A \leftrightarrow [H_{vibronic} + V, A]$, propagates forward in time as

$$\mid \hat{\rho}(t) \rangle\rangle = \mathscr{U}_V(t,t_0;\{F_m(t)\})\mid \hat{\rho}(t_0) \rangle\rangle \quad , \tag{4.34}$$

where the time evolution operator factorizes into a product of the Hermitian conjugate of the bath operator, $\mathscr{U}_B^\dagger(t,t_0)$, and the full time evolution operator, $\mathscr{U}(t,t_0;\{F_m(t)\})$ such that $\mid \rho(t) \rangle\rangle = \mathscr{U}(t,t_0;\{F_m(t)\})\mid \rho(t_0) \rangle\rangle$:

$$\mathscr{U}_V(t,t_0;\{F_m(t)\}) = \mathscr{U}_B^\dagger(t,t_0)\mathscr{U}(t,t_0;\{F_m(t)\}) \tag{4.35}$$

To compute $\mathscr{U}_V(t,t_0;\{F_m(t)\})$, start by writing its derivative,

$$\frac{d}{dt}\mathscr{U}_V(t,t_0;\{F_m(t)\}) = -i\epsilon\hat{\mathscr{L}}_V(t,t_0)\mathscr{U}_V(t,t_0;\{F_m(t)\}) \quad , \tag{4.36}$$

which can be integrated using a time ordered exponential,

$$\mathscr{U}_V(t,t_0;\{F_m(t)\}) = T_+ exp\Big[-i\epsilon\int_{t_0}^{t} d\tau\hat{\mathscr{L}}_V[\{F_m(\tau)\};\tau]\Big] \quad . \tag{4.37}$$

If $|\ \rho(t_0)\ \rangle\rangle = \rho_B|\ \sigma(t_0)\ \rangle\rangle$, then the reduced density matrix can be calculated by operating from the left with the projection operator P,

$$P|\ \rho(t)\ \rangle\rangle = \rho_B|\ \sigma(t)\ \rangle\rangle = P\mathscr{U}_V(t,t_0;\{F_m(t)\})\rho_B|\ \sigma(t_0)\ \rangle\rangle \quad , \tag{4.38}$$

where the nuclear equilibrium density is $\rho_B = e^{-\beta H_B}/Z_B$. Through Eq. 4.38, we see that the time evolution operator of the reduced density matrix is

$$\mathscr{U}_\sigma(t,t_0;\{F_m(t)\}) = \rho_B^{-1}P\mathscr{U}_V(t,t_0;\{F_m(t)\})\rho_B \quad , \tag{4.39}$$

which corresponds to the Hilbert space reduced density matrix,[236, 231]

$$\sigma(t) = \left\langle U(t,t_0;\{F_m(t-i\beta)\})\sigma(0)U^\dagger(t,t_0;\{F_n(t)\})\right\rangle \quad . \tag{4.40}$$

$U(t,t_0;\{F_m(t)\})$ is the full time evolution operator, defined through $\rho(t) = U(t,t_0;\{F_m(t)\})\rho(0)$. The reservoir operators transform as $F_m(t-i\beta) = e^{\beta H_B}F_m(t)e^{-\beta H_B}$. In the path integral formulation of Eq. 4.38,

$$\begin{aligned}\langle\langle\ x_t, x_t'\ |\mathscr{U}_\sigma(t,t_0)|\ x_0, x_0'\ \rangle\rangle = \int_{x(t_0)=x_0}^{x(t)=x_t}\mathcal{D}[x]\int_{x'(t_0)=x_0'}^{x'(t)=x_t'}\mathcal{D}[x']\cdots \\ \cdots\exp\Big[iS[x;t,t_0]\Big]\mathscr{F}\left[x,x'\right]\exp\Big[-iS[x';t,t_0]\Big] \quad ,\end{aligned} \tag{4.41}$$

with the influence functional

$$\begin{aligned}\mathscr{F}[x,x'] \ &= \\ &= \left\langle T_+\exp\Big[-i\epsilon\sum_m\int_{t_0}^t d\tau\mathbf{1}_m[x(\tau)]F_m(\tau-i\beta)\Big]T_-\exp\Big[i\epsilon\sum_n\int_{t_0}^t d\tau\mathbf{1}_n[x'(\tau)]F_n(\tau)\Big]\right\rangle \quad .\end{aligned} \tag{4.42}$$

The hierarchy is now constructed by differentiating Eq. 4.41, ordering terms by powers of ϵ, expanding the bath correlation function in a series of exponential functions,

$$C_m(t) = \sum_{k=0}^{\infty}c_k^{(m)}e^{-\nu_k^{(m)}t} \tag{4.43}$$

and then closing the hierarchical equations of motion through truncation.[231] The Matsubara frequencies are $\nu_0^{(m)} = \Lambda_m$ and $\nu_{k\geq1}^{(m)} = 2\pi k/\beta$. When using the model spectral density for the overdamped Brownian oscillator, $J_m(\omega) = 2\lambda_m\Lambda_m\frac{\omega}{\omega^2+\Lambda_m^2}$ with the cutoff frequency of the bath defined

as Λ_m. The expansion coefficients for the correlation function are $c_0^{(m)} = \frac{2\Lambda_m\lambda_m}{2}\left[cot\left(\beta\Lambda_m/2\right) - i\right]$ and $c_{k\geq 1}^{(m)} = \frac{4\lambda_m\Lambda_m}{\beta}\left(\frac{\nu_k^{(m)}}{{\nu_k^{(m)}}^2 - \Lambda_m^2}\right)$. Details of the HEOM using the spectral density for the overdamped Brownian oscillator can be found elsewhere.[231, 232] Although the HEOM has the advantage of being numerically exact, it is computationally expensive. In the next section we review the Redfield equation and its solutions.

4.3.1.2 Redfield Theory.

Solutions of the Redfield equation should well approximate the true coherent dynamics when $0 < \kappa_m < 1$ for all m, where κ_m is the Kubo parameter for the m^{th} pigment, $\kappa_m = \lambda_m/\Lambda_m$.[88, 237] Coherence can be relaxed by population decay or from system-bath induced frequency shifts in the system. The latter is referred to as "pure dephasing". Redfield theory is derived by invoking the Markovian approximation such that phonons relax to their equilibrium instantaneously, and $C(t) \to 0$ as $t \to \infty$ faster than any characteristic timescale of the system for each pigment.

Unlike the derivation of the HEOM, define an interaction representation through the zeroth order Hamiltonian: $H - V$. In this case the interaction Liouville operator is defined by $\mathscr{L}_V A \leftrightarrow [V, A]$. In a previous publication, we show that the exact solution of the reduced density operator in the interaction representation is[106]

$$\begin{aligned}\frac{d}{dt}P|\ \hat{\rho}(t)\ \rangle\rangle \quad &= \quad -i\epsilon P\hat{\mathscr{L}}_V(t)P|\ \hat{\rho}(t)\ \rangle\rangle \\ &\quad -i\epsilon P\hat{\mathscr{L}}_V(t)\big(1-\Sigma(t)\big)^{-1}\Big(\mathscr{G}_Q^+(t,0)Q|\ \hat{\rho}(0)\ \rangle\rangle + \Sigma(t)P|\ \hat{\rho}(t)\ \rangle\rangle\Big) \qquad (4.44)\end{aligned}$$

with

$$\Sigma(t) = -i\epsilon\int_0^t d\tau\mathscr{G}_Q^+(t,\tau)Q\hat{\mathscr{L}}_V(\tau)Pg_-(t,\tau) \quad , \qquad (4.45)$$

and the forward and reverse propagators,

$$\mathscr{G}_Q^+(t,\tau) = T_+e^{-i\epsilon Q\int_\tau^t ds\hat{\mathscr{L}}_V(s)} \quad , \qquad (4.46)$$

and

$$g_-(t,\tau) = T_-e^{i\epsilon\int_\tau^t ds\hat{\mathscr{L}}_V(s)} \quad , \qquad (4.47)$$

respectively. One can show that the quantum master equation for the reduced operator, dropping the inhomogeneous term, can be written in the time local form,[106]

$$\frac{d}{dt}P|\ \hat{\rho}(t)\ \rangle\rangle = -i\epsilon P\hat{\mathscr{L}}_V(t)P|\ \hat{\rho}(t)\ \rangle\rangle - i\epsilon^2 P\hat{\mathscr{L}}_V(t)\int_0^t d\tau\hat{\mathscr{L}}_V(\tau)P|\ \hat{\rho}(\tau)\ \rangle\rangle + \mathscr{O}(\epsilon^3) \quad (4.48)$$

The second order term in the ϵ expansion has the Liouville/Hilbert space correspondence:

$$P\hat{\mathscr{L}}_V(t)\int_0^t d\tau\hat{\mathscr{L}}_V(\tau)P|\ \hat{\rho}(\tau)\ \rangle\rangle \leftrightarrow \rho_B\int_0^t d\tau Tr_B\Big(\big[\hat{V}(t),[\hat{V}(\tau),\rho_B Tr_B\big(\hat{\rho}(\tau)\big)]\big]\Big)\ . \quad (4.49)$$

If the bath dynamics are much faster than those of the system, the Markovian approximation is valid, and the quantum master equation to second order in ϵ is the Redfield equation,

$$\frac{\partial}{\partial t}\sigma_{j,k}(t) = -i\omega_{j,k}\sigma_{j,k}(t) + \sum_{j',k'} R_{j,k;j',k'}\sigma_{j',k'}(t)\quad , \quad (4.50)$$

with the relaxation superoperator, R, defined as

$$R_{j,k;j',k'} = \Gamma_{k',k,j,j'} + \Gamma^*_{j',j,k,k'} - \delta_{k',k}\sum_l \Gamma_{j,l,l,j'} - \delta_{j',j}\sum_l \Gamma^*_{k,l,l,k'}\quad . \quad (4.51)$$

Eq. 4.50 is the equation of motion for elements of the reduced density operator in the vibronic eigenbasis, $H_{vibronic}|\ j\ \rangle = E_j|\ j\ \rangle$. Populations can be represented in the local pigment basis:

$$\begin{aligned}\sigma_{D,\mu_-}(t) &= \langle\ \mu_-\ |\langle\ e,g\ |\sigma(t)|\ e,g\ \rangle|\ \mu_-\ \rangle & (4.52)\\ &= \sum_{j,k}\langle\ \mu_-\ |\langle\ e,g\ ||\ j\ \rangle\sigma_{j,k}(t)\langle\ k\ ||\ e,g\ \rangle|\ \mu_-\ \rangle & (4.53)\end{aligned}$$

Likewise for the coherences,

$$\sigma_{D,\mu_-;A,\nu_-}(t) = \sum_{j,k}\langle\ \mu_-\ |\langle\ e,g\ ||\ j\ \rangle\sigma_{j,k}(t)\langle\ k\ ||\ g,e\ \rangle|\ \nu_-\ \rangle\quad . \quad (4.54)$$

Recall that μ_- is the anticorrelated vibrational quantum number. The trace property of the reduced density operator is invariant under unitary transformations:

$$Tr\big[\sigma(t)\big] = Tr\big[e^S\sigma(t)e^{-S}\big]\quad . \quad (4.55)$$

The frequency correlation function is

$$\Gamma_{j,k;j',k'} = \sum_{m,n}\sum_{\mu_-,\nu_-}\langle\ j\ ||\ \mu_-\ \rangle\mathbf{1}_m\langle\ \mu_-\ ||\ k\ \rangle\langle\ j'\ ||\ \nu_-\ \rangle\mathbf{1}_n\langle\ \nu_-\ ||\ k'\ \rangle\hat{C}^{(\mu_-,\nu_-)}_{m,n}[\omega_{k',j'}] \quad (4.56)$$

For fluctuations which are intra-pigment correlated, $\hat{C}^{(\mu_-,\nu_-)}_{m,n}[\omega] = \delta_{m,n}\hat{C}[\omega]$. Our approximate treatment of fully uncorrelated fluctuations of vibronic transitions involving only anticorrelated vibrations corresponds to frequency correlation functions of the form:[238, 239]

$$\hat{C}^{(\mu_-,\nu_-)}_{m,n}[\omega] = \delta_{m,n}\delta_{\mu_-,\nu_-}\hat{C}[\omega] \quad . \tag{4.57}$$

As a first approximation we decouple the dynamics of the populations and the dynamics of the coherences. This is known as the secular approximation. We will test the validity of these approximations by comparing the simulated dynamics calculated using Redfield theory and the HEOM directly. The HEOM are truncated at $k = 3$ (4 Matsubara terms) and 7 levels of hierarchy. The HEOM are integrated with the Runge-Kutta-Fehlberg 4/5 adaptive integrator and with time local truncation.[232]

One might expect the energy fluctuations of neighboring pigments to be correlated if the wavelength of the protein motion is much longer than the inter-pigment separation.[223] In 2012, Gelin *et al.*[240] considered a heat bath that induced correlated fluctuations in the local intra-pigment vibrations directly. These fluctuations were uncorrelated from the perspective of the electronic excitation, and the dynamics of $\langle q_+ \rangle(t)$ were only damped by correlated fluctuations while $\langle q_- \rangle(t)$ were only damped by anticorrelated fluctuations. We have shown that for intra-pigment correlated fluctuations, it is only the anticorrelated vibration that couples to the transfer of electronic energy. In Fig. 4.4 we plot the population of the donor pigment with 0 quanta of anticorrelated vibrational energy, fixing the initial population of $|\, e, g \,\rangle|\, 0 \,\rangle$, and also plot the donor population for a dimer exciton model in the absence of any pigment vibrations. In Fig. 4.5 we plot the total population in the acceptor manifold of vibronic states, $|\, g, e \,\rangle|\, 0 \,\rangle$, $|\, g, e \,\rangle|\, 1 \,\rangle$, and $|\, g, e \,\rangle|\, 2 \,\rangle$.

To explore the role of vibrational relaxation in vibronic energy transfer, we next examine simulations of fully uncorrelated fluctuations, $\hat{C}^{(\mu,\nu)}_{m,n}[\omega] = \delta_{m,n}\delta_{\mu,\nu}\hat{C}[\omega]$. In Fig. 4.6 we compare the dynamics of the donor pigment with different quanta of vibrational energy. The populations in Fig. 4.6 are not the total population in the donor manifold of states, but rather the decay of

Figure 4.4: The population of the donor state, $\mid e, g \rangle \mid 0 \rangle$, described in the text, computed using the HEOM and an exciton model in black, and the Redfield theory with the polaron model in blue. The Kubo parameter has been fixed at $\kappa = 0.05$ (a) and $\kappa = 0.8$ (b). The frequency cutoff has been fixed at $\Lambda = 50\ cm^{-1}$. Fluctuations are intra-pigment correlated, with $\hat{C}^{(\mu,\nu)}_{m,n}[\omega] = \delta_{m,n}\hat{C}[\omega]$.

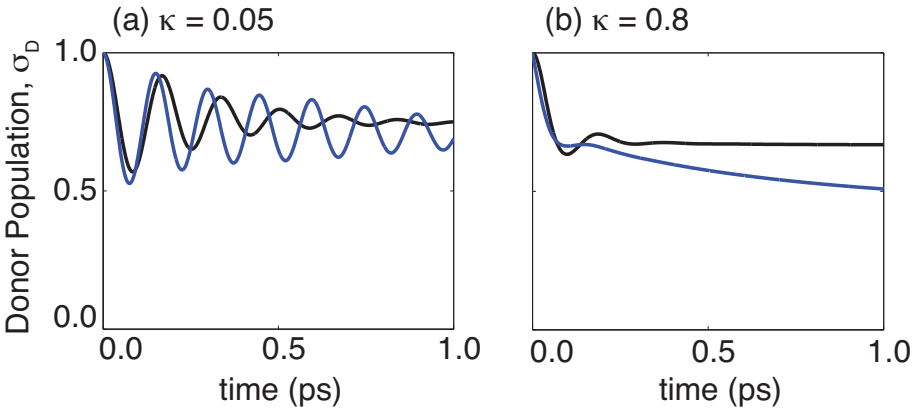

Figure 4.5: The total population of the acceptor state, $\mid g, e \rangle$, described in the text. The Kubo parameter has been fixed at $\kappa = 0.05$ (a) and $\kappa = 0.8$ (b).

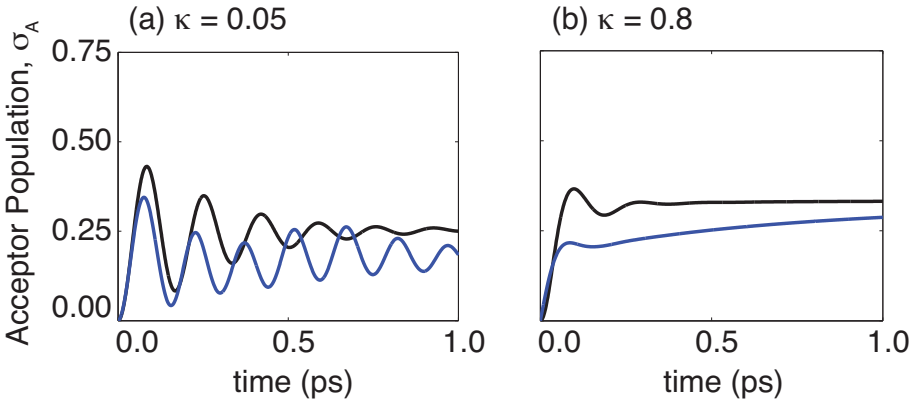

the initial excitation for different choices of initial conditions. We can see from Fig. 4.6 that the

Figure 4.6: The population of the donor state, $\mid e, g \rangle$, with either 0, 1, or 2 quanta of anticorrelated vibrational energy shown in blue, green, and red solid curves, respectively, all computed using the HEOM. The Kubo parameter has been fixed at $\kappa = 0.05$ (a) and $\kappa = 0.8$ (b). The frequency cutoff has been fixed at $\Lambda = 50\ cm^{-1}$. The Redfield dynamics are shown with dashed curves. The exciton dynamics for a dimer without pigment vibrations are shown in black.

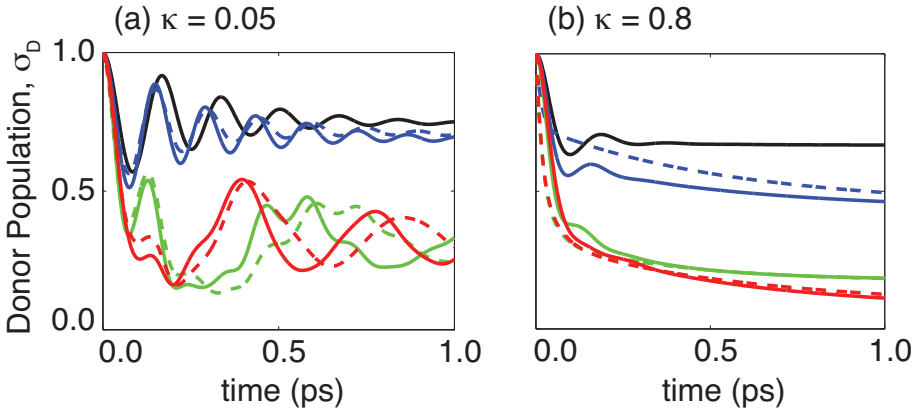

initial relaxation is more rapid for systems initially prepared with anticorrelated vibrational energy. Rapid vibrational cooling is followed by stronger amplitude and longer period quantum beating. The damping of these oscillations increases as the Kubo parameter increases. The Redfield and HEOM are in qualitative agreement, with the Redfield theory missing short-time oscillations for large values of the Kubo parameter. The total population in the acceptor, $\mid g, e \rangle$, corresponding to the calculations shown in Fig. 4.6, is shown in Fig. 4.7. We can see from Fig. 4.7 that the decay of the initial population strongly correlates with the rise of total population in the acceptor manifold of vibronic states. Both the HEOM and the Redfield theory predict increased population in the acceptor pigment when the energy of the initial population increases. For low values of the Kubo parameter, the HEOM and the Redfield theory give similar rates at which σ_A initially rises within $\approx 200\ fs$. As the Kubo parameter increases, the initial rise times predicted by the Redfield theory for 1 and 2 quanta of initial vibrational energy are faster than those calculated from the HEOM, and the short-time quantum beating is more strongly damped for $\sigma(0) = \mid e, g \rangle \mid 0 \rangle \langle 0 \mid \langle e, g \mid$.

Figure 4.7: The total population of the acceptor state, $\mid g, e \rangle$ where the system is prepared with 0, 1, and 2 quanta of anticorrelated vibrational energy in the blue, green, and red solid curves, respectively, computed using the HEOM. The Kubo parameter has been fixed at $\kappa = 0.05$ (a) and $\kappa = 0.8$ (b). The corresponding Redfield theory results are shown with dashed curves.

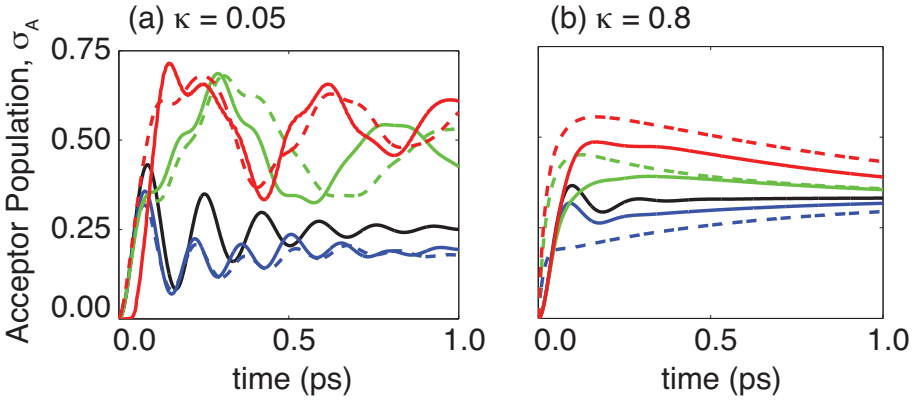

4.4 Zeno and Anti-Zeno Effects

Mohseni *et al.*[213] modeled FMO as a linear array of chromophores, and approximated the initial conditions as a mixture of population at the pigments in contact with the baseplate and reaction center.[213, 241] In our dimer model we can represent the transfer of electronic excitation from the FMO complex to the reaction center as transfer out of the $\mid g, e \rangle$ manifold of vibronic states. Although electronic energy flows to the reaction center, it may do so through pigment intermediates[92], as is illustrated in Fig. 4.8. This "out-transfer" can be modeled as

Figure 4.8: (a) Sketch of the FMO complex with the donor and acceptor pigments shown in blue and green, respectively. (b) An energy level diagram corresponding to the FMO complex in (a), with transfer to either pigments 3 or 4 or the reaction center modeled with a trapping rate, Γ.

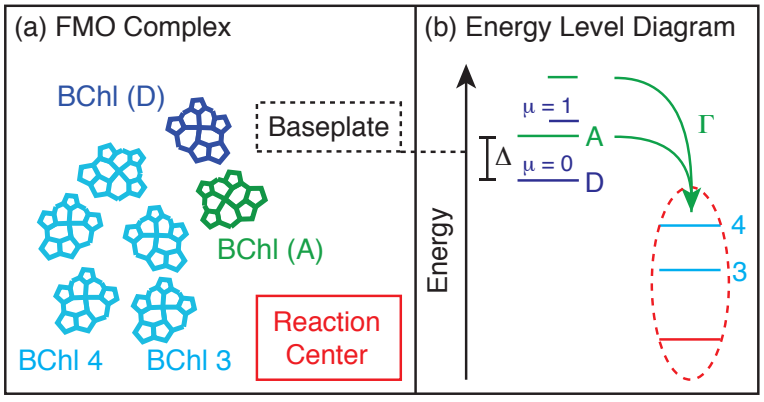

$H = H_{vibronic} + H_B + V + H_{out}$, with an anti-Hermitian operator,[242, 213]

$$H_{out} = -i\Gamma \mid g, e \rangle\langle g, e \mid \quad . \tag{4.58}$$

Transfer out of $\mid g, e \rangle$ is analogous to the short-time measurement of qubits, where increased measurement rates have been known to inhibit decay (the Zeno effect). Conversely, the anti-Zeno effect refers to the enhanced decay when the measurement rate is increased. In Fig. 4.9 we plot the dynamics of the populations calculated using Redfield theory for various out-transfer rates, Γ/Λ. From Fig. 4.9 we see that as Γ/Λ increases, the ratio of total population in the acceptor to the total population in the donor decreases on picosecond timescales. This may suggest a type of Zeno effect,[241] but the rate of transfer from $\mid e, g \rangle$ to $\mid g, e \rangle$ is invariant to changes in Γ/Λ, and

Figure 4.9: The total population of the acceptor state described in the text. The transfer rate out of the acceptor has been fixed at $\Gamma/\Lambda = 1$, 0.1, and 0.01 in blue, green, and red, respectively. Every vibronic splitting is dynamic and is modulated by an independent thermal reservoir using the Redfield theory, plotted in solid lines. Fluctuations in the vibronic splittings are then correlated for each pigment for the dashed lines. The vibronic system initially contains 0 and 1 quantum of anticorrelated vibrational energy in (a) and (b). The ratio of acceptor to donor populations, σ_B/σ_A, corresponding to (a) and (b) are shown in (c) and (d).

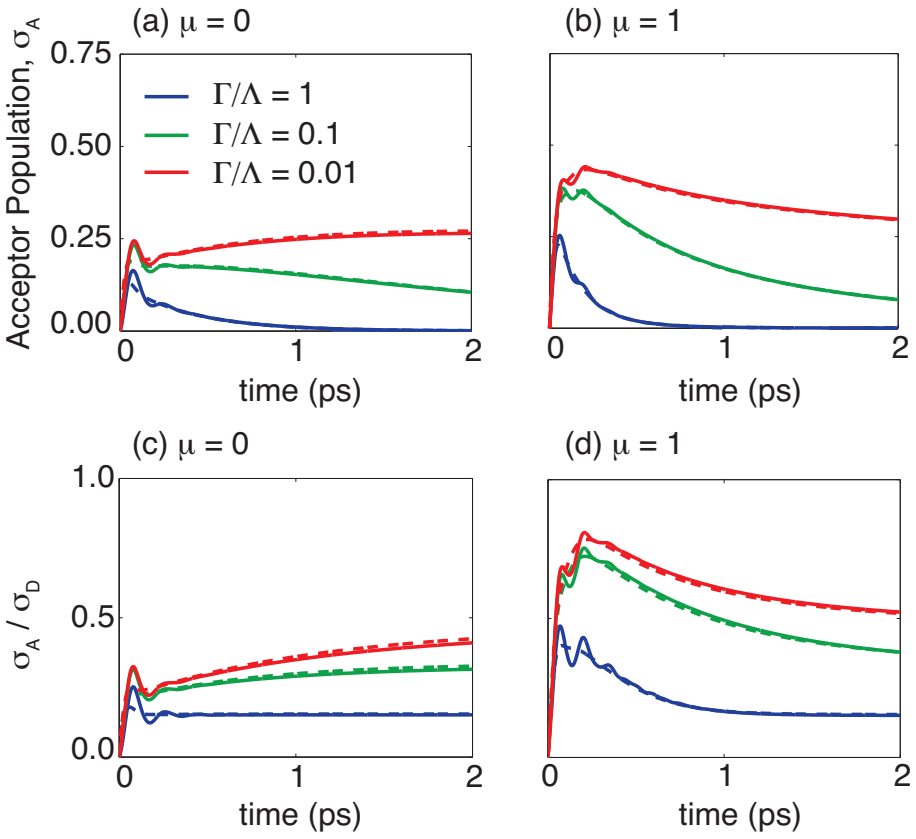

therefore the decay of the population ratio is simply the effect of a drain on the acceptor population. Crossover from Zeno to anti-Zeno behavior has been calculated in the range[243] $0.1 < \Gamma/\Lambda < 1$, but we see no such crossover in our Redfield calculations.

The transfer efficiency can be calculated from the net population that has left the vibronic dimer,[213, 244, 245]

$$\eta = \frac{\Gamma}{\hbar}\int_0^\infty dt\big(1 - \sigma_D(t) - \sigma_A(t)\big) \quad . \tag{4.59}$$

which defines the following trapping time:

$$\tau = \frac{\Gamma}{\eta}\int_0^\infty dt\big(1 - \sigma_D(t) - \sigma_A(t)\big)t \quad . \tag{4.60}$$

In Fig. 4.10 we plot the trapping time as a function of the transfer rate out of the acceptor, choosing a finite upper bound on the time integration to be 2 ps. From Fig. 4.10 we see no clear evidence

Figure 4.10: The trapping time, described in the text, calculated using the Redfield theory for uncorrelated and correlated fluctuations shown with solid and dashed curves, respectively. The trapped population is shown in the inset with the transfer rate out of the acceptor fixed at $\Gamma/\Lambda = 1$, 0.1, and 0.01 in blue, green, and red, respectively.

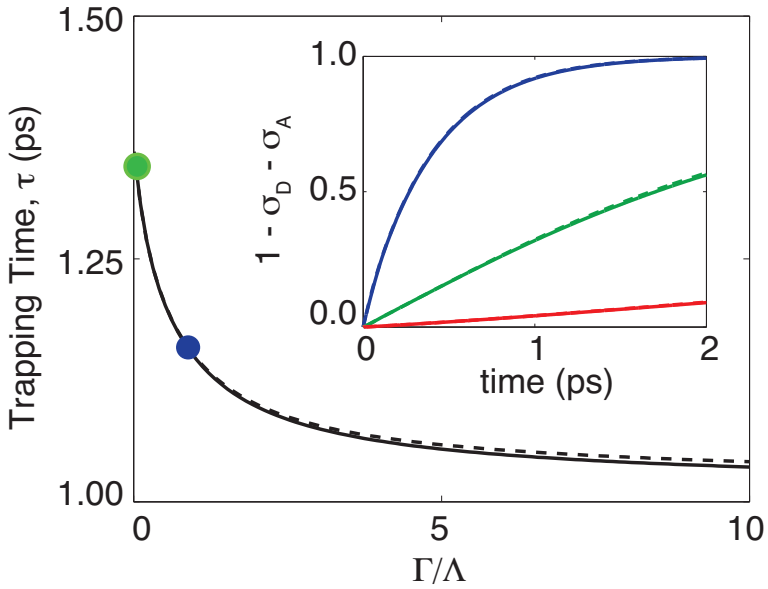

of the quantum Zeno effect. We are left to conclude that, from the perspective of energy transfer within the FMO complex, there is no evidence of a quantum Zeno effect.

4.5 Conclusion

To summarize, we have constructed a model Hamiltonian of electronic excitations and intramolecular vibrations in a dimer of two pigments. Using the polaron transformation, we showed that the correlated pigment vibration does not couple to the electronic energy transfer even when the electronic excitation is linearly coupled to a thermal reservoir. The exact coherent dynamics calculated using the HEOM are in close agreement with the approximate dynamics obtained by solving the Redfield equation. The rate of transfer from the donor to the acceptor pigment is faster when the vibronic system is initially prepared with anticorrelated vibrational energy than when the system is vibrationally cold initially. We show that thermal fluctuations correlated across the dimer enhance the rate of decay out of the vibronic donor state. By incorporating anti-Hermitian decay in our model we were able to comment on the transfer of electronic excitation energy to the reaction center in photosynthesis.

4.6 Appendix 4A - Calculating Low Temperature Transitions with the Numerical Renormalization Group

In this Appendix we describe our attempt to identify low temperature phase transitions using the Numerical Renormalization Group (NRG).[246, 247] When the coupling between the electronic degrees of freedom and the intra-pigment vibrations is negligible, the local pigment energies are degenerate, and fluctuations are anticorrelated across the dimer, $c_{j,D} = -c_{j,A}$, the Hamiltonian maps to the spin-boson model,

$$H = -(\Delta/2)\sigma_z + J\sigma_x + H_B + V \quad . \tag{4.61}$$

By iteratively diagonalizing a coarse-grained version of Eq. 4.61, we can calculate the delocalization of the excitation across the dimer nonperturbatively. To make contact with known NRG results, we approximate our spectral density in the infrared limit as

$$J(\omega) = 2\kappa\omega \quad . \tag{4.62}$$

Eq. 4.62 describes Ohmic dissipation. For a continuous dispersion of a bosonic bath, $g(\epsilon)$, Eq. 4.61 can be written as

$$H = H_S + \int_0^1 d\epsilon g(\epsilon) b_\epsilon^\dagger b_\epsilon - \sigma_z \int_0^1 d\epsilon \; c(\epsilon)\left(b_\epsilon + b_\epsilon^\dagger\right) \quad , \tag{4.63}$$

where the spectral density is related to the coupling function, $c(\epsilon)$, through

$$\frac{1}{\pi} J(\omega) = \frac{d\epsilon(\omega)}{d\omega}\left(\frac{2}{\epsilon} c^2[\epsilon(\omega)]\right) \quad . \tag{4.64}$$

The NRG is constructed using a logarithmic discretization of the system-bath interactions,

$$c(\epsilon) \to c_n = \sqrt{\frac{1}{\Omega^{-n} - \Omega^{-(n+1)}} \int_{\Omega^{-(n+1)}\Lambda}^{\Omega^{-n}\Lambda} \frac{2}{\pi\omega} J(\omega) d\omega} \quad . \tag{4.65}$$

Details of the NRG can be found elsewhere in the literature.[247, 246]. In Fig. 4.11 we plot the flow diagrams using Ohmic dissipation and zero bias. We have not had success with the NRG and

Figure 4.11: The flow diagrams of energies calculated using the NRG and an ohmic spectral density. The bias, electronic coupling, and bath frequency cutoff have been fixed at $\Delta = 0$, $J = -0.005$, and $\Lambda = 1$, respectively. 100 energies were kept at each NRG iteration with 8 new boson degrees of freedom added. The discretization parameter has been fixed at $\Omega = 2$. (Reproduced from ref.[246])

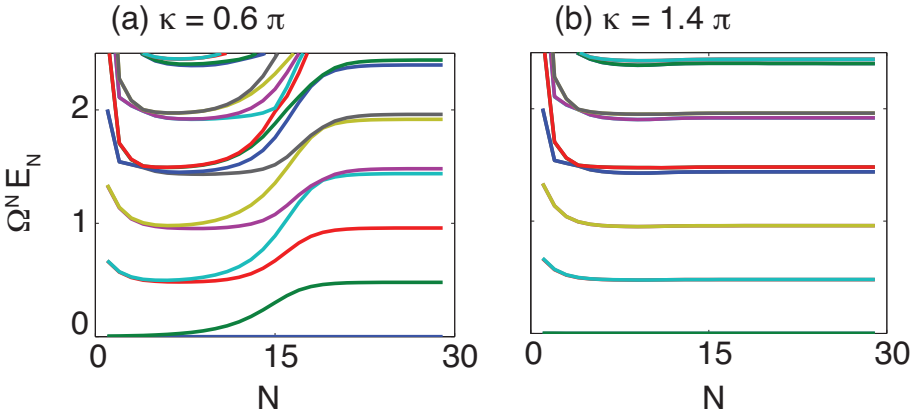

finite bias, which is a necessary condition for any relevant calculation of excitation delocalization throughout the FMO complex.

Bibliography

[1] R. Kubo. Statistical-mechanical theory of irreversible processes. i. general theory and simple applications to magnetic and conduction problems. J. Phys. Soc. Jap., 12:570, 1957.

[2] C. Jacoboni. Theory of electron transport in semiconductors, volume 165. Springer-Verlag, Berlin Heidelberg, 2010.

[3] R. Zwanzig. Nonequilibrium Statistical Mechanics. Oxford Univ. Press, Oxford, 2001.

[4] A. Nitzan. Chemical Dynamics in Condensed Phases. Oxford Univ. Press, Oxford, 2006.

[5] B. J. Berne, G. Ciccotti, and D. F. Coker, editors. Classical and Quantum Dynamics in Condensed Phase Simulations. World Scientific, Singapore, 1998.

[6] U. Weiss. Quantum Dissipative Systems. World Scientific, Singapore, 1993.

[7] R. A. Marcus. On the theory of oxidation-reduction reactions involving electron transfer. J. Chem. Phys., 24:966–978, 1956.

[8] R. A. Marcus and N. Sutin. Electron transfers in chemistry and biology. Biochim. Biophys. Acta, 811:265–322, 1985.

[9] P. Talkner and P. Hänggi. New Trends in Kramers' Reaction Rate Theory. Kluwer Academic Publishers, Boston, 1995.

[10] R. F. Grote and J. T. Hynes. The stable states picture of chemical reactions. ii. rate constants for condensed and gas phase reaction models. J. Chem. Phys., 73:2715, 1980.

[11] A. A. Golosov and D. R. Reichman. Reference system master equation approaches to condensed phase charge transfer processes. i. general formulation. J. Chem. Phys., 115:9848–9861, 2001.

[12] S. Jang, Y. Jung, and R. J. Silbey. Nonequilibrium generalization of förster-dexter theory for excitation energy transfer. Chem. Phys., 275:319–332, 2002.

[13] W. Shockley and H. J. Queisser. Detailed balance limit of efficiency of p-n junction solar cells. J. Appl. Phys., 32:510–519, 1961.

[14] M. C. Hanna and A. J. Nozik. Solar conversion efficiency of photovoltaic and photoelectrolysis cells with carrier multiplication absorbers. J. Appl. Phys., 100:074510(1–8), 2006.

[15] A. Shabaev, A. L. Efros, and A. J. Nozik. Multiexciton generation by a single photon in nanocrystals. Nano Lett., 6:2856–2863, 2006.

[16] M. Grätzel. Photoelectrochemical cells. Nature, 414:338, 2001.

[17] A. J. Nozik, M. C. Beard, J. M. Luther, M. Law, R. J. Ellingson, and J. C. Johnson. Semiconductor quantum dots and quantum dot arrays and applications of multiple exciton generation to third-generation photovoltaic solar cells. Chem. Rev., 110:6873, 2010.

[18] M. B. Smith and J. Michl. Singlet fission. Chem. Rev., 110:6891–6936, 2010.

[19] M. B. Smith and J. Michl. Recent advances in singlet fission. Ann. Rev. Phys. Chem., 64:361–386, 2013.

[20] J. C. Johnson, A. Akdag, M. Zamadar, X. Chen, A. F. Schwerin, I. Paci, M. B. Smith, Z. Havlas, J. R. Miller, M. A. Ratner, A. J. Nozik, and J. Michl. Toward designed singlet fission: solution photophysics of two indirectly coupled covalent dimers of 1,3-diphenylisobenzofuran. J. Phys. Chem. B, 117:4680–4695, 2013.

[21] J. C. Johnson, A. J. Nozik, and J. Michl. The role of chromophore coupling in singlet fission. Accounts Chem. Res., 46:1290–1299, 2013.

[22] A. Akdag, Z. Havlas, and J. Michl. Search for a small chromophore with efficient singlet fission: biradicaloid heterocycles. J. Am. Chem. Soc., 134:14624–14631, 2012.

[23] K. M. Lefler, K. E. Brown, W. A. Salamant, S. M. Dyar, K. E. Knowles, and M. R. Wasielewski. Triplet state formation in photoexcited slip-stacked perylene-3, 4: 9, 10-bis (dicarboximide) dimers on a xanthene scaffold. J. Phys. Chem. A, 117:10333–10345, 2013.

[24] S. W. Eaton, L. E. Shoer, S. D. Karlen, S. M. Dyar, E. A. Margulies, B. S. Veldkamp, C. Ramanan, D. A. Hartzler, S. Savikhin, T. J. Marks, and M. R. Wasielewski. Singlet exciton fission in polycrystalline thin films of a slip-stacked perylenediimide. J. Am. Chem. Soc., 135:14701–14712, 2013.

[25] J. E. Bullock, M. T. Vagnini, C. Ramanan, D. T. Co, T. M. Wilson, J. W. Dicke, T. J. Marks, and M. R. Wasielewski. Photophysics and redox properties of rylene imide and diimide dyes alkylated ortho to the imide groups. J. Phys. Chem. B, 114:1794–1802, 2010.

[26] P. J. Vallett, J. L. Snyder, and N. H. Damrauer. Tunable electronic coupling and driving force in structurally well-defined tetracene dimers for molecular singlet fission: A computational exploration using density functional theory. J. Phys. Chem. A, 117:10824–10838, 2013.

[27] P. W. Anderson. Localized magnetic states in metals. Phys. Rev., 124:41, 1961.

[28] R. C. Johnson and R. E. Merrifield. Effect of magnetic fields on the mutual annihilation of triplet excitons in anthracene crystals. Phys. Rev. B, 1:896–902, 1970.

[29] R. E. Merrifield. Theory of magnetic field effects on the mutual annihilation of triplet excitons. J. Chem. Phys., 48:4318–4319, 1968.

[30] J. B. Parkinson and D. J. J. Farnell. An Introduction to Quantum Spin Systems, volume 816. Springer, Berlin Heidelberg, 2010.

[31] K. Modi and V. Vedral. Unification of quantum and classical correlations and quantumness measures. AIP Conf. Proc., 1384:69, 2011.

[32] V. Tiwari, W. K. Peters, and D. M. Jonas. Electronic resonance with anticorrelated pigment vibrations drives photosynthetic energy transfer outside the adiabatic framework. Proc. Natl. Acad. Sci., 110:1203, 2013.

[33] Y. C. Cheng and G. R. Fleming. Dynamics of light harvesting in photosynthesis. Ann. Rev. Phys. Chem., 60:241, 2009.

[34] F. Müh, M. El-Amine Madjet, J. Adolphs, A. Abdurahman, B. Rabenstein, H. Ishikita, E. Knapp, and T. Renger. α-helices direct excitation energy flow in the fenna-matthews-olson protein. Proc. Natl. Acad. Sci., 104:16862, 2007.

[35] C. Y. Wong, R. M. Alvey, D. B. Turner, K. E. Wilk, D. A. Bryant, P. M. G. Curmi, R. J. Silbey, and G. D. Scholes. Electronic coherence lineshapes reveal hidden excitonic correlations in photosynthetic light harvesting.

[36] K. A. Fransted, J. R. Caram, D. Hayes, and G. S. Engel. Two-dimensional electronic spectroscopy of bacteriochlorophyll a in solution: Elucidating the coherence dynamics of the fenna-matthews-olson complex using its chromophore as a control. J. Chem. Phys., 137:125101, 2012.

[37] D. Abramavicius and S. Mukamel. Quantum oscillatory exciton migration in photosynthetic reaction centers. J. Chem. Phys., 133:064510, 2010.

[38] A. D. Patel. Efficient energy transport in photosynthesis: Roles of coherence and entanglement. AIP Conf. Proc., 1384:102, 2011.

[39] D. M. Jonas. Two-dimensional femtosecond spectroscopy. Annu. Rev. Phys. Chem., 54:425, 2003.

[40] K. L. M. Lewis and J. P. Ogilvie. Probing photosynthetic energy and charge transfer with two-dimensional electronic spectroscopy. J. Phys. Chem. Lett., 3:503, 2012.

[41] T. Manal, N. Christensson, V. Luke, F. Milota, O. Bixner, H. F. Kauffmann, and J. Hauer. System-dependent signatures of electronic and vibrational coherences in electronic two-dimensional spectra. J. Phys. Chem. Lett., 3:1497, 2012.

[42] N. Christensson, H. F. Kauffmann, T. Pullerits, and T. Manal. Origin of long-lived coherences in light-harvesting complexes. J. Phys. Chem. B, 116:7449, 2012.

[43] A. J. Nozik. Nanoscience and nanostructures for photovoltaics and solar fuels. Nano Lett., 10:2735–2741, 2010.

[44] A. Franceschetti, J. M. An, and A. Zunger. Impact ionization can explain carrier multiplication in pbse quantum dots. Nano Lett., 6:2191–2195, 2006.

[45] M. R. Antognazza, L. Luer, D. Polli, R. L. Christensen, R. R. Schrock, G. Lanzani, and G. Cerullo. Ultrafast excited state relaxation in long-chain polyenes. Chem. Phys., 373:115–121, 2010.

[46] T. S. Kuhlman, J. Kongsted, K. V. Mikkelsen, K. B. Møller, and T. I. Sølling. Interpretation of the ultrafast photoinduced processes in pentacene thin films. J. Am. Chem. Soc., 132:3431–3439, 2010.

[47] M. W. B. Wilson, A. Rao, J. Clark, R. S. S. Kumar, D. Brida, G. Cerullo, and R. H. Friend. Ultrafast dynamics of exciton fission in polycrystalline pentacene. J. Am. Chem. Soc., 133:11830–11833, 2011.

[48] W. L. Chan, M. Ligges, A. Jailaubekov, L. Kaake, L. Miaja-Avila, and X. Y. Zhu. Observing the multiexciton state in singlet fission and ensuing ultrafast multielectron transfer. Science, 334:1541–1545, 2011.

[49] H. Yamagata, J. Norton, E. Hontz, Y. Olivier, D. Beljonne, J. L. Brédas, R. J. Silbey, and F. C. Spano. The nature of singlet excitons in oligoacene molecular crystals. J. Chem. Phys., 134:204703, 2011.

[50] P. J. Jadhav, A. Mohanty, J. Sussman, J. Lee, and M. A. Baldo. Singlet exciton fission in nanostructured organic solar cells. Nano Lett., 11:1495–1498, 2011.

[51] J. Lee, P. Jadhav, and M. A. Baldo. High efficiency organic multilayer photodetectors based on singlet exciton fission. Appl. Phys. Lett., 95:033301, 2009.

[52] P. M. Zimmerman, Z. Zang, and C. B. Musgrave. Singlet fission in pentacene through multi-exciton quantum states. Nat. Chem., 2:648–652, 2010.

[53] P. M. Zimmerman, F. Bell, D. Casanova, and M. Head-Gordon. Mechanism for singlet fission in pentacene and tetracene: from single exciton to two triplets. J. Am. Chem. Soc., 133:19944, 2011.

[54] E. C. Greyson, J. Vura-Weis, J. Michl, and M. A. Ratner. Maximizing singlet fission in organic dimers: Theoretical investigation of triplet yield in the regime of localized excitation and fast coherent electron transfer. J. Phys. Chem. B, 114:14168–14177, 2010.

[55] S. Tornow, R. Bulla, F. B. Anders, and A. Nitzan. Dissipative two-electron trasfer: A numerical renormalization group study. Phys. Rev. B, 78:035434(1–14), 2008.

[56] E. C. Greyson, B. R. Stepp, X. Chen, A. F. Schwerin, I. Paci, M. B. Smith, A. Akdag, J. C. Johnson, A. J. Nozik, J. Michl, and M. A. Ratner. Singlet exciton fission for solar cell applications: Energy aspects of interchromophore coupling. J. Phys. Chem. B, 114:14223–14232, 2010.

[57] M. D. Todd, A. Nitzan, and M. A. Ratner. Electron transfer via superexchange: a time-dependent approach. J. Phys. Chem., 97:29–33, 1993.

[58] J. Brédas, D. Beljonne, V. Coropceanu, and J. Cornil. Charge-transfer and energy-transfer processes in π-conjugated oligomers and polymers: a molecular picture. Chem. Rev., 104:4971–5004, 2004.

[59] N. E. Gruhn, D. A. da Silva Filho, T. G. Bill, M. Malagoli, V. Coropceanu, A. Kahn, and J. Brédas. The vibrational reorganization energy in pentacene: Molecular influences on charge transport. J. Am. Chem. Soc., 124:7918–7919, 2002.

[60] D. P. McMahon and A. Troisi. Evaluation of the external reorganization energy of polyacenes. J. Phys. Chem. Lett., 1:941–946, 2010.

[61] G. C. Schatz and M. A. Ratner. Quantum Mechanics in Chemistry. Dover, New York, 2002.

[62] M. Pope and C. E. Swenberg. Electronic Processes in Organic Crystals and Polymers. Oxford University Press, Oxford, U.K., 1999.

[63] V. K. Thorsmølle, R. D. Averitt, J. Demsar, D. L. Smith, S. Tretiak, R. L. Martin, X. Chi, B. K. Crone, A. P. Ramirez, and A. J. Taylor. Photoexcited carrier relaxation dynamics in pentacene probed by ultrafast optical spectroscopy: Influence of morphology on relaxation processes. Phys. B (Amsterdam, Neth.), 404:3127–3130, 2009.

[64] V. K. Thorsmølle, R. D. Averitt, J. Demsar, D. L. Smith, S. Tretiak, R. L. Martin, X. Chi, B. K. Crone, A. P. Ramirez, and A. J. Taylor. Morphology effectively controls singlet-triplet exciton relaxation and charge transport in organic semiconductors. Phys. Rev. Lett., 102:017401, 2009.

[65] M. L. Tiago, J. E. Northrup, and S. G. Louie. Ab initio calculation of the electronic and optical properties of solid pentacene. Phys. Rev. B, 67:115212, 2003.

[66] P. F. Barbara, T. J. Meyer, and M. A. Ratner. Contemporary issues in electron transfer research. J. Phys. Chem., 100:13148–13168, 1996.

[67] Th. Förster. In Modern Quantum Chemistry, Pt. III. Academic, New York, 1965.

[68] A. Perdomo, L. Vogt, A. Najmaje, and A. Aspuru-Guzik. Engineering directed excitonic energy transfer. Appl. Phys. Lett., 96:093114(1–3), 2010.

[69] D. Chandler and J. S. Bader. Computer simulation of photochemically induced electron transfer. Chem. Phys. Lett., 157:501–504, 1989.

[70] J. S. Bader, R. A. Kuharski, and D. Chandler. Role of nuclear tunneling in aqueous ferrous-ferric electron transfer. J. Chem. Phys., 93:230–236, 1990.

[71] S. J. Rosenthal, R. Jimenez, G. R. Fleming, P. V. Kumar, and M. Maroncelli. Solvation dynamics in methanol: Experimental and molecular dynamics simulation studies. J. Mol. Liq., 60:25–26, 1994.

[72] J. D. Eaves, A. Tokmakoff, and P. L. Geissler. Electric field fluctuations drive vibrational dephasing in water. J. Phys. Chem. A, 109:9424–9436, 2005.

[73] J. Kouteckýý. Some properties of semiempirical hamiltonians. J. Chem. Phys., 47:1501–1511, 1967.

[74] R. Pariser and R. G. Parr. A semi-empirical theory of the electronic spectra and electronic structure of complex unsaturated molecules. i. J. Chem. Phys., 21:466–471, 1953.

[75] J. A. Pople. Trans. Faraday Soc., 49:1375–1385, 1953.

[76] G. D. Mahan. Many Particle Physics 3rd ed. Kluwer Academic/Plenum Publishers, New York, 2000.

[77] J. Jortner. Temperature dependent activation energy for electron transfer between biological molecules. J. Chem. Phys., 64:4860–4867, 1976.

[78] M. Bixon and J. Jortner. Solvent relaxation dynamics and electron transfer. Chem. Phys., 176:467–481, 1993.

[79] M. Bixon and J. Jortner. Quantum effects on electron-transfer processes. Faraday Discuss. Chem. Soc., 74:17–29, 1982.

[80] J. Jortner and J. Ulstrup. The effect of intramolecular quantum modes on free energy relationships for electron transfer reactions. J. Chem. Phys., 63:4358–4368, 1975.

[81] M. Sparpaglione and S. J. Mukamel. Dielectric friction and the transition from adiabatic to nonadiabatic electron transfer. i. solvation dynamics in liouville space. J. Chem. Phys., 88:3263–3280, 1988.

[82] T. Chang and J. Skinner. Non-markovian population and phase relaxation and absorption lineshape for a two-level system strongly coupled to a harmonic quantum bath. Phys. A (Amsterdam, Neth.), 193:483–539, 1993.

[83] S. Jang, Y. Cheng, D. R. Reichman, and J. D. Eaves. Theory of coherent resonance energy transfer. J. Chem. Phys., 129:101104(1–4), 2008.

[84] E. Sim and N. Makri. Filtered propagator functional for iterative dynamics of quantum dissipative systems. Comput. Phys. Commun., 99:335–354, 1997.

[85] A. A. Golosov, R. A. Friesner, and P. Pechukas. Efficient memory equation algorithm for reduced dynamics in spin-boson models. J. Chem. Phys., 110:138–146, 1999.

[86] D. G. Evans, A. Nitzan, and M. A. Ratner. Photoinduced electron transfer in mixed-valence compounds: Beyond the golden rule regime. J. Chem. Phys., 108:6387–6393, 1998.

[87] B. B. Laird, J. Budimir, and J. L. Skinner. Quantum-mechanical derivation of the bloch equations: Beyond the weak-coupling limit. J. Chem. Phys., 94:4391–4404, 1991.

[88] G. R. Fleming and A. Ishizaki. On the adequacy of the redfield equation and related approaches to the study of quantum dynamics in electronic energy transfer. J. Chem. Phys., 130:234110(1–8), 2009.

[89] W. B. Bosma, Y. J. Yan, and S. Mukamel. Impulsive pump-probe and photon-echo spectroscopies of dye molecules in condensed phases. Phys. Rev. A, 42:6920–6923, 1990.

[90] Y. Tanimura and S. Mukamel. Real-time path-integral approach to quantum coherence and dephasing in nonadiabatic transitions and nonlinear optical response. Phys. Rev. E, 47:118–136, 1993.

[91] G. R. Fleming and M. Yang. Influence of phonons on exciton transfer dynamics: Comparison of the redfield, förster, and modified redfield equations. Chem. Phys., 275:355–372, 2002.

[92] A. Ishizaki and G. R. Fleming. Theoretical examination of quantum coherence in a photosynthetic system at physiological temperature. Proc. Natl. Acad. Sci. U. S. A., 106:17255–17260, 2009.

[93] J. J. Burdett, G. B. Piland, and C. J. Bardeen. Magnetic field effects and the role of spin states in singlet fission. Chem. Phys. Lett., 585:1–10, 2013.

[94] G. B. Piland, J. J. Burdett, D. Kurunthu, and C. J. Bardeen. Magnetic field effects on singlet fission and fluorescence decay dynamics in amorphous rubrene. J. Phys. Chem. C, 117:1224–1236, 2013.

[95] J. J. Burdett and C. J. Bardeen. The dynamics of singlet fission in crystalline tetracene and covalent analogs. Accounts Chem. Res., 46:1312–1320, 2013.

[96] J. J. Burdett and C. J. Bardeen. Quantum beats in crystalline tetracene delayed fluorescence due to triplet pair coherences produced by direct singlet fission. J. Am. Chem. Soc., 134:8597–8607, 2012.

[97] J. J. Burdett, A. M. Mueller, D. Gosztola, and C. J. Bardeen. Excited state dynamics in solid and monomeric tetracene: The roles of superradiance and exciton fission. J. Chem. Phys., 133:144506, 2010.

[98] W. L. Chan, T. C. Berkelbach, M. R. Provorse, N. R. Monahan, J. R. Tritsch, M. S. Hybertsen, D. R. Reichman, J. Gao, and X. Y. Zhu. The quantum coherent mechanism for singlet fission: Experiment and theory. Accounts Chem. Res., 46:1321–1329, 2013.

[99] W. L. Chan, M. Ligges, and X. Y. Zhu. The energy barrier in singlet fission can be overcome through coherent coupling and entropic gain. Nat. Chem., 4:840–845, 2012.

[100] S. T. Roberts, R. E. McAnally, J. N. Mastron, D. H. Webber, M. T. Whited, R. L. Brutchey, M. E. Thompson, and S. E. Bradforth. Efficient singlet fission discovered in a disordered acene film. J. Am. Chem. Soc., 134:6388–6400, 2012.

[101] E. M. Grumstrup, J. C. Johnson, and N. H. Damrauer. Enhanced triplet formation in polycrystalline tetracene films by femtosecond optical-pulse shaping. Phys. Rev. Lett., 105:257403, 2010.

[102] R. J. Dillon, G. B. Piland, and C. J. Bardeen. Different rates of singlet fission in monoclinic versus orthorhombic crystal forms of diphenylhexatriene. J. Am. Chem. Soc., 135:17278–17281, 2013.

[103] M. W. B. Wilson, A. Rao, K. Johnson, S. Gelinas, R. di Pietro, J. Clark, and R. H. Friend. Temperature-independent singlet exciton fission in tetracene. J. Am. Chem. Soc., 135:16680–16688, 2013.

[104] X. Feng, A. V. Luzanov, and A. I. Krylov. Fission of entangled spins: An electronic structure perspective. J. Phys. Chem. Lett., 4:3848–3852, 2013.

[105] P. M. Zimmerman, C. B. Musgrave, and M. Head-Gordon. A correlated electron view of singlet fission. Accounts Chem. Res., 46:1339, 2013.

[106] P. E. Teichen and J. D. Eaves. A microscopic model of singlet fission. J. Phys. Chem. B, 116:11473–11481, 2012.

[107] T. C. Berkelbach, M. S. Hybertsen, and D. R. Reichman. Microscopic theory of singlet exciton fission. i. general formulation. J. Chem. Phys., 138:114102, 2013.

[108] T. C. Berkelbach, M. S. Hybertsen, and D. R. Reichman. Microscopic theory of singlet exciton fission. ii. application to pentacene dimers and the role of superexchange. J. Chem. Phys., 138:114103, 2013.

[109] A. B. Kolomeisky, X. Feng, and A. I. Krylov. A simple kinetic model for singlet fission: A role of electronic and entropic contributions to macroscopic rates. J. Phys. Chem. C, 118:5188–5195, 2014.

[110] J. N. Schrauben, J. L. Ryerson, J. Michl, and J. C. Johnson. Mechanism of singlet fission in thin films of 1,3-diphenylisobenzofuran. J. Am. Chem. Soc., 136:7363, 2014.

[111] F. Mirjani, N. Renaud, N. Gorczak, and F. C. Grozema. Theoretical investigation of singlet fission in molecular dimers: The role of charge transfer states in quantum interference. J. Phys. Chem. C, 118:14192, 2014.

[112] N. Renaud and F. C. Grozema. Intermolecular vibrational modes speed up singlet fission in perylenediimide crystals. J. Phys. Chem. Lett., 6:360, 2015.

[113] D. Casanova. Electronic structure study of singlet fission in tetracene derivatives. J. Chem. Theory Comput., 10:324, 2014.

[114] S. M. Parker, T. Seideman, M. A. Ratner, and T. Shiozaki. A model hamiltonian analysis of singlet fission from first principles. J. Phys. Chem. C, 118:12700, 2014.

[115] F. Ambrosio and A. Troisi. Singlet fission in linear chains of molecules. J. Chem. Phys., 141:204703, 2014.

[116] X. Feng, A. B. Kolomeisky, and A. I. Krylov. Dissecting the effect of morphology on the rates of singlet fission: Insights from theory. J. Phys. Chem. C, 118:19608, 2014.

[117] S. R. Yost, E. Hontz, S. Yeganeh, and T. Van Voorhis. Triplet vs singlet energy transfer in organic semiconductors: The tortoise and the hare. J. Phys. Chem. C, 116:17369–17377, 2012.

[118] R. M. Lynden-Bell and H. M. McConnell. Theory of paramagnetic excitons in solid free radicals. J. Chem. Phys., 37:794, 1962.

[119] D. B. Chesnut and A. Suna. Fermion behavior of one-dimensional excitons. J. Chem. Phys., 39:146–149, 1963.

[120] G. D. Scholes and G. Rumbles. Excitons in nanoscale systems. Nat. Mat., 5:683–696, 2006.

[121] S. K. Lower and M. A. El-Sayed. The triplet state and molecular electronic processes in organic molecules. Chem. Rev., 66:199, 1966.

[122] J. Jortner, S. A. Rice, J. L. Katz, and S. I. Choi. Triplet excitons in crystals of aromatic molecules. J. Chem. Phys., 42:309, 1965.

[123] B. A. West, J. M. Womick, L. E. McNeil, K. J. Tan, and A. M. Moran. Ultrafast dynamics of frenkel excitons in tetracene and rubrene single crystals. J. Phys. Chem. C, 114:10580, 2010.

[124] T. S. Ahn, A. M. Mueller, R. O. Al-Kaysi, F. C. Spano, J. E. Norton, D. Beljonne, J. L. Brédas, and C. J. Bardeen. Experimental and theoretical study of temperature dependent exciton delocalization and relaxation in anthracene thin films. J. Chem. Phys., 128:054505, 2008.

[125] J. J. Burdett, D. Gosztola, and C. J. Bardeen. The dependence of singlet exciton relaxation on excitation density and temperature in polycrystalline tetracene thin films: Kinetic evidence for a dark intermediate state and implications for singlet fission. J. Chem. Phys., 135:214508, 2011.

[126] P. Cudazzo, M. Gatti, and A. Rubio. Excitons in molecular crystals from first-principles many-body perturbation theory: Picene versus pentacene. Phys. Rev. B, 86:195307, 2012.

[127] D. Beljonne, H. Yamagata, J. L. Brédas, F. C. Spano, and Y. Olivier. Charge-transfer excitations steer the davydov splitting and mediate singlet exciton fission in pentacene. Phys. Rev. Lett., 110:226402, 2013.

[128] S. Sharifzadeh, P. Darancet, L. Kronik, and J. B. Neaton. Low-energy charge-transfer excitons in organic solids from first-principles: The case of pentacene. J. Phys. Chem. Lett., 4:2197, 2013.

[129] L. Grisanti, Y. Olivier, L. Wang, S. Athanasopoulos, J. Cornil, and D. Beljonne. Roles of local and nonlocal electron-phonon couplings in triplet exciton diffusion in the anthracene crystal. Phys. Rev. B, 88:035450, 2013.

[130] Z. G. Soos and H. M. McConnell. Motion of localized triplet excitons. J. Chem. Phys., 43:3780, 1965.

[131] D. N. Congreve, J. Lee, N. J. Thompson, E. Hontz, S. R. Yost, P. D. Reusswig, M. E. Bahlke, S. Reineke, T. Van Voorhis, and M. A. Baldo. External quantum efficiency above 100 % in a singlet-exciton-fission-based organic photovoltaic cell. Science, 340:334–337, 2013.

[132] C. A. Nelson, N. R. Monahan, and X. Y. Zhu. Exceeding the shockley-queisser limit in solar energy conversion. Energy and Environmental Science, 6:3508, 2013.

[133] X. Y. Zhu. Exceeding the limit in solar energy conversion with multiple excitons. Accounts of chemical research, 46:1239, 2013.

[134] R. E. Merrifield. Interaction of excitation waves in a one-dimensional crystal. J. Am. Chem. Soc., 31:522–525, 1959.

[135] A. Suna. Kinematics of exciton-exciton annihilation in molecular crystals. Phys. Rev. B, 1:1716–1739, 1970.

[136] F. C. Spano. Excitons in conjugated oligomer aggregates, films, and crystals. Annu. Rev. Phys. Chem., 57:217, 2006.

[137] T. C. Berkelbach, M. S. Hybertsen, and D. R. Reichman. Microscopic theory of singlet exciton fission. iii. crystalline pentacene. J. Chem. Phys., 141:074705, 2014.

[138] G. B. Piland, J. J. Burdett, R. J. Dillon, and C. J. Bardeen. Singlet fission: from coherences to kinetics. Phys. Chem. Lett., 5:2312, 2014.

[139] X. Qiao, L. Luan, Y. Liu, Z. Yu, and B. Hu. Inter-triplet spin-spin interaction effects on inter-conversion between different spin states in intermediate triplet-triplet pairs towards singlet fission. Org. Electron., 2014. http://dx.doi.org/10.1016/j.orgel.2014.06.015.

[140] H. Najafov, B. Lee, Q. Zhou, L. C. Feldman, and V. Podzorov. Observation of long-range exciton diffusion in highly ordered organic semiconductors. J. Phys. Chem. C, 9:938, 2010.

[141] K. Kolata, T. Breuer, G. Witte, and S. Chatterjee. Molecular packing determines singlet exciton fission in organic semiconductors. ACS Nano, 8:7377, 2014.

[142] R. G. Della Valle, E. Venuti, A. Brillante, and A. Girlando. Inherent structures of crystalline tetracene. J. Phys. Chem. A, 110:10858, 2006.

[143] Th. Holstein. Studies of polaron motion: Part i. the molecular-crystal model. Annals of Physics, 8:325, 1959.

[144] Th. Holstein. Studies of polaron motion: Part ii. the "small" polaron. Annals of Physics, 8:343, 1959.

[145] V. Coropceanu, J. Cornil, D. A. da Silva Filho, Y. Olivier, R. Silbey, and J. L. Brédas. Charge transport in organic semiconductors. Chem. Rev., 107:926, 2007.

[146] R. D. Mattuck. A Guide to Feynman Diagrams in the Many-Body Problem. McGraw-Hill, New York, 1976.

[147] M. S. Hybertsen and S. G. Louie. First-principles theory of quasiparticles: calculation of band gaps in semiconductors and insulators. Phys. Rev. Lett., 55:1418, 1985.

[148] M. S. Hybertsen and S. G. Louie. Electron correlation in semiconductors and insulators: Band gaps and quasiparticle energies. Phys. Rev. B., 34:5390, 1986.

[149] F. Roth, R. Schuster, A. König, M. Knupfer, and H. Berger. Momentum dependence of the excitons in pentacene. J. Chem. Phys., 136:204708, 2012.

[150] M. C. M. Wright. Green function or green's function? Nature Physics, 2:646, 2006.

[151] M. Chabr and D. F. Williams. Fission of singlet excitons into triplet-exciton pairs in molecular crystals. Phys. Rev. B, 16:1685–1693, 1977.

[152] J. S. Bell. On the einstein-podolsky-rosen paradox. Physics, 1:195, 1964.

[153] M. M. Sahrapour and N. Makri. Tunneling, decoherence, and entanglement of two spins interacting with a dissipative bath. J. Chem. Phys., 138:114109, 2013.

[154] N. Makri and D. E. Makarov. Tensor propagator for iterative quantum time evolution of reduced density matrices. i. theory. J. Chem. Phys., 102:4600, 1995.

[155] N. Makri and D. E. Makarov. Tensor propagator for iterative quantum time evolution of reduced density matrices. ii. numerical methodology. J. Chem. Phys., 102:4611, 1995.

[156] P. P. Orth, D. Roosen, W. Hofstetter, and K. Le Hur. Dynamics, synchronization, and quantum phase transitions of two dissipative spins. Phys. Rev. B, 82:144423, 2010.

[157] B. Bellomo, R. Lo Franco, and G. Compagno. Entanglement dynamics of two independent qubits in environments with and without memory. Phys. Rev. A, 77:032342, 2008.

[158] B. Bellomo, R. Lo Franco, and G. Compagno. Non-markovian effects on the dynamics of entanglement. Phys. Rev. Lett., 99:160502, 2007.

[159] Z. Z. Li, X. T. Liang, and X. Y. Pan. The entanglement dynamics of two coupled qubits in different environments. Phys. Lett. A, 373:4028, 2009.

[160] M. Lucamarini, S. Paganelli, and S. Mancini. Two-qubit entanglement dynamics in a symmetry-broken environment. Phys. Rev. A, 69:062308, 2004.

[161] T. Van Voorhis, B. Kowalczyk, B. Kaduk, L. P. Wang, C. L. Cheng, and Q. Wu. The diabatic picture of electron transfer, reaction barriers, and molecular dynamics. Annu. Rev. Phys. Chem., 61:149–170, 2010.

[162] M. Marchi, J. N. Gehlen, D. Chandler, and M. Newton. Diabatic surfaces and the pathway for primary electron transfer in a photosynthetic reaction center. J. Am. Chem. Soc., 115:4178, 1993.

[163] A. Camposeo, M. Polo, S. Tavazzi, L. Silvestri, P. Spearman, R. Cingolani, and D. Pisignano. Polarized superradiance from delocalized exciton transitions in tetracene single crystals. Phys. Rev. B, 81:033306, 2010.

[164] S. H. Lim, T. G. Bjorklund, F. C. Spano, and C. J. Bardeen. Exciton delocalized and superradiance in tetracene thin films and nanoaggregates. Phys. Rev. Lett., 92:107402, 2004.

[165] F. C. Spano and E. S. Manas. Theory of coherent transient spectroscopy in molecular aggregates: The effects of interacting excitons. J. Chem. Phys., 103:5939, 1995.

[166] F. C. Spano. Pump-probe spectrum of interacting one-dimensional excitons: biexcitons and j-aggregates. Chem. Phys. Lett., 234:29, 1995.

[167] F. C. Spano and S. Mukamel. Nonlinear susceptibilities of molecular aggregates: Enhancement of $\chi^{(3)}$ by size. Phys. Rev. A, 40:5783, 1989.

[168] F. C. Spano. Nonlinear optical response of one-dimensional molecular crystals: Breakdown of the local field approximation. J. Chem. Phys., 96:8109, 1992.

[169] J. A. Leegwater and S. Mukamel. Exciton-scattering mechanism for enhanced nonlinear response of molecular nanostructures. Phys. Rev. A, 46:452, 1992.

[170] G. Juzeliūnas and P. Reineker. Pump-probe spectra of linear molecular aggregates: Effect of exciton-exciton interaction and higher molecular levels. J. Chem. Phys., 109:6919, 1998.

[171] M. Bednarz and J. Knoester. The linear absorption and pump-probe spectra of cylindrical molecular aggregates. J. Phys. Chem. B, 105:12913–12923, 2001.

[172] G. Juzeliūnas and J. Knoester. Pump-probe spectrum of molecular assemblies of arbitrary structure and dimension. J. Chem. Phys., 112:2325, 2000.

[173] S. Mukamel. Principles of nonlinear optical spectroscopy. Oxford University Press, New York, 1995.

[174] M. Ogata and H. Shiba. Bethe-ansatz wave function, momentum distribution, and spin correlation in the one-dimensional strongly correlated hubbard model. Phys. Rev. B, 41:2326, 1990.

[175] T. Giamarchi. Quantum physics in one dimension. Oxford Univ. Press, Oxford, 2003.

[176] T. Radtke and S. Fritzsche. Simulation of n-qubit quantum systems. ii. separability and entanglement. Comp. Phys. Comm., 175:145–166, 2006.

[177] T. Radtke and S. Fritzsche. Simulation of n-qubit quantum systems. v. quantum measurements. Comp. Phys. Comm., 181:440–453, 2010.

[178] F. Mintert, A. R. R. Carvalho, M. Kuś, and A. Buchleitner. Measures and dynamics of entangled states. Phys. Rep., 415:207–259, 2005.

[179] A. S. Davydov. Theory of Molecular Excitons. Plenum, New York, 1971.

[180] V. M. Agranovich. Theory of Excitons. Moscow, Nauka, 1968.

[181] V. M. Agranovich. Electronic Excitation Energy Transfer in Condensed Matter. North-Holland, Amsterdam, 1982.

[182] L. D. Bakalis and J. Knoester. Optical properties of one-dimensional exciton systems: Beyond the heitler-london approximation. J. Chem. Phys., 106:6964, 1997.

[183] V. M. Agranovich and D. M. Basko. Frenkel excitons beyond the heitler-london approximation. J. Chem. Phys., 112:8156, 2000.

[184] Z. Q. You and C. P. Hsu. Theory and calculation for the electronic coupling in excitation energy transfer. Int. J. of Quantum Chem., 114:102, 2014.

[185] C. P. Hsu, Z. Q. You, and H. C. Chen. Characterization of the short-range couplings in excitation energy transfer. J. Phys. Chem. C, 112:1204, 2008.

[186] N. J. Turro, V. Ramamurthy, and J. C. Scaiano. Principles of Molecular Photochemistry: an introduction. University Science Books, 2009.

[187] R. E. Blankenship, M. T. Madigan, and C. E. Bauer, editors. Anoxygenic Photosynthetic Bacteria, volume 2. Springer, 1995.

[188] G. M. Akselrod, P. B. Deotare, N. J. Thompson, J. Lee, W. A. Tisdale, M. A. Baldo, V. M. Menon, and V. Bulović. Visualization of exciton transport in ordered and disordered molecular solids. Nat. Comm., 5:3646, 2014.

[189] S. R. Yost, J. Lee, M. W. B. Wilson, T. Wu, D. P. McMahon, R. R. Parkhurst, N. J. Thompson, D. N. Congreve, A. Rao, K. Johnson, M. Y. Sfeir, M. G. Bawendi, T. M. Swager, R. H. Friend, M. A. Baldo, and T. Van Voorhis. A transferable model for singlet-fission kinetics. Nat. Chem., 6:492, 2014.

[190] F. C. Spano, V. Agranovich, and S. Mukamel. Biexciton states and two-photon absorption in molecular monolayers. J. Chem. Phys., 95:1400, 1991.

[191] E. Lieb, T. Schultz, and D. Mattis. Two soluble models of an antiferromagnetic chain. Annals of Physics, 16:407–466, 1961.

[192] V. May and O. Kühn. Charge and Energy Transfer Dynamics in Molecular Systems. John Wiley and Sons, 2008.

[193] We choose a phase convention when writing the nonconservative operator in terms of the jordan-wigner fermions such that the singlet-two triplet interaction smoothly approaches zero as we approach the triplet pair state which violates pauli exclusion.

[194] E. N. Economou. Green's Functions in Quantum Physics. Springer, Berlin, 2006.

[195] M. C. Sweeney and J. D. Eaves. Carrier transport in heterojunction nanocrystals under strain. J. Chem. Phys. Lett., 3:791–795, 2012.

[196] U. Fano. Effects of configuration interaction on intensities and phase shifts. Phys. Rev., 124:1866, 1961.

[197] J. J. Sakurai. Modern Quantum Mechanics, volume 104. Addison-Wesley, 2009.

[198] S. Mukamel. Communications: Signatures of quasiparticle entanglement in multidimensional nonlinear optical spectroscopy of aggregates. J. Chem. Phys., 132:241105, 2010.

[199] S. Pabst, L. Greenman, P. J. Ho, and D. A. Mazziotti. Decoherence in attosecond photoionization. Phys. Rev. Lett., 106:053003, 2011.

[200] C. N. Yang. Some exact results for the many-body problem in one dimension with repulsive delta-function interaction. Phys. Rev. Lett., 19:1312, 1967.

[201] S. Murakami and M. Wadati. Two-component δ-function fermions and bethe ansatz eigenstates. Chaos, Solitons and Fractals, 7:93, 1996.

[202] X. W. Guan, M. T. Batchelor, and C. Lee. Fermi gases in one dimension: From bethe ansatz to experiments. Rev. Mod. Phys., 85:1633, 2013.

[203] B. S. DeWitt. Quantum mechanics and reality. Physics Today, 23:30, 1970.

[204] R. Paškauskas and L. You. Quantum correlations in two-boson wave functions. Phys. Rev. A, 64:042310, 2001.

[205] J. Schliemann, J. I. Cirac, M. Kuś, M. Lewenstein, and D. Loss. Quantum correlations in two-fermion systems. Phys. Rev. A, 64:022303, 2001.

[206] W. Wimmer. Algorithm 923: Efficient numerical computation of the pfaffian for dense and banded skew-symmetric matrices. ACM Trans. Math. Softw., 38:1, 2012.

[207] M. Almeida, Y. Omar, and V. Rocha Vieira. Strongly correlated systems, coherence and entanglement. World Scientific Publishing Co. Pte. Ltd., 2007.

[208] S. Hamieh, J. Qi, D. Siminovitch, and M. K. Ali. Extracting classical correlations from a bipartite quantum system. Phys. Rev. A, 67:014301, 2003.

[209] S. Hamieh, R. Kobes, and H. Zaraket. Positive-operator-valued measure optimization of classical correlations. Phys. Rev. A, 70:052325, 2004.

[210] S. Oh and J. Kim. Entanglement of electron spins of noninteracting electron gases. Phys. Rev. A, 69:054305, 2004.

[211] V. M. Agranovich, O. A. Dubovsky, D. M. Basko, G. C. La Rocca, and F. Bassani. Kinematic frenkel biexcitons. J. Lum., 85:221–232, 2000.

[212] T. Renger, V. May, and O. Kühn. Ultrafast excitation energy transfer dynamics in photosynthetic pigment-protein complexes. Phys. Rep., 343:137, 2001.

[213] M. Mohseni, P. Rebentrost, S. Lloyd, and A. Aspuru-Guzik. Environment-assisted quantum walks in photosynthetic energy transfer. J. Chem. Phys., 129:174106, 2008.

[214] C. Ng, M. Z. DeMaere, T. J. Williams, F. M. Lauro, M. Raftery, J. A. E. Gibson, C. Andrews-Pfannkoch, M. Lewis, J. M. Hoffman, T. Thomas, and R. Cavicchioli. Metaproteogenomic analysis of a dominant green sulfur bacterium from ace lake, antarctica. The ISME Journal, 4:1002, 2010.

[215] P. Nalbach, C. A. Mujica-Martinez, and M. Thorwart. Vibronic speed-up of the excitation energy transfer in the fenna-matthews-olson complex. arXiv, 1311.6363, 2013.

[216] D. B. Turner, R. Dinshaw, K. K. Lee, M. S. Belsley, K. E. Wilk, M. P. Curmi, and G. D. Scholes. Quantitative investigations of quantum coherence for a light-harvesting protein at conditions simulating photosynthesis. Phys. Chem. Chem. Phys., 14:4857, 2012.

[217] V. Butkus, D. Zigmantas, and D. Abramavicius. Vibrational vs. electronic coherences in 2d spectrum of molecular systems. Chem. Phys. Lett., 545:40, 2012.

[218] J. Strümpfer and K. Schulten. The effect of correlated bath fluctuations on exciton transfer. J. Chem. Phys., 134:095102, 2011.

[219] S. Jesenko and M. Žnidarič. Excitation energy transfer rates: comparison of approximate methods to the exact solution. arXiv, 1405.4156, 2014.

[220] A. G. Dijkstra and Y. Tanimura. Correlated fluctuations in the exciton dynamics and spectroscopy of dna. New. J. Phys., 12:055005, 2010.

[221] F. Fassioli, A. Nazir, and A. Olaya-Castro. Quantum state tuning of energy transfer in a correlated environment. J. Phys. Chem. Lett., 1:2139, 2010.

[222] A. V. Akimov and O. V. Prezhdo. Persistent electronic coherence despite rapid loss of electron-nuclear correlation. J. Phys. Chem. Lett., 4:3857, 2013.

[223] A. Ishizaki and G. Fleming. Quantum superpositions in photosynthetic light harvesting: delocalization and entanglement. New J. Phys., 12:055004, 2010.

[224] B. Palmieri, D. Abramavicius, and S. Mukamel. Lindblad equations for strongly coupled populations and coherences in photosynthetic complexes. J. Chem. Phys., 130:204512, 2009.

[225] T. C. Berkelbach, D. R. Reichman, and T. E. Markland. Reduced density matrix hybrid approach: An efficient and accurate method for adiabatic and non-adiabatic quantum dynamics. J. Chem. Phys., 136:034113, 2012.

[226] T. C. Berkelbach, T. E. Markland, and D. R. Reichman. Reduced density matrix hybrid approach: Application to electronic energy transfer. J. Chem. Phys., 136:084104, 2012.

[227] P. Heman, U. Kleinekathöfer, I. Barvk, and M. Schreiber. Exciton scattering in light-harvesting systems of purple bacteria. J. Lum., 94-95:447, 2001.

[228] L. Valkunas, D. Abramavicius, and T. Mančas. Molecular excitation dynamics and relaxation. Wiley-VCH, Weinheim, 2013.

[229] P. Nalbach, J. Eckel, and M. Thorwart. Quantum coherent biomolecular energy transfer with spatially correlated fluctuations. New J. Phys., 12:065043, 2010.

[230] V. I. Prokhorenko, A. M. Nagy, L. S. Brown, and R. J. Dwayne Miller. On the mechanism of weak-field coherent control of retinal isomerization in bateriorhodopsin. Chem. Phys., 341:296, 2007.

[231] R. X. Xu, P. Cui, X. Q. Li, Y. Mo, and Y. Yan. Exact quantum master equation via the calculus on path integrals. J. Chem. Phys., 122:041103, 2005.

[232] J. Strümpfer and K. Schulten. Open quantum dynamics calculations with the hierarchy equations of motion on parallel computers. J. Chem. Theory and Comp., 8:2808, 2012.

[233] R. P. Feynman and A. R. Hibbs. Quantum Mechanics and Path Integrals. Mc Graw-Hill, New York, 1965.

[234] R. P. Feynman. Statistical Mechanics. Benjamin, Reading, 1972.

[235] L. S. Schulman. Techniques and Applications of Path Integration. Wiley, 1981.

[236] A. Ishizaki and Y. Tanimura. Quantum dynamics of system strongly coupled to low-temperature colored noise bath: reduced hierarchy equations approach. J. Phys. Soc. Jap., 74:3131, 2005.

[237] A. Ishizaki and Y. Tanimura. Nonperturbative non-markovian quantum master equation: Validity and limitation to calculate nonlinear response functions. Chem. Phys., 347:185, 2008.

[238] O. Kühn, T. Renger, and V. May. Theory of exciton-vibrational dynamics in molecular dimers. Chem. Phys., 204:99, 1996.

[239] T. Renger, J. Voigt, V. May, and O. Kühn. Dissipative exciton motion in a chlorophyll a/b dimer of the light harvesting complex of photosystem ii: Simulation of pump-probe spectra. Phys. Chem., 100:15654, 1996.

[240] M. F. Gelin, L. Z. Sharp, D. Egorova, and W. Domcke. Bath-induced correlations and relaxation of vibronic dimers. J. Chem. Phys., 136:034507, 2012.

[241] P. Rebentrost, M. Mohseni, I. Kassal, S. Lloyd, and A. Aspuru-Guzik. Environment-assisted quantum transport. New J. Phys., 11:033003, 2009.

[242] M. Bixon and J. Jortner. Electron transfer- from isolated molecules to biomolecules. J. Adv. Chem. Phys., 106:35, 1999.

[243] D. Segal and D. R. Reichman. Zeno and anti-zeno effects in spin-bath models. Phys. Rev. A, 76:012109, 2007.

[244] P. Rebentrost, M. Mohseni, and A. Aspuru-Guzik. Role of quantum coherence and environmental fluctuations in chromophoric energy transport. J. Phys. Chem. B, 113:9942, 2009.

[245] I. Kassal and A. Aspuru-Guzik. Environment-assisted quantum transport in ordered systems. New J. Phys., 14:053041, 2012.

[246] R. Bulla, H. J. Lee, N. H. Tong, and M. Vojta. Numerical renormalization group for quantum impurities in a bosonic bath. Phys. Rev. B, 71:045122, 2005.

[247] R. Bulla, N. H. Tong, and M. Vojta. Numerical renormalization group for bosonic systems and application to the sub-ohmic spin-boson model. Phys. Rev. Lett., 91:170601, 2003.

[248] NREL. Reference Solar Spectral Irradiance: Air Mass 1.5, 1999.

[249] V. Blanchet, M. Z. Zgierski, T. Seideman, and A. Stolow. Discerning vibronic molecular dynamics using time-resolved photoelectron spectroscopy. Nature, 401:52, 1999.

[250] M. Seel and W. Domcke. Model studies on femtosecond time-resolved ionization spectroscopy of excited-state vibrational dynamics and vibronic coupling. Chem. Phys., 151:59, 1991.

[251] S. Haessler, J. Caillat, W. Boutu, C. Giovanetti-Teixeira, T. Ruchon, T. Auguste, Z. Diveki, P. Breger, A. Maquet, B. Carré, R. Taïeb, and P. Salières. Attosecond imaging of molecular electronic wavepackets. Nat. Phys., 6:200, 2010.

[252] T. Pfeifer, M. J. Abel, P. M. Nagel, A. Jullien, Z. H. Loh, M. J. Bell, D. M. Deumark, and S. R. Leone. Time-resolved spectroscopy of attosecond quantum dynamics. Chem. Phys. Lett., 463:11, 2008.

[253] G. Sansone, F. Kelkensberg, J. F. Pérez-Torres, F. Morales, M. F. Kling, W. Siu, O. Ghafur, P. Johnsson, M. Swoboda, E. Benedetti, F. Ferrari, F. Lépine, J. L. Sanz-Vicario, S. Zherebtsov, I. Znakovskaya, A. L'Huillier, M. Y. Ivanov, M. Nisoli, F. Martín, and M. J. J. Vrakking. Electron localization following attosecond molecular photoionization. Nature, 465:763, 2010.

[254] A Kramers. Physica (amsterdam) 7, 284 (1940); m. buttiker, e. p. harris, and r. landauer. Phys. Rev. B, 28:1268, 1983.

[255] L. D. Zusman. Outer-sphere electron transfer in polar solvents. Chem. Phys., 49:295, 1980.

[256] M. Born and J. R. Oppenheimer. Zur quantentheorie der molekeln. Ann. Phys., 84:457, 1927.

[257] R. F. Snider, G. W. Wei, and J. G. Muga. Moderately dense gas quantum kinetic theory: Aspects of pair correlations. J. Chem. Phys., 105:3057, 1996.

[258] K. Bärwinkel and S. Grossmann. The pair distribution function of moderately dense quantum fluids. Zeitschrift für Physik, 230:141, 1970.

[259] K. Bärwinkel, J. Schnack, and U. Thelker. Quasi-particle picture for monatomic gases. Physica A: Statistical mechanics and its applications, 262:496, 1999.

[260] K. Bärwinkel and J. Schnack. van der waals revisited. Physica A: Statistical mechanics and its applications, 387:4581, 2008.

[261] B. J. Baumgartl. Second and third virial coefficient of a quantum gas from two-particle scattering amplitude. Zeitschrift für Physik, 198:148, 1967.

[262] D. Kremp, W. D. Kraeft, and W. Ebeling. Quantum-statistical second virial coefficient and scattering theory. Physica, 51:146, 1971.

[263] A. Hackl and M. Vojta. Pressure-induced magnetic transition and volume collapse in feas superconductors: an orbital-selective mott scenario. New J. Phys., 11:055064, 2009.

[264] K. Nasu. Extended peierls-hubbard model for one-dimensional n-sites n-electrons system. i. phase diagram by mean field theory. J. Phys. Soc. Jpn., 52:3865, 1983.

[265] M. Valiente and D. Petrosyan. Two-particle states in the hubbard model. J. Phys. B: At. Mol. Opt. Phys., 41:161002, 2008.

[266] M. Valiente and D. Petrosyan. Scattering resonances and two-particle bound states of the extended hubbard model. J. Phys. B: At. Mol. Opt. Phys., 42:121001, 2009.

[267] R. D. Averitt. Nat. Phys., 4:14, 2008.

[268] D. G. Evans and R. D. Coalson. Simulation of electron transfer in polar solvents: Effects of nonequilibrium initial state preparation. J. Chem. Phys., 104:3598, 1996.

[269] D. G. Evans and R. D. Coalson. Incorporating backflow into a relaxation theory treatment of the dynamics of nonequilibrium nonadiabatic transition processes. J. Chem. Phys. , 102:5658, 1995.

[270] R. D. Coalson, D. G. Evans, and A. Nitzan. A nonequilibrium golden rule formula for electronic state populations in nonadiabatically coupled systems. J. Chem. Phys. , 101:436, 1994.

[271] Q. Shi, L. Chen, G. Nan, R. Xu, and Y. Yan. Electron transfer dynamics: Zusman equation versus exact theory. J. Chem. Phys., 130:164518, 2009.

[272] K. Han and C. Tianshu, editors. Reaction Rate Constant Computations: Theories and Applications. Royal Society of Chemistry, 2013.

[273] D. A. McQuarrie. Statistical Mechanics. University Science Books, Sausalito, 2000.

[274] J. L. McHale. Molecular Spectroscopy. Prentice Hall, New Jersey, 1999.

[275] G. R. Fleming and M. Cho. Chromophore-solvent dynamics. Annu. Rev. Phys. Chem., 47:109–134, 1996.

[276] C. J. Fecko, J. D. Eaves, and A. Tokmakoff. Isotropic and anisotropic raman scattering from molecular liquids measured by spatially masked optical kerr effect spectroscopy. J. Chem. Phys., 117:1139–1154, 2002.

[277] M. Busse. Entanglement in open quantum systems. PhD thesis, Max-Planck-Institut, 2006.

[278] S. Y. Shiau, M. Combescot, and Y. C. Chang. Electronic structure and absorption spectrum of biexciton obtained by using exciton basis. Annals of Physics, 336:309, 2013.

[279] E. O. Potma and D. A. Wiersma. Exciton superradiance in aggregates: The effect of disorder, higher order exciton-phonon coupling and dimensionality. J. Chem. Phys., 108:4894, 1998.

[280] L. Amico, R. Fazio, A. Osterloh, and V. Vedral. Entanglement in many-body systems. Rev. Mod. Phys., 517:80, 2008.

[281] E. Schrödinger. Discussion of probability relations between separated systems. Math Proc. Cambridge, 31:555, 1935.

[282] S. Longhi. Bound states in the continuum in a single-level fano-anderson model. Eur. Phys. J. B, 57:45, 2007.

[283] M. Combescot and W. Pogosov. Composite boson many-body theory for frenkel excitons. Eur. Phys. J. B, 68:161, 2009.

[284] V. Chernyak, N. Wang, and S. Mukamel. Four-wave mixing and luminescence of confined excitons in molecular aggregates and nanostructures. many-body green function approach. Phys. Rep., 263:213, 1995.

[285] H. A. Bethe. On the theory of metals. i. eigenvalues and eigenfunctions of a linear chain of atoms. Z. Phys., 71:205, 1931.

[286] B. J. Walker, A. J. Musser, D. Beljonne, and R. H. Friend. Singlet exciton fission in solution. Nat. Chem., 5:1019, 2013.

[287] L. D. Bakalis and J. Knoester. Pump-probe spectroscopy and the exciton delocalization length in molecular aggregates. J. Phys. Chem. B, 103:6620, 1999.

[288] V. M. Axt and T. Kuhn. Femtosecond spectroscopy in semiconductors: a key to coherences, correlations and quantum kinetics. Rep. Prog. Phys., 67:433, 2004.

[289] M. C. Tichy, F. Mintert, and A. Buchleitner. Essential entanglement for atomic and molecular physics. J. Phys. B: At. Mol. Opt. Phys., 44:192001, 2011.

[290] C. Bulutay and B. Tanatar. Dynamical correlations in quasi-one dimensional electron gas. Europhys. Lett., 43:572, 1998.

[291] X. S. Ma, M. T. Cheng, G. X. Zhao, and A. M. Wang. Quantum discord of electron spins of noninteracting electron gases. Eur. Phys. J. D, 66:46, 2012.

[292] C. Wang and M. J. Tauber. High-yield singlet fission in a zeaxanthin aggregate observed by picosecond resonance raman spectroscopy. J. Am. Chem. Soc., 132:13988, 2010.

[293] A. Rao, M. W. B. Wilson, J. M. Hodgkiss, S. Albert-Seifried, H. Bässler, and R. H. Friend. Exciton fission and charge generation via triplet excitons in pentacene/c_{60} bilayers. J. Am. Chem. Soc., 132:12698, 2010.

[294] M. A. Nielsen, C. M. Dawson, J. L. Dodd, A. Gilchrist, D. Mortimer, T. J. Osborne, M. J. Bremner, A. W. Harrow, and A. Hines. Quantum dynamics as a physical resource. Phys. Rev. A, 67:052301, 2003.

[295] P. J. Jadhav, P. R. Brown, N. Thompson, B. Wunsch, A. Mohanty, S. R. Yost, E. Hontz, T. V. Voorhis, M. G. Bawendi, V. Bulović, and M. A. Baldo. Triplet exciton dissociation in singlet exciton fission photovoltaics. Adv. Mater., 24:6169–6174, 2012.

[296] G. Vidal. Entanglement of pure states for a single copy. Phys. Rev. Lett., 83:1046–1049, 1999.

[297] J. C. Johnson, A. J. Nozik, and J. Michl. High triplet yield from singlet fission in a thin film of 1,3-diphenylisobenzofuran. J. Am. Chem. Soc., 132:16302–16303, 2010.

[298] P. W. Brouwer, C. Mudry, B. D. Simons, and A. Altland. Delocalization in coupled one-dimensional chains. Phys. Rev. Lett., 81:862–865, 1998.

[299] S. Kouachi. Eigenvalues and eigenvectors of tridiagonal matrices. J. Linear Algebra, 15:115–133, 2006.

[300] M. Sarovar, A. Ishizaki, G. R. Fleming, and K. Birgitta Whaley. Quantum entanglement in photosynthetic light-harvesting complexes. Nat. Phys., 6:462–467, 2010.

[301] D. Abramavicius and S. Mukamel. Quantum oscillatory exciton migration in photosynthetic reaction centers. J. Chem. Phys., 133:064510, 2010.

[302] H. Benk and H. Sixl. Theory of two coupled triplet states: Application to bicarbene structures. Mol. Phys., 42:779, 1981.

[303] A. Franceschetti, J. M. An, and A. Zunger. Impact ionization can explain carrier multiplication in pbse quantum dots. Nano Lett., 6:2191–2195, 2006.

[304] M. Malagoli, V. Coropceanu, D. A. da Silva Filho, and J. L. Brédas. A multimode analysis of the gas-phase photoelectron spectra in oligoacenes. J. Chem. Phys., 120:7490, 2004.

[305] Y.-C. Chang and I. Chao. An important key to design molecules with small internal reorganization energy: Strong nonbonding character in frontier orbitals. J. Phys. Chem. Lett., 1:116–121, 2009.

[306] D. Segal, A. Nitzan, W. B. Davis, M. R. Wasielewski, and M. A. Ratner. Electron transfer rates in bridged molecular systems 2. a steady-state analysis of coherent tunneling and thermal transitions. J. Phys. Chem. B, 104:3817–3829, 2000.

[307] M. Mejatty, J. L. Monge, V. Ern, and H. Bouchriha. Applicability of the kinematic pair-density-matrix theory to optically detected magnetic-resonance spectra of two-dimensional molecular crystals. Phys. Rev. B, 43:2558–2564, 1991.

[308] C. H. Bennett, S. Popescu, D. Rohrlich, J. A. Smolin, and A. V. Thapliyal. Exact and asymptotic measures of multipartite pure-state entanglement. Phys. Rev. A, 63:012307, 2000.

[309] V. Vedral, M. B. Plenio, M. A. Rippin, and P. L. Knight. Quantifying entanglement. Phys. Rev. Lett., 78:2275–2279, 1997.

[310] A. Lagendijk, B. van Tiggelen, and D. S. Wiersma. Fifty years of anderson localization.

[311] N. Mott. Metal-insulator transitions. Physics Today, 31:42, 1978.

[312] D. H. Dunlap, H. L. Wu, and P. W. Phillips. Absence of localization in a random-dimer model. Phys. Rev. Lett., 65:88–91, 1990.

[313] F. M. Izrailev, T. Kottos, A. Politi, S. Ruffo, and G. P. Tsironis. Quantum diffusion and localization of wavepackets in disordered media. Europhys. Lett., 34:441–446, 1996.

[314] P. A. Lee and D. S. Fisher. Anderson localization in two dimensions. Phys. Rev. Lett., 47:882–885, 1981.

[315] M. Jammer. The Philosophy of Quantum Mechanics. Wiley, New York, 1974.

[316] M. Borda. Fundamentals in Information Theory and Coding, volume 6. Springer, New York, 2011.

[317] N. W. Ashcroft and N. D. Mermin. Solid State Physics. Brooks/Cole, Belmont, 2004.

[318] A. A. Abrikosov, L. P. Gorkov, and I. E. Dzyaloshinksy. Quantum Field Theoretical Methods in Statistical Physics. Oxford, New York, 1965.

[319] J. M. Ziman. Elements of advanced quantum theory. Cambridge Univ. Press, New York, 1969.

[320] G. Jaeger. Entanglement, information, and the interpretation of quantum mechanics. Springer-Verlag, Berlin Heidelberg, 2009.

[321] H. Hossein-Nejad, V. V. Albert, E. J. O'Reilly, and G. D. Scholes. Corrigendum: Energy transfer, entanglement and decoherence in a molecular dimer interacting with a phonon bath. New J. Phys., 16:019502, 2014.

[322] C. Kreisbeck, T. Kramer, and A. Aspuru-Guzik. Disentangling electronic and vibronic coherences in two-dimensional echo spectra. J. Phys. Chem. B, 117:9380, 2013.

[323] J. M. Anna, G. D. Scholes, and R. van Grondelle. A little coherence in photosynthetic light harvesting. BioScience, 64:14, 2014.

[324] L. G. Mourokh and F. Nori. Energy transfer efficiency in the fmo complex strongly coupled to a vibronic mode. arXiv, 1402.7031v1, 2014.

[325] M. F. Gelin, A. V. Pisliakov, and W. Domcke. Time- and frequency-gated spontaneous emission as a tool for studying vibrational dynamics in the excited state. Phys. Rev. A, 65:062507, 2002.

[326] J. D. Hybl, A. A. Ferro, and D. M. Jonas. Two-dimensional fourier transform electronic spectroscopy. J. Chem. Phys., 115:6606, 2001.

[327] E. R. Smith and D. M. Jonas. Alignment, vibronic level splitting, and coherent coupling effects on the pump- probe polarization anisotropy. J. Phys. Chem. A, 115:4101, 2011.

[328] A. Matro and J. A. Cina. Theoretical study of time-resolved fluorescence anisotropy from coupled chromophore pairs. J. Phys. Chem., 99:2568, 1995.

[329] S. Savikhin, D. R. Buck, and W. S. Struve. Oscillating anisotropies in a bacteriochlorophyll protein: Evidence for quantum beating between exciton levels. Chem. Phys., 223:303, 1997.

[330] J. Strümpfer and K. Schulten. Light harvesting complex ii b850 excitation dynamics. J. Chem. Phys., 131:225101, 2009.

[331] Y. C. Cheng and G. R. Fleming. Coherence quantum beats in two-dimensional electronic spectroscopy. J. Phys. Chem. A, 112:4254, 2008.

[332] W. M. Zhang, T. Meier, V. Chernyak, and S. Mukamel. Exciton-migration and three-pulse femtosecond optical spectroscopies of photosynthetic antenna complexes. J. Chem. Phys., 108:7763, 1998.

[333] S. Berweger, J. M. Atkin, X. G. Xu, R. L. Olmon, and M. B. Raschke. Femtosecond nanofocusing with full optical waveform control. Nano Lett., 11:4309, 2011.

[334] S. Berweger, J. M. Atkin, R. L. Olmon, and M. B. Raschke. Adiabatic tip-plasmon focusing for nano-raman spectroscopy. J. Phys. Chem. Lett., 1:3427, 2010.

[335] M. D'Amore, F. Auriemma, C. De Rosa, and V. Barone. Disordered chain conformations of poly(tetrafluoroethylene) in the high-temperature crystalline form i. Macromolecules, 37:9473, 2004.

[336] A. Serov, A. Choukourov, I. Melnichuk, A. Shelemin, A. Kuzminova, O. Kylián, J. Hanuš, J. Kousal, M. Drábik, D. Slavínská, and H. Biederman. Poly(tetrafluoroethylene) sputtering in a gas aggregation source for fabrication of nano-structured deposits. Surface and Coatings Technology, 254:319, 2014.

[337] C. Wang, G. Duscher, and J. Paddison. Electron energy loss spectroscopy of polytetrafluoroethylene: experiment and first principles calculations. Microscopy, 0:1, 2013.

[338] C. Quarti, A. Milani, and C. Castiglioni. Ab initio calculation of the ir spectrum of ptfe: Helical symmetry and defects. J. Phys. Chem. B, 117:706, 2013.

[339] K. F. Freed and A. A. Villaeys. Coherence transfer processes in vibrational relaxation of polyatomic molecules in condensed media. Chem. Phys., 39:51, 1979.

[340] A. Tokmakoff, B. Sauter, and M. D. Fayer. Temperature-dependent vibrational relaxation in polyatomic liquids: Picosecond infrared pump-probe experiments. J. Chem. Phys., 100:9035, 1994.

[341] M. Gruebele. Mechanism and control of molecular energy flow: a modeling perspective. Theor. Chem. Acc., 109:53, 2003.

[342] M. Bixon and J. Jortner. Intramolecular radiationless transitions. J. Chem. Phys., 48:715, 1968.

[343] M. Khalil, N. Demirdoeven, and A. Tokmakoff. Vibrational coherence transfer characterized with fourier-transform 2d ir spectroscopy. J. Chem. Phys., 121:362, 2004.

[344] A. Godec and R. Metzler. Finite-time effects and ultraweak ergodicity breaking in superdiffusive dynamics. Phys. Rev. Lett., 110:020603, 2013.

[345] R. Bittl and K. Schulten. A static ensemble approximation for stochastically modulated quantum systems. J. Chem. Phys. , 90:1794, 1989.

[346] B. Harland and S. X. Sun. Path ensembles and path sampling in nonequilibrium stochastic systems. J. Chem. Phys. , 127:104103, 2007.

[347] S. X. Sun. Equilibrium free energies from path sampling of nonequilibrium trajectories. J. Chem. Phys. , 118:5769, 2003.

[348] P. Alonso-González. Resolving the electromagnetic mechanism of surface-enhanced light scattering at single hot spots. Nat. Comm., 3:684, 2012.

[349] B. Mishra and T. Schlick. The notion of error in langevin dynamics. i. linear analysis. J. Chem. Phys., 105:299, 1996.

[350] C. H. Chou, T. Yu, and B. L. Hu. Exact master equation and quantum decoherence of two coupled harmonic oscillators in a general environment. Phys. Rev. E, 77:011112, 2008.

[351] R. L. S. Farias, R. O. Ramos, and L. A. da Silva. Stochastic langevin equations: Markovian and non-markovian dynamics. Phys. Rev. E, 80:031143, 2009.

[352] A. I. Burshtein and V. S. Malinovsky. Free-induction decay in the framework of sudden-modulation theory. J. Opt. Soc. Am. B, 8:1098, 1991.

[353] S. Chandrasekhar. Stochastic problems in physics and astronomy. Rev. Mod. Phys., 15:1, 1943.

[354] J. W. Gadzuk. Vibrational lineshapes of adsorbates: the role of substrate electronic excitations. Chem. Phys. Lett., 80:5, 1981.

[355] G. W. Ford and M. Kac. On the quantum langevin equation. J. of Stat. Phys., 46:803, 1987.

[356] B. Knoll and F. Keilmann. Enhanced dielectric constrast in scattering-type scanning near-field optical microscopy. Optics Comm., 182:321, 2000.

[357] B. Pollard, E. A. Muller, K. Hinrichs, and M. B. Raschke. Vibrational nano-spectroscopic imaging correlating structure with intermolecular coupling and dynamics. Nat. Comm., 5:1, 2014.

[358] X. G. Xu and M. B. Raschke. Near-field infrared vibrational dynamics and tip-enhanced decoherence. Nano Lett., 13:1588, 2013.

[359] S. Berweger, J. M. Atkin, R. L. Olmon, and M. B. Raschke. Light on the tip of a needle: Plasmonic nanofocusing for spectroscopy on the nanoscale. Phys. Chem. Lett., 3:945, 2012.

[360] R. Adato, A. A. Yanik, J. J. Amsden, D. L. Kaplan, F. G. Omenetto, M. K. Hong, S. Erramilli, and H. Altug. Ultra-sensitive vibrational spectroscopy of protein monolayers with plasmonic nanoantenna arrays. P. Natl. Acad. Sci., 106:19227, 2009.

[361] D. Dregely, F. Neubrech, H. Duan, R. Vogelgesang, and H. Giessen. Vibrational near-field mapping of planar and buried three-dimensional plasmonic nanostructures. Nat. Comm., 4:1, 2013.

[362] R. L. Olmon, P. M. Krenz, A. C. Jones, G. D. Boreman, and M. B. Raschke. Near-field imaging of optical antenna modes in the mid-infrared. Optics Express, 16:20295, 2008.

[363] M. B. Raschke, S. Berweger, and J. M. Atkin. Plasmonics: Theory and Application, Challenges and Advances in Computational Chemistry and Physics (CH. 7), volume 15. Springer, New York, 2013.

[364] M. Grigoriu. Applied Non-Gaussian Processes. PTR Prentice Hall, Englewood Cliffs, 1995.

[365] P. Hänggi. Stochastic Dynamics., volume 484 of Lecture Notes in Physics. Springer, Berlin, 1997.

[366] W. H. Press, S. A. Teukolsky, W. T. Vetterling, and B. P. Flannery. Numerical Recipes. Cambridge University Press, New York, 2007.

Appendix A

Stochastic Modeling of the Vibrational FID in s-SNOM of PTFE

A.1 Introduction

The advent of scattering-scanning near-field optical microscopy (s-SNOM) has made possible the imaging of condensed matter on nanometer length scales.[334, 358, 357] By propagating surface plasmon polaritons along nanoantenna capable of supporting strong local fields, S. Berweger *et al.*[334] enhanced the sensitivity of s-SNOM with near-infrared excitation. In recent years, s-SNOM and femtosecond (fs) infrared (IR) vibrational spectroscopy have been combined to image micro chemical environments.[358, 357] In 2013, Xu and Raschke[358] studied the vibrational free-induction decay (FID) of polytetrafluoroethylene (PTFE), also known as Teflon, and found that the tip-sample coupling provides control of vibrational decoherence. Since then, the Raschke group has also examined poly(methyl methacrylate) (PMMA).[357]

FID arises from the near-field dipole-dipole coupling between the AFM tip and molecular vibrations. The near-field signal is a coherent superposition of a frequency independent nonresonant instantaneous response and a resonant vibrational contribution.[348] In this appendix, we assume that s-SNOM impulsively excites vibrational coherence in PTFE that then decays through interactions with segments of PTFE many nanometers removed from the probed subensemble as well as through interactions with neighboring PTFE chains.

In the classical description of FID, a radiating dipole moment is represented as a local harmonic vibration. Normal oscillations are damped by friction, and thermal fluctuations randomly perturb the vibration. The transition dipole operator for N oscillators, each interacting with the

IR field, is $\hat{\mu} = \sum_{i=0}^{N-1} \left(\frac{\partial \mu}{\partial q_i}\right)_0 q_i$, where q_i is the vibrational coordinate of the i^{th} oscillator. The linear response function for linear optical measurements is governed by the time correlation function, $C(t) = \langle\ \mu(t)\mu(0)\ \rangle$. C. Quarti *et al.* have shown,[338] using density functional theory with the B3LYP/TZVP functional, that the intensity of the local symmetric stretch frequency is dramatically reduced when infinite chains are replaced with finite length oligomers. We will simulate the dynamics of $q_i(t)$ using the quantum Langevin equation to explore how s-SNOM might predict the vibrational composition of PTFE at nanometer resolutions, and how spectral features of FID depend on chain length.

A.2 Nonergodic FID at Nanometer s-SNOM Resolution

At room temperature, the CF_2 groups are arranged in PTFE chains in a zig zag conformation such that local CF_2 dipole moments alternate along the carbon backbone. If these CF_2 groups are only weakly interacting, then the Fourier transformation of the FID will possess two strong features at $\Omega_s \approx 1160\ cm^{-1}$ and $\Omega_{as} \approx 1220\ cm^{-1}$, corresponding to the local symmetric and antisymmetric stretch frequencies, respectively.[336, 358, 337] To make progress, we ignore phase transitions that can occur across a range of temperatures[338, 337, 335] from $0 - 50$ °C, and choose an approximate zeroth order basis of local symmetric and antisymmetric stretch modes.[337, 336, 358]

Friction damps the harmonic motion of the local stretches and also damps thermal fluctuations arising from the chemical environment surrounding the subensemble of local oscillations probed by s-SNOM. If friction is uncorrelated with respect to each local normal mode, then the dynamics of each vibration are independent, and we start with a model Hamiltonian of a single displacement, q, subject to a potential, $V(q)$, with the momentum canonical to the position defined as p. If the mass responds linearly to displacements of vibrations in a heat bath, then the Hamiltonian in mass-weighted coordinates is[355, 3, 4, 6]

$$H = p^2/2 + V(q) + \sum_j \left[k_j^2/2 + \omega_j^2(x_j - \lambda_j q)^2/2\right] \tag{A.1}$$

having let $\hbar = 1$. The equilibrium position of the j^{th} bath mode is $\chi_j = \lambda_j q$. Using $[q, p] = i$,

$[x_j, k_k] = i\delta_{j,k}$, and $\frac{d}{dt}A = -i[A, H]$ one can derive the Heisenberg equations of motion:

$$\frac{d}{dt}q = p \tag{A.2}$$

and

$$\frac{d}{dt}p = -\frac{d}{dq}V(q) + \sum_j \omega_j^2 \lambda_j (x_j - \lambda_j q) \quad , \tag{A.3}$$

having used $\frac{d}{dt}q = \frac{\partial H}{\partial p}$ and $\frac{d}{dt}p = -\frac{\partial H}{\partial q}$, and

$$\frac{d}{dt}x_j = k_j \quad , \quad \frac{d}{dt}k_j = \omega_j^2(\lambda_j q - x_j) \quad . \tag{A.4}$$

Eqs. A.2, A.3, and A.4 define a system of inhomogeneous differential equations:

$$\frac{d^2}{dt^2}q = -\frac{d}{dq}V(q) + \sum_j \omega_j^2 \lambda_j (x_j - \lambda_j q) \tag{A.5}$$

$$\frac{d^2}{dt^2}x_j = \omega_j^2(\lambda_j q - x_j) \quad . \tag{A.6}$$

Solutions of these differential equations are common, and we leave the derivation of the general solution,[365]

$$\begin{aligned} x_j(t) &= X_j(t) + \tilde{x}_j(t) = \\ &= \big(x_j - \lambda_j q(0)\big) cos(\omega_j t) + \frac{k_j}{\omega_j} sin(\omega_j t) + \lambda_j q(t) - \lambda_j Ref_j(t) \quad , \end{aligned} \tag{A.7}$$

to the reader. Insert this result into Eqn. A.3 to arrive at

$$\frac{d^2}{dt^2}q + \int_0^t d\tau R(t-\tau)\frac{d}{d\tau}q(\tau) + \frac{d}{dq}V(q) = F(t) \quad , \tag{A.8}$$

with the stochastic forcing function given by

$$F(t) = \sum_j \left[\big(x_j - \lambda_j q(0)\big)\omega_j^2 \lambda_j cos(\omega_j t) + k_j \omega_j \lambda_j sin(\omega_j t)\right] \quad , \tag{A.9}$$

and the response function defined as $R(t) = \sum_j \omega_j^2 \lambda_j^2 cos(\omega_j t)$. Friction is said to be memoryless if it does not depend on the history of the velocity, such that the response function is proportional to a scalar friction, γ.

x_j and k_j are sampled from the equilibrium distribution of free harmonic oscillators, $\rho_B = exp\big[-H_B/k_BT\big]$ with $H_B = \sum_j \big[k_j^2/2 + \omega_j^2 x_j^2/2\big]$. The initial conditions are: $\langle x_j\rangle = \langle k_j\rangle = 0$ for all j, $\frac{1}{2}\langle k_j k_k\rangle = \frac{\omega_j^2}{2}\langle x_j x_k\rangle = \frac{k_BT}{2}\delta_{j,k}$, and $\langle x_j k_k\rangle = 0$ for all j and k. Thermal energy fixes the ratio of the stochastic correlation to the response, $k_BT = \langle F(t)F(0)\rangle/R(t)$. In the Markovian limit, all noise is white noise, and $\langle F(t)F(0)\rangle = \sigma\delta(t)$ with $\sigma = 2\gamma k_BT$. Here the force varies rapidly relative to all other timescales in the problem, and the dynamics are governed by the quantum Langevin equation,

$$\frac{d^2}{dt^2}q + \gamma\frac{d}{dt}q + \frac{d}{dq}V(q) = F(t) \quad . \tag{A.10}$$

The expectations of variance in the position and momentum in the ensemble limit are k_BT/ω^2 and k_BT, respectively. To test deviations from ensemble expectation values of the linear polarization when s-SNOM accesses a small ensemble of local vibrations, we first launch N stochastic trajectories in the harmonic potential, $V(q) = \frac{1}{2}\Omega_s^2 q^2$. In the semi-impulsive limit, the driving field is a short pulse,

$$E(t) \approx Ee^{i\Omega_p t}\delta(t) \approx Ee^{i\Omega_p t}\frac{\tau/\pi}{\tau^2 + t^2} \quad , \tag{A.11}$$

and

$$\frac{d^2}{dt^2}q + \int_0^t d\tau R(t-\tau)\frac{d}{d\tau}q(\tau) + \frac{d}{dq}V(q) = eE(t) + F(t) \quad . \tag{A.12}$$

where e is one unit of elementary charge. In this Appendix we fix $E = e = 1$. If the Markovian approximation is valid, the displacement can be solved using the Fourier space Green's function, $\hat{G}(\omega)$, and is given by

$$q(t) = \int_{-\infty}^{\infty} d\omega e^{i\omega t}\hat{G}(\omega)\big(e\hat{E}(\omega) + \hat{F}(\omega)\big) \quad , \tag{A.13}$$

with $\hat{E}(\omega) = \int_{-\infty}^{\infty} dt e^{-i\omega t}E(t)$ and $\hat{F}(\omega) = \int_{-\infty}^{\infty} dt e^{-i\omega t}F(t)$. The Green's function is

$$\hat{G}(\omega) = \big[-\omega^2 + i\gamma\omega + \Omega^2\big]^{-1} \quad . \tag{A.14}$$

To simulate a subensemble of N vibrations, we launch N trajectories that each experience a statistically independent "noisy" chemical environment, enumerated by i:

$$q_i(t) = \int_{-\infty}^{\infty} d\omega e^{i\omega t} \hat{G}(\omega)\big(e\hat{E}(\omega) + \hat{F}_i(\omega)\big) \quad .(A.15)$$

The underlying frequency fluctuations can be described using Kubo theory, where the correlation of Gaussian fluctuations exponentially decay in time,

$$\langle \delta\Omega(t)\delta\Omega(0)\rangle = \Delta^2 e^{-\Gamma t} \quad . \tag{A.16}$$

In Fig. A.1 we calculate the autocorrelation function, $C(t) = \langle\ q(t)q(0)\ \rangle$, fixing the friction and inverse Kubo decay time to $\gamma = \Gamma = (680\text{ fs})^{-1}$. From Fig. A.1 we see that, as the number of independent trajectories is reduced from 100 to 10, both the Kubo response function and the autocorrelation function are not fully damped on picosecond timescales. More work is needed to set quantitative albeit numerical thresholds for what constitutes recurrence at long times, and whether such noisy dynamics fall outside the scope of ergodic theory.

In Fig. A.2 we simulate a mixed ensemble of N symmetric ($\Omega_s = 1160\ cm^{-1}$ and $\gamma_s = (680\ fs)^{-1}$) and N antisymmetric ($\Omega_{as} = 1220\ cm^{-1}$ and $\gamma_{as} = (340\ fs)^{-1}$) local vibrations. From Fig. A.2 we see the same nonergodic and noisy dynamics when the number of trajectories is reduced from 100 to 10, but now with a recurrence in $C(t)$ corresponding to the interference of the symmetric and antisymmetric stretch frequencies.

A.3 Coherence Transfer between Local Vibrations

The finite set of local symmetric and antisymmetric stretch modes is an approximate representation for the response of PTFE to strong local IR fields. The accuracy of our simulations in this zeroth order picture may be compromised as the extent of crystallinity is reduced such that PTFE becomes a disordered solid, and if elements of the Hessian strongly couple nearest-neighbor stretches. At temperatures between 0 and 50 °C there is conformational disorder in the crystalline

Figure A.1: The Kubo response function (a) and autocorrelation function (b), described in the text, for a PTFE sample at 300 K driven by a short pulse ($\tau = 200\ fs$) with frequency $\Omega_p = 1160\ cm^{-1}$. Simulations of subensembles of 100 and 10 oscillators are shown in blue and green, respectively. An inset of $\varrho = -\frac{1}{\pi} Im[\hat{G}(\omega)]$ is shown in (a).

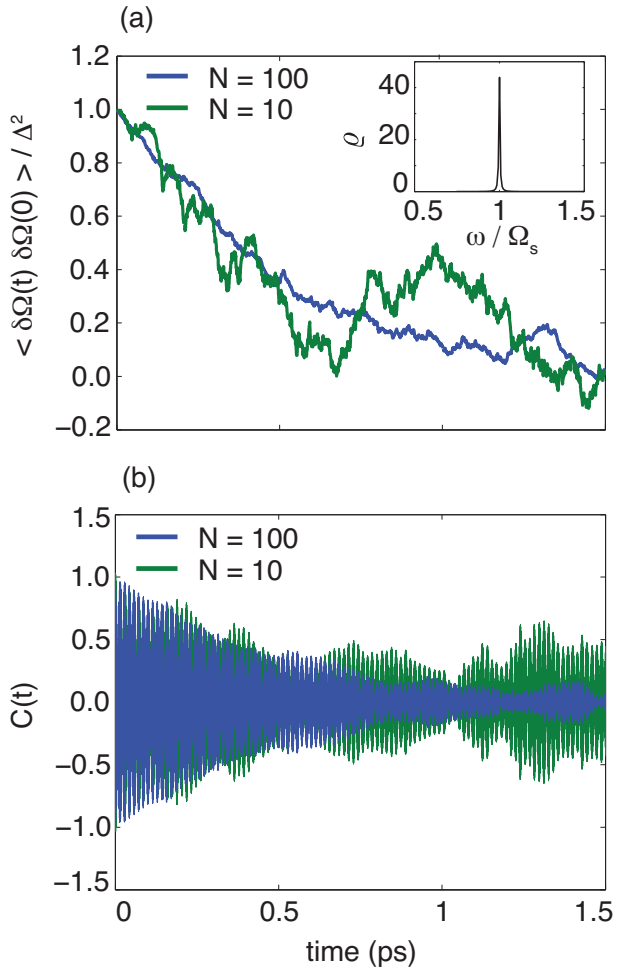

Figure A.2: The Kubo response function (a) and autocorrelation function (b), described in the text, for a PTFE sample at 300 K driven by a short pulse ($\tau = 200\ fs$) with frequency $\Omega_p = 1190\ cm^{-1}$. Simulations of subensembles of 100 and 10 oscillators are shown in blue and green, respectively. An inset of $\varrho = -\frac{1}{\pi} Im[\hat{G}(\omega)]$ is shown in (a).

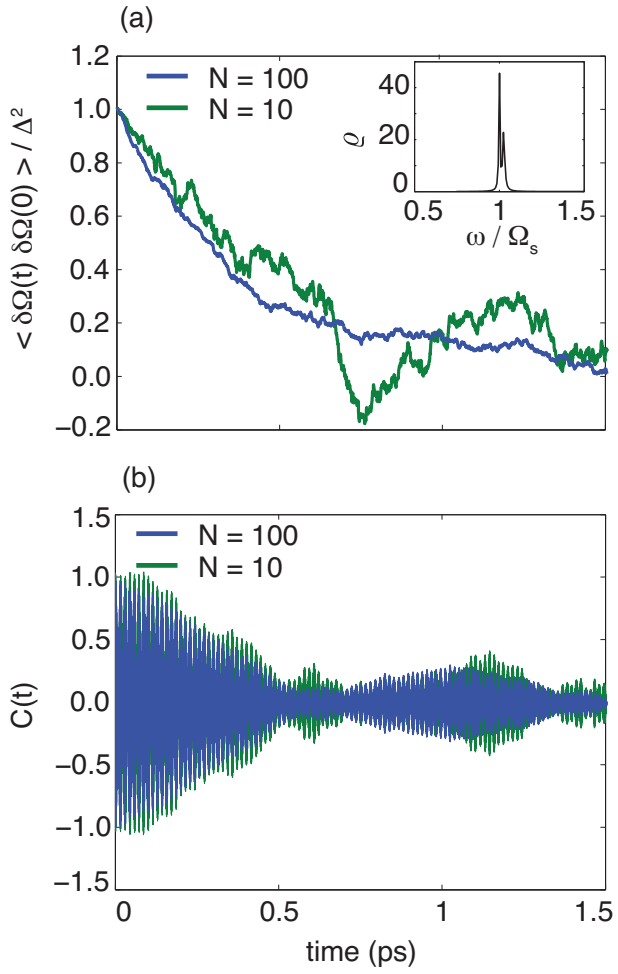

phase of PTFE.[338] PTFE is primarily found in the zig zag and pseudohexagonal 15_7 helix conformations at 30 °C, in a hexagonal 15_7 helix conformation at lower temperatures ($19 - 30$ °C), and below 19 °C is most stable as the 13_6 helices.[338, 337, 336] The15_7 and 13_6 oligomers refer to configurations which contain 15 CF_2 groups in 7 turns and 13 CF_2 groups in 6 turns, respectively.

13_6 and 15_7 are split by energies approximately equal to dispersive interaction energies. It is thought that the 13_6 phase is dominated by inter-chain interactions while 15_7 is dominated by intra-chain interactions.[338, 335] In the future we will study two intra-chain interactions, (i) nonlocal interactions between stretch modes localized at neighboring CF_2 groups and (ii) anharmonicities within a single CF_2 group leading to interactions between the symmetric and antisymmetric stretch modes.